ABSTRACT

Title of dissertation: CROSS-CORRELATIONS AND ENTANGLEMENT IN CAVITY QED

Matthew L. Terraciano,
Doctor of Philosophy, 2006

Dissertation directed by: Professor Luis A. Orozco
Department of Physics

Every quantum system subjected to measurements is an open quantum system. The cavity QED system is elegant in that it probes the interaction between two quantum systems, the atom and the field, while its loss mechanisms are well understood and can be externally monitored. The study of cross-correlations in cavity QED is important for understanding how entanglement evolves in open quantum systems. As quantum information science grows we need to learn more about entanglement and how it can be quantified and measured.

Correlation functions have been used to compare an electromagnetic field (intensity) of one mode with the electromagnetic field (intensity) of the same mode at a later time or different spatial location. In quantum optics, correlation functions have been calculated and measured to probe the nonclassical field that results from the interaction of a single mode of the electromagnetic field and an ensemble of two-level atoms (the canonical cavity QED system). This field can exhibit antibunching, squeezing, and can violate inequalities required for a classical field.

Entanglement in the steady state of a cavity QED system cannot be measured directly with traditional correlation functions (Hanbury-Brown and Twiss type experiments). Cross-correlations, however, interrogate directly both modes of the entangled pair, the transmitted (cavity) and the fluorescent (atom) intensities, and can act as an entanglement witness.

This thesis presents the implementation of a cross-correlation measurement in a cavity QED system. The work has required the construction of an apparatus that incorporates laser cooling and trapping with quantum optics to carefully control both the external (center of mass motion) and internal (atomic state) degrees of freedom of a collection of atoms that interact with a single mode of a high finesse Fabry-Perot cavity. We examine theoretically and experimentally a new intensity cross-correlation function $g^{(2)}_{TF}(\tau)$ which probes the evolution of the cavity field conditioned on the detection of a fluorescent photon from an atom in the cavity. The results open the possibility to generalize the dynamics of entanglement as a physical resource necessary for the nascent quantum information science.

CROSS-CORRELATIONS AND ENTANGLEMENT IN CAVITY QED

by

Matthew L. Terraciano

Dissertation submitted to the Faculty of the Graduate School of the
University of Maryland, College Park in partial fulfillment
of the requirements for the degree of
Doctor of Philosophy
2006

Advisory Commmittee:

Professor Luis A. Orozco, Chair/Advisor, University of Maryland
Professor Wendell T. Hill III, Dean's Representative, University of Maryland
Professor Howard M. Milchberg, University of Maryland
Professor Perry R. Rice, Miami University
Professor Steven L. Rolston, University of Maryland

DEDICATION

Dedicated to the memory of Rose Terraciano.

ACKNOWLEDGMENTS

There are many people to whom I owe a great debt for supporting me throughout the past years. First I mention two people whose support has been so valuable I dare say that I could have completed my Ph.D. without it. The first is my advisor, Luis Orozco. I was first attracted to his laboratory because of his passion for science, his integrity in carrying out scientific research, and his eagerness and ability to teach. Over the years he has imparted me with knowledge, not just of physics, but in many aspects of life outside of our laboratory. His guidance has helped me grow as a scientist and his influence on me is immeasurable.

The second person who has had a profound effect on my life is my future wife, Vanessa Capanzano. We met years ago while we were students at Stony Brook University and she has patiently stuck with me through my move to Maryland and the tough years to follow. Her support and love have strengthened me at the time of my life when I most needed it. I may never be able to repay my debt to her, although I will try as we begin our lives together as a married couple.

I would like to thank my parents, grandparents, siblings, aunts and uncles for their loving encouragement. Vanessa's family has been extremely supportive of Vanessa and myself as we continued our education in Maryland.

At Stony Brook there are many friends and lab mates who made my first years of graduate school an absolute pleasure. Among them are: Matt Carmell, Evan

Crocker, Jamil Egdemir, Lisa Bjorndal, Sue Metz, T. J. Walls, Doug Bennett, Dave Cardoza, Joe Reiner, Eduardo Gomez, Seth Aubin, Wade Smith, Mirna Lerotic, Almar Lange, Florian Baumer, and Josh Grossman. This is by no means a complete list. After moving our laboratory to the University of Maryland our group has recuited many wonderful people who have helped build a strong program in AMO physics. I would like to thank the students Rebecca Olson, Basudev Roy, Michael Scholten, David Norris, Elohim Becerra, Nick Cummings, Dong Sheng, and Adrian Perez-Galvan. We have had three postdocs during my time at Maryland who have aided significantly in the progress of research in our group: Daniel Friemund, Daniela Manoel, and Yanting Zhao.

Our group is essentially married to the group of Steve Rolston, another person to whom I owe many thanks for his advise and interest in our experiments. In his group I would like to thank the following "Rolstonians" for their help and friendship: Scott Fletcher, Emily Edwards, Matt Beeler, Brendan Wyker, Xianli Zhang, Tommy Willis, Jennifer Robinson, and Ilya Arakelyan.

In particular I am grateful to Perry Rice for his continued collaboration with Luis and myself. We have both benefited from his contributions to our work and I have personally learned a great deal from him during his visits to Maryland and my visit to Ohio. Also our collaborative efforts with James Clemens, Julio Gea-Banacloche, Hicem Eleuch, and Howard Carmichael have been extremely fruitful.

I would like to thank the National Science Foundation and the National Institute of Standards and Technology for their support of this work.

TABLE OF CONTENTS

LIST OF FIGURES

Chapter 1

Introduction

Cavity quantum electrodynamics (QED) is a subset of a broad area of study which encompasses electromagnetism and quantum mechanics. Its main components are the cavity, a resonator for electromagnetic radiation, and a medium coupled to the electromagnetic field mode defined by the cavity. Since its inception the number of physical realizations of cavity QED systems has grown dramatically. Examples of such systems include: Rydberg atoms in microwave cavities [1], quantum dots imbedded in micropillar cavities [2], and trapped ions [3] or neutral atoms in optical cavities [4]. Each system has its advantages and disadvantages from an experimental point of view, but they all are common in that they study the interaction between a single mode of the electromagnetic field and the matter within.

Jaynes and Cummings considered the interaction of a single two-level atom with a single mode of a quantized field [5]. Simultaneously in East Germany, Paul developed an equivalent model [6], however the Hamiltonian that describes the interaction is commonly referred to as the Jaynes and Cummings (JC) Hamiltonian.

$$H_{JC} = \frac{1}{2}\hbar\omega_a\sigma^z + \hbar\omega_c a^\dagger a + \hbar g(\sigma^- a^\dagger + \sigma^+ a) \tag{1.1}$$

The first term describes the state of the atom, where σ^z is the population operator of a two-level atom. The following term is the field Hamiltonian where $a^\dagger$ and a are the field raising and lowering operators respectively. Last is the term that describes

the interaction of the field with the atom in the rotating wave approximation with a coupling strength given by g. Here σ^+ and σ^- are respectively the atomic raising and lowering operators.

The eigenstates of the Hamiltonian are the ground state

$$|n, g\rangle \tag{1.2}$$

and the excited states

$$|\pm\rangle = \frac{1}{\sqrt{2}}(|n, e\rangle \pm |n+1, g\rangle), \tag{1.3}$$

where $|n, g(e)\rangle$ represent the bipartite bare state of the atom-cavity system with n photons in the mode and an atom in the ground (excited) state. The dressed states, $|\pm\rangle$, differ from that of the degenerate excited states of the uncoupled system. A doublet is formed by a splitting of the excited states of $\pm g\sqrt{n}$, lifting the degeneracy. This is the so-called vacuum Rabi splitting of cavity QED [7].

The Jaynes and Cummings model discussed above is a simplified picture of the interaction between light and matter in cavity QED. While it illustrates how energy changes between the two constitute systems, it does not account for dissipation. An excitation in the atom or the field can couple to modes outside the cavity via a spontaneous emission event or a photon escaping the cavity due to finite mirror transmission. These modes of decay into the two available reservoirs allow an observer to interrogate the system.

The cavity QED system, in the presence of dissipation, is characterized by three rates; the coherent coupling rate, g, between the atom and the cavity mode, the spontaneous emission rate γ, and the escape of photons from the mode of the

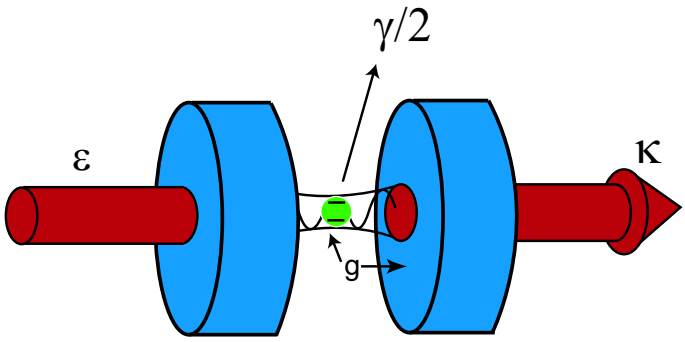

Figure 1.1: Cavity QED System.

cavity 2κ. Here g is given by

$$g = \sqrt{\frac{\mu^2 \omega}{2\hbar\epsilon_0 V}} \tag{1.4}$$

where μ and ω are the dipole matrix element and the frequency of the atomic transition, respectively, and V is the volume of the mode. $2g$ represents the Rabi frequency associated with the field of a single photon inside the resonator.

Quantum systems and their interactions with external reservoirs have been of interest since the birth of quantum mechanics, however new quantum information protocols demand that these interactions be understood to a much higher level. The cavity QED system is an ideal system for probing the nature of open quantum systems. The mechanisms to lose information to external reservoirs are well understood and are exactly the avenues by which the system can be interrogated.

There are many measurements in cavity QED that illuminate the dynamical exchange of energy between the atoms and the cavity mode. Here we will characterize these measurements into two broad categories, frequency (spectral) [8, 9] and time (correlation) [10] measurements.

Spectral measurements can be performed by driving a cavity on the TEM_{00} mode by a weak classical field, ε. This field typically derives from an attenuated laser beam and is resonant with both the atom and the cavity. Detuning the laser frequency with respect to the atomic and cavity resonance reveals the probe spectrum of the coupled system. The coupling of the atoms to the cavity mode lifts the degeneracy of excited states, resulting in a doublet in the probe spectrum. The separation of this so-called vacuum Rabi splitting in the weak excitation regime ($n < 1$) is given by $g\sqrt{N}$ in the limit of strong coupling, $g >> \kappa, \gamma$. Here N represents the number of maximally coupled atoms in the mode.

Two-time correlation measurements of cavity emitted photons reveal the non-classical nature of the cavity QED through effects such as photon antibunching [11, 12, 13] and violations of inequalities required for a classical field [14]. A common correlation function is the autocorrelation of the type used by Hanbury-Brown and Twiss [15] for stellar interferometry, $g^{(2)}(\tau)$, where τ is the time in between two detection events. An autocorrelation function of this type cannot measure the entanglement between the atoms and the cavity mode as it does not measure both components of the entangled pair.

Although the JC model does not account for dissipation in the system, it reveals the underlying entanglement between the atom and the field in the absence of higher order excitations. Entanglement can be described as a property of two or more composite quantum systems that are in some way intertwined such that they can no longer be thought of as independent despite the physical distance that may separate them. It is a measure of how much information can be learned about one

subsystem by making a measurement on the other.

Entanglement remains a complicated subject, despite the passage of over seventy years since Einstein, Podolsky, and Rosen discussed it in their seminal paper [16]. Schrodinger responded to this discussion by proposing the now infamous Schrodinger cat thought experiment [17]. The tone of these discussions reflect the internal struggles of these prominent physicists with a concept that seemingly defies reality.

Entanglement is often described in a mathematical sense as the inability to write the total wave function for the combined system as the product of separate wave functions for the individual subsystems. A state that is not separable is said to be entangled.

The probing question of the nature of entanglement in quantum mechanics was formalized by Bell [18] with the introduction of an inequality that cannot be violated by a classically correlated system with local hidden variables. The study of nonlocality in nature eventually spawned a series of measurements [19], which show how entangled quantum states violate, in particular circumstances, Bell's inequality. The emphasis on entanglement has shifted from a mere curious property of quantum mechanics to an invaluable resource with the emergence of the nascent quantum information. The possibility to teleport quantum states [20], communicate securely [21], and build a quantum computer [22] relies intrinsically on entanglement.

Cross-correlations between spontaneously emitted light (atomic state information) and light emitted from the cavity (field mode information) have the possibility to probe entanglement. This measurement is experimentally challenging because

a direct measurement of the fluorescence is required. An atom inside the cavity can emit in all directions out of the sides of the cavity, complicating the detection process.

The goal of this work is to measure entanglement in cavity QED through an experimental realization of a cavity QED experiment. To accomplish this we examine the use of correlation functions which correlate fluctuations (photons) in two modes: one for the cavity, the other for spontaneous emission of the atoms. This thesis describes cross-correlations and its relationship to entanglement. The results described here are relevant for the understanding of how entanglement evolves in open quantum systems. Chapter 2 introduces the theoretical background. Chapter 3 elaborates on this discussion with new theoretical calculations of entanglement in a driven cavity QED system. Chapter 4 describes the experimental apparatus. Chapter 5 explains our results of a measurement of the probe spectrum of spontaneously emitted light into the mode of the cavity. Chapter 6 discusses quantum auto- and cross-correlation measurements on a two-mode cavity QED system and chapter 7 presents the conclusions.

Chapter 2

Cavity QED: Theoretical Background

This chapter reviews current theoretical models for cavity QED. We begin with a semiclassical description that provides a guiding principle for predicting the steady state behavior. This leads naturally to a discussion of optical bistability in cavity QED and the vacuum Rabi splitting, both steady state semiclassical phenomenon. Quantum models give an intuitive sense of the dynamical evolution of the system wave function after a detection event. This guide provides a background for the following chapters that describe the experiments, results, and further modifications to the theory. Throughout this work we characterize the cavity QED system with two dimensionless parameters that weigh the influence of the atom and light on the system: the single atom cooperativity $C_1 = g^2/(\kappa\gamma)$ and the saturation photon number $n_0 = (\gamma^2/(8g^2))b$, where b depends on the mode function of the cavity. For a travelling plane wave cavity, $b = 1$, and for a standing wave Gaussian cavity, $b = 8/3$ (see article by Kimble in Ref. [4]). For N atoms the cooperativity, C, scales as NC_1.

2.1 Semiclassical Model

2.1.1 Maxwell-Bloch Equations

The Maxwell-Bloch equations give a semiclassical treatment of cavity QED. These consist of (1) an equation for the mode of the cavity which is driven classically

by a field, ε, and (2) the Bloch equations that describe how a two-level atom couples to this field. In a cavity QED system there is a feedback mechanism due to the light traversing the atomic sample many times before exiting the cavity, imposing boundary conditions on the field [23]. For a plane wave ring cavity the Maxwell-Bloch equations are:

$$\frac{dx}{dt} = -\kappa(x - y - 2CP) \tag{2.1}$$

$$\frac{dP}{dt} = \frac{\gamma}{2}(xD - P) \tag{2.2}$$

$$\frac{dD}{dt} = -\gamma\left[\frac{1}{2}(xP^* + x^*P) + D + 1\right] \tag{2.3}$$

Here $x \equiv \langle a\rangle/\sqrt{n_0}$ is the field inside the cavity in the presence of atoms, $y \equiv \epsilon/(\kappa\sqrt{n_0})$ is the field without atoms, P is the normalized atomic polarization, and D is the normalized atomic inversion, where D = -1 represents all the atoms in the ground state.

For the case of a weak driving field x $\ll$ 1, we can safely assume that all the atoms remain in the ground state and can set D = -1. In steady state this results in a linear relationship between the intracavity fields with and without atoms.

$$y = x(1 + 2C), \tag{2.4}$$

for x$\ll$1.

Detunings between the driving laser field and the atomic and cavity resonances, Δ and Θ are respectively defined as

$$\Delta = \frac{\omega_a - \omega_l}{\gamma/2} \tag{2.5}$$

$$\Theta = \frac{\omega_c - \omega_l}{\kappa} \tag{2.6}$$

where ω_a, ω_c, ω_l are the frequencies of the atomic and cavity resonances, and the probing laser. These detunings are incorporated into this semiclassical picture by making the following substitutions [24].

$$\gamma/2 \rightarrow \gamma/2(1 + i\Delta),\ \kappa \rightarrow \kappa(1 + i\Theta) \tag{2.7}$$

Departing from the weak field limit we now can express the state equation for the cavity QED system under the assumption of a plane wave ring cavity as

$$y = x\left[\left(1 + \frac{2C}{1 + \Delta^2 + x^2}\right) + ix\left(\Theta - \frac{2C\Delta}{1 + \Delta^2 + x^2}\right)\right], \tag{2.8}$$

for all x. Here we have solved the Maxwell-Bloch equations using the substitutions of Eq. 2.7 to allow for detunings. Note that Eq. 2.8 reduces to Eq. 2.4 in the resonant weak driving limit.

2.1.2 Optical Bistability

The state equation reveals the intrinsic nonlinearity of the system. A two-level atom in the excited state cannot be excited to a higher energy level, but can only decay through spontaneous or stimulated emission; in contrast, the cavity is a harmonic oscillator and its energy can increase without bound. For a weak driving field, $x,\ y \ll 1$, the linearity is restored as the atom spends very little time in the excited state.

Taking the absolute value squared of both sides of Eq. (2.8) relates the intracavity intensities with and without atoms respectively ($X = |x|^2, Y = |y|^2$). Here the system can have two stable output intensities for a given drive intensity, commonly referred to as optical bistability [23]. The system chooses the appropriate solution depending on its past history. For a very weak driving field the atoms absorb most of the light, spontaneously emitting a photon randomly with a dipolar pattern. As the driving field increases, the atoms saturate and a field builds up quickly. This field constructively interferes inside the cavity and the resulting field is equivalent to the driving field minus a small amount due to absorption and spontaneous emission of the atomic sample. The system resides in the upper branch of the bistability curve. As the driving field decreases the field remains strong inside the cavity until the drive is sufficiently low that the atoms scatter more photons than the drive can provide. The field drops rapidly and the system shifts back to the lower branch.

2.1.3 Vacuum Rabi Splitting

The response of a resonantly driven cavity QED system that resides on the lower branch of the bistability curve is analogous to a pair of coupled oscillators. Here the oscillators are the cavity mode and the atomic polarization, coupled together by the radiating dipole. This assumption is valid when there is at most one excitation in the system. Like its classical counterpart, the atom-cavity system can exchange energy from one oscillator to the other. This energy exchange occurs at the rate $2g$ (for a single atom in the strong coupling limit), which is the Rabi fre-

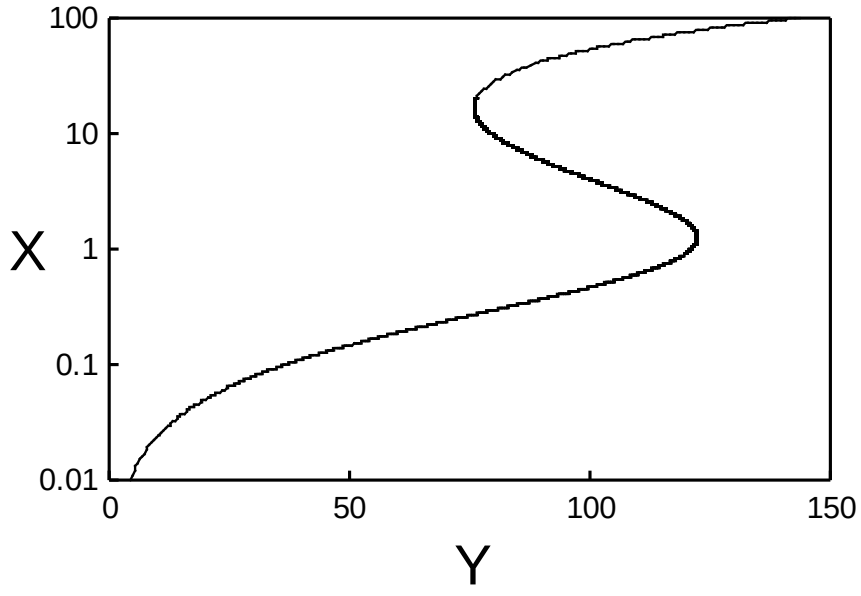

Figure 2.1: Optical bistability. Plot of the state equation for a cavity QED system with $C = 10$.

quency associated with the field of a single photon inside the cavity. This coupling is enhanced by the cavity compared to the free space coupling. Because g depends inversely on $\sqrt{V}$ many optical cavity QED experiments employ cavities with very small mirror separation ($L < 100$ μm) to maximize the coupling.

The probe spectrum of cavity QED with low excitation shows a doublet in the first excited state of the system. The degeneracy between the bare atomic and cavity resonances ($\omega_e - \omega_g = \omega_c$) is lifted as g surpasses a threshold given by the decay rates which determine the linewidth of the double peaks. For N atoms this coupling is enhanced due to the cooperative nature of the cavity QED system. The N atoms generate a collective atomic dipole in the mode of the cavity with a strength $\sqrt{N}$ times larger than that of a single atom.

This doublet is dubbed the vacuum Rabi splitting, a misnomer as it is the excited state that is split, not the vacuum. In a quantum mechanical picture it can be viewed as a dressing of the transition, however this quantum description is not required. Semiclassically, using the formalism we describe above, we can rewrite the intensity state equation (square of Eq. 2.8) in the low intensity regime as

$$\frac{X}{Y} = \frac{1}{\left(1 + \frac{2C}{1+\Omega^2/\kappa^2}\right)^2 + \left(2\Omega/\gamma - \frac{2C\Omega/\kappa}{1+\Omega^2/\kappa^2}\right)^2} \tag{2.9}$$

where $\Omega = \Delta\kappa = \Theta\gamma/2$ is the probe frequency detuning. The expression for the peak positions follow [25]

$$\Omega_{\pm} = \pm\sqrt{-\left(\frac{\gamma}{2}\right)^2 + g^2N\sqrt{1 + \frac{\gamma}{g^2N}\left(\frac{\gamma}{2} + \kappa\right)}} \tag{2.10}$$

and they have been found to match very well with experimental observations at low intensity done previously in our laboratory [8, 26].

2.2 Quantum Model

2.2.1 Steady State Wave Function

The model for a realistic cavity QED system in the optical regime starts with the JC Hamiltonian and incorporates dissipation and external drives. A consistent treatment of dissipation requires a master equation approach, which allows for the system to interact with external reserviors (modes other than the cavity mode). These external modes are connected to the system through the processes of atomic

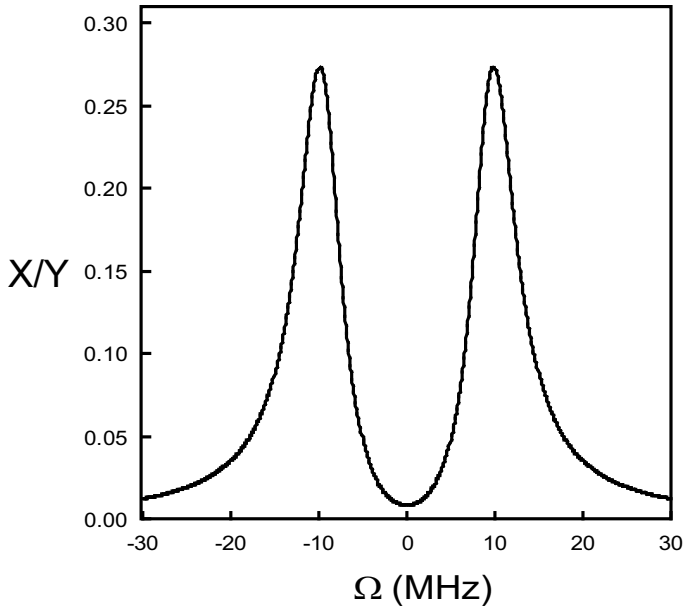

Figure 2.2: Probe spectrum for cavity QED system with $g = \kappa = \gamma/2 = 3$, $N = 10$, $C = 5$. For this case $\omega_c = \omega_a$.

polarization and cavity decay. The master equation describes the evolution of a density matrix for the system.

We follow the treatment of Carmichael [27] to elucidate the master equation using as a guiding principle the detection process and the quantum trajectory formalism. For a driven cavity QED system with N atoms defined by a density operator ρ, the master equation describing its time evolution is

$$\begin{aligned} \frac{d\rho}{dt} &= \epsilon[a^\dagger - a, \rho] + g[a^\dagger J^- - aJ^+, \rho] + \kappa(2a\rho a^\dagger - a^\dagger a\rho - \rho a^\dagger a) \\ &\quad + \frac{\gamma}{2}\sum_{j=1}^{N}(2\sigma_j^-\rho\sigma_j^+ - \sigma_j^+\sigma_j^-\rho - \rho\sigma_j^+\sigma_j^-) \end{aligned} \tag{2.11}$$

We use here the collective raising and lowering operators

$$J^+ = \sum_{j=1}^{N}\sigma_j^+ \tag{2.12}$$

$$J^- = \sum_{j=1}^{N} \sigma_j^-. \tag{2.13}$$

For a sufficiently weak driving field, ε, the system will evolve into a steady state that is nearly a pure state. This assumption is valid when photodetections occur only infrequently compared with the timescales that govern the evolution of the system, namely $1/g$, $1/\kappa$, and $1/\gamma$. This pure steady state can be written in a basis of up to two excitations. At this point we abandon the semiclassical treatment and can no longer assume that the atom is never in the excited state [28].

Expansion of the master equation to leading order in ϵ/κ with the substitution $\rho = |\Psi(t)\rangle\langle\Psi(t)|$ where,

$$|\Psi(t)\rangle = |0,g\rangle + A_{1g}(t)|1,g\rangle + A_{0e}(t)|0,e\rangle + A_{1e}(t)|1,e\rangle + A_{2g}(t)|2,g\rangle, \tag{2.14}$$

leads to rate equations for the coefficients of the basis states. Solving these rate equations in the steady state results in a steady state wave function

$$|\Psi_{SS}\rangle = |0,g\rangle + A_{1g}|1,g\rangle + A_{0e}|0,e\rangle + A_{2g}|2,g\rangle + A_{1e}|1,e\rangle \tag{2.15}$$

where the A_{ij} are known [28, 24]. They are

$$A_{1g} = \alpha \tag{2.16}$$

$$A_{0e} = \beta \tag{2.17}$$

$$A_{1e} = \alpha\beta q \tag{2.18}$$

$$A_{2g} = \alpha^2 pq/\sqrt{2}. \tag{2.19}$$

where α is the mean cavity field and β is the mean atomic polarization. The quantities p and q are equal to 1 for coupled harmonic oscillators. In cavity QED they

differ from unity due to the nonlinear, or saturable, nature of the atom. The squares of coefficients of single excitation, A_{1g} and A_{0e}, give the probabilities of detecting single photons through the output mirror or in fluorescence (steady state). The squares of the double excitation coefficients, A_{1e} and A_{2g}, give the probabilities of detection of two photons either in coincidence (one through the mirror, and one in fluorescence) or both out of the mirror. The variables are

$$\alpha = \frac{\epsilon}{\kappa(1+2C_1)} \tag{2.20}$$

$$\beta = \frac{-2g}{\gamma}\alpha \tag{2.21}$$

$$p = 1 - 2C_1' \tag{2.22}$$

$$q = \frac{(1+2C_1)}{(1+2C_1-2C_1')} \tag{2.23}$$

$$C_1 = \frac{g^2}{\kappa\gamma} \tag{2.24}$$

$$C_1' = C_1\frac{2\kappa}{(2\kappa+\gamma)} \tag{2.25}$$

The one-excitation amplitudes, A_{1g} and A_{0e}, are proportional to the driving field ε; the two-excitation amplitudes, A_{2g} and A_{1e}, are proportional to the square of the driving field, ε^2 [28]. The norm of this wave function is $||\Psi\rangle| = \sqrt{1+O(\varepsilon^2)}$; hence to lowest order in ε, the coefficient of the vacuum should be $(1-(1/2)O(\varepsilon^2))$.

2.2.2 Correlation Functions

Correlation functions derive formally from coherence theory in classical optics. A simple example comes from the interference of two monochromatic fields. For two overlapping fields with the same frequency, the interference term can be written as a cross-correlation, $\langle E_1(t)E_2^*(t+\tau)\rangle$, where τ represents a relative time delay

between the two fields, E_1 and E_2. The brackets represent an average over times typically long compared to the optical frequency. Classical coherence theory reveals how correlations of this type can be used to measure the degree of coherence of a light source as well as the spectrum through the Wiener-Khintchine theorem.

In 1956, Hanbury-Brown and Twiss proposed an optical stellar interferometer based on measuring correlations of intensity fluctuations. The proposed second order (in intensity) correlation function, $\langle I(t)I(t+\tau)\rangle$, represents two-time correlations of the intensity I.

The normalized form for a single source,

$$g^{(2)}(\tau) = \frac{\langle I(t)I(t+\tau)\rangle}{\langle I(t)\rangle^2} \tag{2.26}$$

illustrates the differences between classical and quantum mechanical sources. The intensity can be written as $I(t) = \langle I\rangle + \Delta I(t)$ where $\Delta I(t)$ represents the variance of the intensity at time t from the average. Inserting this into Eq. 2.26 gives

$$g^{(2)}(\tau) = 1 + \frac{\langle \Delta I(t)\Delta I(t+\tau)\rangle}{\langle I\rangle^2}. \tag{2.27}$$

The second term above is always positive for a classical source with fluctuations, therefore, $g^{(2)}(0) \geq 1$. A laser operating well above threshold obeys Poissonian statistics, $g^{(2)}(0) = 1$, while for a chaotic source, $g^{(2)}(0) = 2$, exhibiting super-Poissonian statistics. A chaotic source exhibits bunching, $g^{(2)}(0) > g^{(2)}(\tau)$, indicating that photons emitted from the source are more likely to be emitted in bunches.

The foundation of quantum coherence theory was primarily laid by Glauber in a series of articles in 1963 [29, 30]. His contributions to the field earned him a Nobel

prize in 2005. The formalism of classical coherence theory is replaced by quantum mechanical normal and time ordered operators which act on a quantum state. The second order correlation function can exhibit behavior for quantum mechanical systems that is forbidden by classical mechanics. An example is a measurement of $g^{(2)}(\tau)$ for resonance fluorescence [31]. A perfect measurement would result in subPoissonian statistics, $g^{(2)}(0) < 1$, and antibunching, $g^{(2)}(0) < g^{(2)}(\tau)$, due to the time that it takes for an atom to get reexcited after emitting a photon.

A general normalized second order correlation function for a quantum system is

$$g^{(2)}(\tau) = \frac{\langle \Psi | a^\dagger(t) a^\dagger(t+\tau) a(t+\tau) a(t) | \Psi \rangle}{\langle \Psi_{SS} | a^\dagger a | \Psi_{SS} \rangle^2} \tag{2.28}$$

where $|\Psi\rangle$ is the wave function for the system. A weakly driven cavity QED system in the steady state is described as a pure state by the wave function of Eq. 2.15. Here the delicate nature of the quantum state is revealed. The finite mirror transmission allows an intracavity photon to escape, collapsing the wave function. This conditioned state, $|\Psi_c\rangle = a|\Psi_{ss}\rangle / \sqrt{\langle a^\dagger a \rangle}$, is the same for all photodetections if we regard the system as pure. This is a good approximation when photodetections occur infrequently, less than one per several lifetimes of the system: $1/\kappa$, $1/\gamma$. The second order correlation function can be considered as the expectation value of the field at time $t+\tau$, conditioned a photodetection at time t.

$$g^{(2)}(\tau) = \frac{\langle \Psi_c | a^\dagger(t+\tau) a(t+\tau) | \Psi_c \rangle}{\langle \Psi_{ss} | a^\dagger a | \Psi_{ss} \rangle} \tag{2.29}$$

An analytical expression for $g^{(2)}(\tau)$ for a weakly driven cavity QED system is

derived in [28]

$$g^{(2)}(\tau) = \left(1 + (\Delta\alpha/\alpha) exp\left[-1/2(\kappa+\gamma/2)\tau\right]\left[cosh\chi\tau + \frac{1}{2}(\kappa+\gamma/2)\frac{sinh\chi\tau}{\chi}\right]\right)^2 \tag{2.30}$$

where

$$\Delta\alpha/\alpha = -2C_1'\left[2C/(1+2C-2C_1')\right] \tag{2.31}$$

and

$$\chi = \sqrt{\frac{\kappa-\gamma/2}{4} - Ng^2}. \tag{2.32}$$

This correlation function can exhibit nonclassical behavior such as photon anti-bunching as well as violation of inequalities required for a classical field, such as $|g^{(2)}(\tau) - 1| < |g^{(2)}(0) - 1|$.

Chapter 3

Steady State Entanglement in Cavity QED and Cross Correlations

Two particles (or systems), A and B are said to be in an entangled state if the wave function of the complete system does not factorize, that is $|AB\rangle \neq |A\rangle|B\rangle$. One consequence of this form of the wave function is that a measurement on system A yields information about system B without any direct interaction with system B. An example that is of relevance to this work is the maximally entangled state of an atom and a field mode, $|\Psi\rangle = (1/\sqrt{2})\,(|1,g\rangle + |0,e\rangle)$. A measurement of the state of the atom immediately tells us the number of photons in the field mode; or a measurement of the photon number immediately tells us the state of the atom.

Quantifying the amount of entanglement present in a quantum state is a topic of much debate. Until recently, measurements of violations of Bell's inequalities have been thought to serve as an indicator of entanglement. However it has been shown that not all entangled states violate Bell's inequalities [32]. For a pure bipartite state the Von Neumann entropy, $E = -(tr_A \rho_A log_2 \rho_A)$, quantifies the entanglement. Here ρ_A is the reduced density matrix after tracing over the states of the subsystem B, $\rho_A = tr_B \rho_{AB}$. For mixed states, on the other hand, quantifying the amount of entanglement in a partially entangled state is not, in general, simple. The natural generalization of the pure-state measure indicated above is known as the entanglement of formation. This utilizes a decomposition of the quantum state

$\rho = \sum_j P_j|\psi_j\rangle\langle\psi_j| = \sum_j P_j\rho_j$, and then defines $E = min(\sum_j P_j E_j)$ where E_j is the von Neumann entropy for the density matrix $\rho_j = |\psi_j\rangle\langle\psi_j|$, and the minimum is taken over all the possible decompositions, which is in general a very challenging task [33, 34]. As a result of this, alternative measures have been proposed, such as the logarithmic negativity [35]. It is also possible that some particular measurement scheme may result in a most natural unraveling of the density operator, in the sense of the quantum trajectories approach [36] (especially for systems that are continually monitored), and in that case it may be physically meaningful to focus only on the entanglement of the (conditionally pure) states obtained via that particular unraveling.

Another measure of entanglement is the concurrance, first introduced by Wootters for two qubits [34]. In the case of a mixed state of two qubits it can be shown that the concurrance is equivalent to the entanglement of formation. This chapter discusses how entanglement in a steady state cavity QED system can be quantified and measured using cross-correlations.

3.1 Quantifying Entanglement in a Steady State Cavity QED System

Recall from chapter 2 the wave function of cavity QED under a weak drive,

$$|\Psi(t)\rangle = |0,g\rangle + A_{1g}(t)|1,g\rangle + A_{0e}(t)|0,e\rangle + A_{1e}(t)|1,e\rangle + A_{2g}(t)|2,g\rangle. \quad (3.1)$$

The entanglement of formation for this system is calculated from the density matrix after tracing over the field variables:

$$\rho_{atom} = Tr_{field}|\Psi\rangle\langle\Psi| \quad (3.2)$$

$$= \begin{pmatrix} 1 + A_{1g}^2 + A_{2g}^2 & A_{1e}A_{1g} + A_{0e} \\ A_{1e}A_{1g} + A_{0e} & A_{1e}^2 + A_{0e}^2 \end{pmatrix} \tag{3.3}$$

The eigenvalues of this matrix are, to lowest nonvanishing order,

$$\begin{aligned} \lambda_1 &= (A_{1g}A_{0e} - A_{1e})^2 \\ &= |A_{1g}|^2 |A_{0e}|^2 (q-1)^2 \\ &= \left(\frac{\varepsilon}{\kappa}\right)^4 \xi^2 \qquad (3.4) \\ \lambda_2 &= 1 - (A_{1g}A_{0e} - A_{1e})^2 \\ &= 1 - \left(\frac{\varepsilon}{\kappa}\right)^4 \xi^2 \qquad (3.5) \end{aligned}$$

where q is defined in Eq. (2.23), and we have defined

$$\xi = \frac{2g}{\gamma(1+2C_1)^2}(q-1) \tag{3.6}$$

The entropy $E = -\lambda_1 \log_2 \lambda_1 - \lambda_2 \log_2 \lambda_2$ is then (again to lowest leading order)

$$\begin{aligned} E &= -\left(\frac{\varepsilon}{\kappa}\right)^4 \xi^2 \log_2 \left[\left(\frac{\varepsilon}{\kappa}\right)^4 \xi^2\right] - \left(1 - \left(\frac{\varepsilon}{\kappa}\right)^4 \xi^2\right) \log_2 \left(1 - \left(\frac{\varepsilon}{\kappa}\right)^4 \xi\right) \\ &\approx -\left(\frac{\varepsilon}{\kappa}\right)^4 \xi^2 \left(\log_2 \left(\frac{\varepsilon}{\kappa}\right)^4 + \log_2(\xi^2) - 1\right) \\ &\approx -\left(\frac{\varepsilon}{\kappa}\right)^4 \log_2 \left(\frac{\varepsilon}{\kappa}\right)^4 \xi^2. \qquad (3.7) \end{aligned}$$

where we have taken the weak field limit, $\varepsilon/\kappa \ll 1$. The approximation (3.7) will hold provided $(\varepsilon/\kappa)^2 \ll |\xi|$. This entropy is the same as that obtained by using the density matrix for the field alone, traced over the atomic degrees of freedom.

The concurrence can also be used to characterize entanglement between two quantum systems of arbitrary dimension [37, 38, 39, 40]. The concurrence for our system is

$$\begin{aligned}\mathcal{C} &= \sqrt{2(1-Tr\rho_{atom}^2)} \\ &= \sqrt{4\left(A_{1g}A_{0e}-A_{1e}\right)^2} \\ &= 2\left(\frac{\varepsilon}{\kappa}\right)^2|\xi| \end{aligned} \tag{3.8}$$

which is closely related to the square root of the entropy, of Eq. 3.7, with the absence of the *log* factor [41]. To see why $|\xi| \propto |A_{1e} - A_{0e}A_{1g}|$ may be a good indication of entanglement, consider what happens if the wave function is a product state. We could write the steady state wave function for the cavity QED system as a product state

$$\begin{aligned}|\Psi\rangle_P &= |\psi_C\rangle \otimes |\phi_A\rangle \\ &= (D_0|0\rangle + D_1|1\rangle + D_2|2\rangle) \otimes (C_g|g\rangle + C_e|e\rangle) \\ &= D_0C_g|0,g\rangle + D_1C_g|1,g\rangle + D_0C_e|0,e\rangle + D_2C_g|2,g\rangle + D_1C_e|1,e\rangle \end{aligned} \tag{3.9}$$

where the $C_{g(e)}$ and D_n coefficients represent the probability amplitudes for the respective atomic and cavity wave functions. For weak excitations, the coefficient of the ground state of the system is $D_0C_g = 1$, or $C_g = D_0 = 1$. Then the product state is

$$|\Psi\rangle_P = |0,g\rangle + D_1|1,g\rangle + C_e|0,e\rangle + D_2|2,g\rangle + D_1C_e|1,e\rangle \tag{3.10}$$

Just knowing the one excitation amplitudes does not yield any information about entanglement, as it is possible to have $A_{1g} = D_1$ and $A_{0e} = C_e$. The coefficient of $|2,g\rangle$ gives no information about entanglement, just nonclassical effects in the field, as it only involves field excitation. For weak fields D_2 is exactly A_{2g}. The

entanglement shows up in the value of the coefficient of $|1,e\rangle$, A_{1e}; if this value does not satisfy $A_{1e} = D_1 C_e = A_{0e} A_{1g}$, then it is not possible to write the state as a product state.

In the presence of a non-zero vacuum contribution (as any real quantum state will have), one can learn nothing about entanglement simply by measurement of one-excitation amplitudes or probabilities. For example, the state $|0,g\rangle + \alpha(|1,g\rangle + |0,e\rangle)$ is entangled, but only if one is certain that the probability amplitudes for higher excitation are truly zero. A state of the form $|0,g\rangle + \alpha(|1,g\rangle + |0,e\rangle) + O(\varepsilon^2)$ cannot be said to be entangled without information on the relative size of the probability amplitude A_{1e}. Measurement of one-excitation amplitudes conditioned by a previous measurement *can* yield information about entanglement. This can be accomplished by utilizing cross-correlation functions.

Equation (3.8) gives the amount of entanglement in the system as a function of the one and two excitation amplitudes. In terms of specific system parameters the concurrence is:

$$\mathcal{C} = |2\alpha\beta(q-1)| = \frac{16\, g^3\, \varepsilon^2\, \kappa}{\left(2\, g^2 + \gamma\, \kappa\right)^2 \left(2\, g^2 + \kappa\, (\gamma + 2\, \kappa)\right)}. \tag{3.11}$$

Here we analyze the sensitivity of the concurrence to the different parameters that appear in Eq. (3.11), while trying to give physical reasons for their influence on the entanglement. Despite the fact that the rates of decay could be the same through the two reservoirs, spontaneous emission (γ) reduces entanglement more than cavity loss (κ). This is due to the fact that a γ event (spontaneous emission) *must* come from the atom, while a κ event (cavity transmission) could come from either the drive or

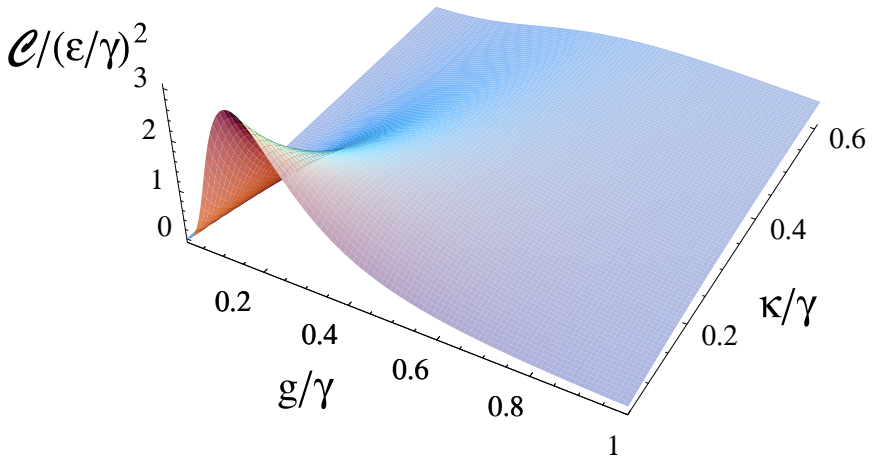

Figure 3.1: A plot of $\mathcal{C}$ scaled by $(\varepsilon/\gamma)^2$ as a function of κ/γ and g/γ for weak excitation.

a photon emitted by the atoms into the cavity mode. A spontaneous emission event unambiguously leaves the atom in the ground state, and the system wave function factorizes.

Figure 3.1 shows a remarkable result in the entanglement of the system as a function of the three rates in the problem. There is an optimal value for the coupling constant g given a set of dissipation rates κ, γ. For many interesting cavity QED effects, stronger coupling is generally better, such as the enhancement of the spontaneous emission by a factor of $1 + 2C_1 = 1 + 2g^2/(\kappa\gamma)$ (this formula strictly holds only in the bad cavity limit $\kappa >> g,\ \gamma$). However, here increasing the coupling of the atom and field mode eventually decreases the amount of entanglement [41]. To explain this it is instructive to recall that the concurrence $\mathcal{C} = |2\alpha\beta(q-1)|$, where α

is the mean cavity field, and $\beta = -g\alpha/\gamma$ is the mean atomic dipole. As the coupling g increases, for a fixed weak driving field ε, the intracavity field $\alpha = \varepsilon/(\kappa + 2g^2/\gamma)$ decreases. The intracavity field is the sum of the driving field in the cavity ε/κ, and the field radiated by the atom, $(-2C_1/(1+2C_1))\varepsilon/\kappa$; the minus sign resulting from the fact that the radiated field is π out of phase with the driving field on resonance. We see that as g and C_1 increase, the intracavity field decreases. This means that the steady-state wave function has a larger vacuum component, and consequently less entanglement. Another way to view this is that the cavity enhancement of the spontaneous emission rate means a larger loss rate for the system as the coupling increases, which is bad for entanglement.

More formally, consider what happens if the two-excitation amplitudes in Eq. (2.15) are arbitrarily set to zero, which amounts to setting $q = 0$ in Eq. (3.11), in which case the entanglement is only determined by the prefactor $|\alpha\beta|$. The steady-state wave function becomes

$$|\psi\rangle_{ss} = |0,g\rangle + \alpha(|1,g\rangle - \frac{g}{\gamma}|0,e\rangle). \tag{3.12}$$

There are two interesting limits on this Eq. (3.12) for the parameter $f = g/\gamma$. If $f \gg 1$, the steady state wave function is approximately $|\psi\rangle_{ss} = |0\rangle(|g\rangle - f\alpha|e\rangle)$, which is a product state. Also, if $f \ll 1$, the steady state wave function is approximately $|\psi\rangle_{ss} = |g\rangle(|0\rangle + \alpha|1\rangle)$, which again is a product state. To have entanglement between the atom and cavity mode, we must have the parameter $f \simeq 1$, so as to prepare a steady state wave function of the form $|\psi\rangle_{ss} = |0,g\rangle + \alpha(|1,g\rangle - |0,e\rangle) = |0,g\rangle + \alpha|-\rangle$, a mixture of the vacuum with a small entangled state component.

The decrease of the prefactor $|\alpha\beta|$ is the dominant reason why the concurrence decreases with increasing g for large coupling. Close inspection of Fig. 3.1 also shows that there is an optimal cavity loss rate, κ, for entanglement for a fixed g and γ. This is a result of reaching a maximum in the population of the states different from the vacuum (Eq. (2.15)). Our results here are consistent with the numerical results of Nha and Carmichael [36].

When the system is driven off resonance, its response is typically characterized by transmission and fluorescent spectra [25, 42]. Although these are important probes of the system, they do not, in this limit, carry information about the entanglement, since they are derived from only the one-excitation amplitudes.

The concurrence as a function of the detuning of the driving laser shows that the steady state entanglement decreases typically by a factor of $1/\Delta$ for large detuning, where $\Delta = (\omega - \omega_l)$ with ω the resonant frequency of the atom and cavity, and ω_l the frequency of the driving probe laser. But in the case where g is larger than κ and γ, the response is maximized at the vacuum-Rabi peaks [43]. Figure 3.2 shows a contour plot of $\mathcal{C}$ for parameters in the regime of cavity QED where the two decay rates are similar: $2\kappa/\gamma = 1.0$. The concurrence increases with increasing g on resonance up to a saddle point, and then decreases. However the entanglement persists for detunings on the order of g, the approximate location of the vacuum-Rabi peaks in the spectra of the system.

Detuning to a vacuum-Rabi peak ($\Delta = \pm g$), generates a steady state wave

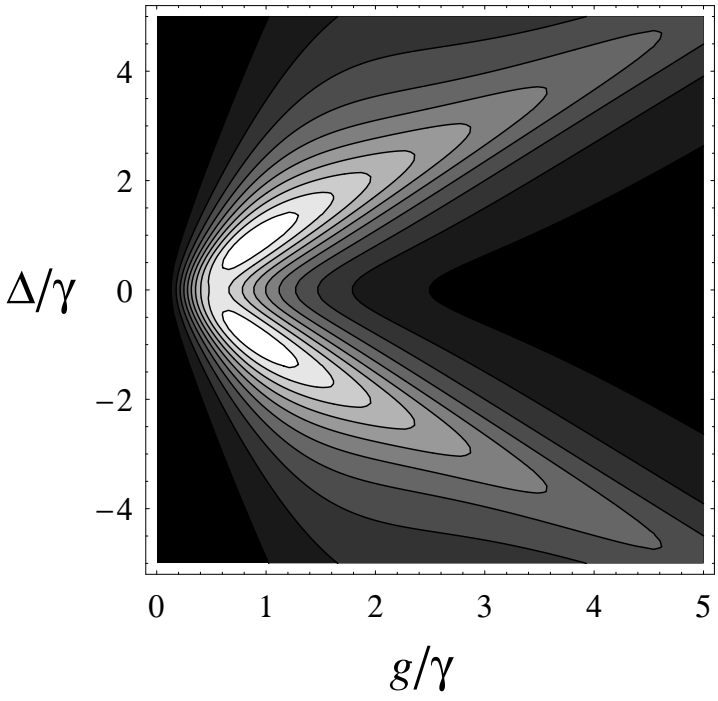

Figure 3.2: Contour plot of $\mathcal{C}$ as a function of g/γ and Δ/γ for $\kappa/\gamma = 0.5$

function of the form

$$|\psi\rangle_{ss} = |0, g\rangle + \alpha\Gamma_1(g/\gamma)|1, \pm\rangle + \alpha^2\Gamma_2(g/\gamma)|2, \pm\rangle, \tag{3.13}$$

where $|n, \pm\rangle = (1/\sqrt{2})(|n, g\rangle \pm |n-1, e\rangle)$ is the n photon dressed atom-field state one is tuned near and $\Gamma_1(g/\gamma)$ and $\Gamma_2(g/\gamma)$ are functions that are maximal when $g \simeq \gamma$. This is a state of mainly vacuum, plus a part that has entanglement between the atom and the cavity. It would seem that by continuing to tune to a vacuum-Rabi peak as g increases, it would be possible to maintain the entanglement, but Fig. 3.2 shows that this is not the case. Rather, as argued (for the on-resonance case) above, the crucial parameter for maximizing entanglement is $f = g/\gamma \propto 1/\sqrt{n_0}$, where $n_0 = \gamma^2/3g^2$ is the saturation photon number (recall from chapter 2) [41]. Recall

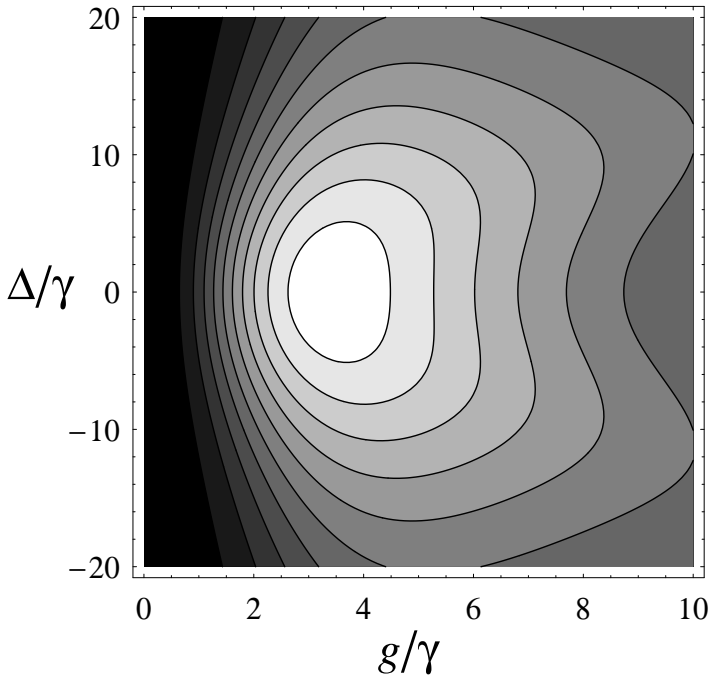

Figure 3.3: Contour plot of $\mathcal{C}$ as a function of g/γ and Δ/γ for $\kappa/\gamma = 10$

that, if these were two driven coupled harmonic oscillators, $q = 1$ and there would be no entanglement. A nonlinear interaction between the two harmonic oscillators would be needed to entangle them, as in the signal and idler modes in optical parametric oscillation. Even though the driving field is weak and the atom never nears saturation, there can only be entanglement with a linear atom-field coupling if the atom has a nonlinear response, as two-level atoms do.

The concurrence shows its sensitivity to different parameters. Figure 3.3 shows a contour plot of $\mathcal{C}$ versus g/γ and Δ/γ for a case where the cavity decay rate is larger than the spontaneous emission rate ($\kappa/\gamma = 10.0$). The entanglement is largest near $g/\gamma = 4.0$, before the vacuum-Rabi splitting of the spectrum, which does not occur in this case until $g/\gamma \sim 10.0$, at which point the entanglement is already

diminishing. The size of the maximum concurrence decreases by increasing κ/γ from 0.5 to 10.0 by a factor of about 30.

3.2 Cross-correlations for Entanglement Measurements

The calculation of entanglement leads now to the question of how to implement measurements that give the full information in the case of this cavity QED system under weak excitation. The previous section shows that the concurrence is related to the probability of single photon counts and coincidence counts from the cavity and fluorescence. These are the quantities associated in quantum optics with correlation functions, first introduced by Glauber [29, 30, 44, 45]. Generally these correlation functions involve comparing a field (intensity) of one mode with the field (intensity) of the same mode at a later time (or different spatial location), with some exceptions [46, 47, 48, 49, 50, 51]. However, entanglement in cavity QED has two components: atom and cavity mode. It is natural to look at cross-correlations between the cavity mode and the fluorescent light that falls in the mode of the detector [41].

Consider a general cross-correlation function for two modes of the electromagnetic field:

$$G = \langle f_b(b^\dagger, b) f_c(a^\dagger, a)\rangle / \langle f_b(b^\dagger, b)\rangle \langle f_c(a^\dagger, a)\rangle. \tag{3.14}$$

with f_b and f_c well behaved functions, in the sense of a convergent Taylor series on the Hilbert space of interest. If $|\psi\rangle$ is a product state, the correlation function $G(a, b)$ factorizes and then is unity. If it is not a product state, then this will manifest itself in a non-unit value for the normalized cross-correlation functions.

The simplest cross correlation function to consider is $j^{(1)}(\tau)$. This could be obtained by measuring the visibility of the fringe pattern formed by interfering the transmitted and fluorescent light. For the weakly driven cavity QED system, this is

$$\begin{aligned} j^{(1)}(\tau) &= \frac{\langle \sigma_+(0)a(\tau)\rangle}{\langle \sigma_+\rangle\langle a\rangle} \\ &= \frac{\alpha\beta}{\alpha\beta} \\ &= 1 \end{aligned} \tag{3.15}$$

so to lowest order, there is no information in this correlation function about entanglement.

To obtain information about entanglement the correlation function has to probe the two-excitation part of the state. A possibility to do this is the intensity cross correlation:

$$j^{(2)}(\tau) = \frac{\langle \sigma_+(0)a^\dagger(\tau)a(\tau)\sigma_-(0)\rangle}{\langle a^\dagger a\rangle_{ss}\langle \sigma_+\sigma_-\rangle_{ss}} \tag{3.16}$$

This yields the probability that a transmitted photon is detected at time τ conditioned on the detection of a fluorescent photon at $\tau = 0$. For simultaneous detection of a fluorescent and transmitted photon, $j^{(2)}(0) = q^2$. This normalized correlation function is directly related to the coefficient of double excitations (See Eqs. (2.15), (2.18), (2.23)). If $q = 1$ then $j^{(2)}(0) = 1$ and there is no entanglement; so a non-unit value of q indicates entanglement. Using second-order intensity correlations has been proposed in the context of entangled coherent states by Stobińska and Wódkiewicz [52].

The cross-correlation function $j^{(2)}(\tau)$ contains information about the average photon number after a measurement of the fluorescence relative to the average pho-

ton number in the absence of any interrogation of the fluorescence.

$$j^{(2)}(0) = \frac{|A_{1e}|^2}{|A_{1g}A_{0e}|^2} = q^2, \tag{3.17}$$

and $j^{(2)}(0) - 1 = q^2 - 1$ is an indicator of entanglement.

A way to measure q directly utilizes a field-intensity correlation function $h_\theta(\tau)$ [53], that can be implemented as a homodyne measurement conditioned on the detection of a fluorescent photon,

$$\begin{aligned} h^{TF}_{\theta=0}(0) &= \frac{\langle I_F E_T \rangle}{\langle I_F \rangle \langle E_T \rangle} \\ &= \frac{\langle (a^\dagger + a)\sigma_+\sigma_- \rangle}{\langle a^\dagger + a \rangle \langle \sigma_+\sigma_- \rangle} \\ &= \frac{A_{1e}}{A_{0e}A_{1g}} \\ &= q \end{aligned} \tag{3.18}$$

So $h^{TF}_{\theta=0}(0) - 1 = q - 1$ is also an indicator of entanglement in this system. What makes this measurement possible experimentally is the conditioning that selects only times when there is a fluctuation and the rest of the time (when the vacuum is present) no data is collected [54]. For one mode, the homodyned transmitted field conditioned by detection of a photon from that mode, is a measure of squeezing in that mode [53]. A homodyne measurement of the transmitted field conditioned by detection of a fluorescent photon is a measure of the two-mode squeezing, with the cavity field and atomic dipole as the two components. Generally, two-mode squeezing is an indicator of entanglement between the two modes. Gea Banacloche *et al.* explored this correlation function in a different regime of cavity QED and found it to be a witness of the dynamics of entanglement [55].

Non-classicality and entanglement are not necessarily simultaneously present. For example for two oscillators one could have $|\psi\rangle = (1/\sqrt{2})(|A, B\rangle + |B, A\rangle)$, where A and B are coherent state amplitudes. In this state, there is entanglement, but each individual mode shows no non-classical behavior. Conversely, one can have non-classical behavior with no entanglement, say for example the atom in the ground state and the field in a squeezed coherent state.

Chapter 4

Experimental Apparatus

This chapter gives an overview of the experimental hardware used in the cavity QED experiments described in the following chapters. There are three main components to the apparatus: the optical components, including the optical cavity, the atomic source, and the photon counting detectors and hardware.

4.1 Optical Components

4.1.1 Optical Cavity

The heart of the apparatus is the optical cavity. The requirements for mechanical stability are daunting. A typical cavity finesse is about 10,000. A reasonable condition for measurements of nonclassical features requires the cavity to be locked to within one tenth of the lesser of the cavity and atomic linewidths. This translates to stabilizing the separation of the mirrors over a large bandwidth (10 kHz) to an rms deviation of $\lambda/(2 \times 10^5)$, less than a Bohr radius for $\lambda = 780$ nm. The mirrors of the cavity are highly reflective at 780 nm, the frequency of the D_2 line of rubidium which we use as our atomic transition. The mirrors are custom ordered from Research Electro-Optics (Boulder, CO) for specified reflectivity and curvature. We use two mirrors with different reflectivities to define a preferential output port. The input and output mirrors transmit approximately 15 ppm and 300 ppm and have

radii of curvatures of 25 cm and 10 cm respectively. Losses due to absorption on the coatings are low (< 5 ppm). A stable Fabry-Perot cavity is formed from these mirrors when they are facing each other with the center of curvature of each mirror in the direction of the opposite mirror.

The cavity design allows optical access to the cavity volume from nearly all directions. Figure 4.1 shows the design of our cavity. The base is a 2.0 cm $\times$ 6.0 cm $\times$ 0.5 cm piece of polished stainless steel. The hole drilled through the center of the base allows for atoms or light to propagate through the piece to the center of the cavity. Two flat, rectangular piezo-electric transducers (PZTs) are glued to the steel base with a metallic epoxy. The glue connects electrically the bottom of the PZTs to the base which serves as ground. The importance of this cannot be understated. Extreme care must be taken in attaching the PZTs to the base. Previous attempts to glue the PZTs with nonmetallic epoxy from the side resulted in a partially elevated PZT. Although the electrical connection was sufficient, the combination of the partially elevated PZT with a mirror attached acted like a springboard with a resonant frequency < 1 kHz. The use of the metallic epoxy eliminated this resonance.

The mirrors are glued to the top of the PZTs with a nonmetallic epoxy one at a time using a HeNe laser to guide the placement of the mirrors with respect to an axis defined by the laser beam. Translation and tilt of the the mirrors are controlled as the mirrors are placed on the epoxy while the final placement is determined by monitoring the reflections and transmission of the HeNe reference beam.

The spacing of the cavity mirrors, 2.2 mm, is determined by measuring the

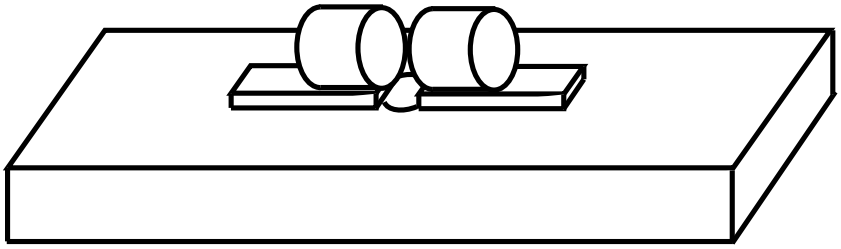

Figure 4.1: Cavity Design

frequency change needed to traverse one free spectral range. The free spectral range (FSR)is equal to $c/2L$ where c is the speed of light in vacuum and L is the length of the cavity. A figure of merit for the cavity is the finesse given by $FSR/2\kappa$. We measure 2κ by putting FM sidebands on the cavity beam with an electro-optic modulator and applying a linear ramp voltage to one of the PZTs, scanning the cavity length. The transmission of the cavity is detected with a photomultiplier tube. From the profile of the transmission, 2κ can be determine by relating the FWHM of the resonance to the spacing of the sidebands. For our system $2\kappa = 6.5$ MHz, $FSR = 68$ GHz and the cavity finesse is 10,000. The mode waist of the cavity is calculated from the cavity dimensions as 56 μm. For the experiments described in the following chapters, the cavity is driven with linearly polarized light, driving π transitions in the atom. We take the maximum dipole matrix element for the atomic transition and apply the appropriate correction factor to account for the reduction of strength when driving these π transitions. With these parameters we determine $g/2\pi$ for our system as 1.5 MHz and a single atom cooperativity of $C_1 = 0.12$.

4.1.2 Vacuum System

The cavity is placed under high vacuum (better than 1 x 10^{-8} Torr) in a cubical vacuum chamber (Kurt Lesker). This chamber connects to either a secondary chamber or a glass cell for the atomic source used in the experiments described in the following chapters. A 20 L/s ion pump (Varian) with no moving parts provides the vacuum. The ion pump has a finite lifetime and cannot operate at pressures above 1 mTorr. A vacuum tee connects the chamber to the pump where a valve opens a port for mechanical pump to prepump the system. A turbo pump is used to bring the chamber well below 1 mTorr before closing the valve and starting the ion pump. The turbo pump is removed from the system once the ion is on.

4.1.3 Main Laser

The cavity is driven on-axis with a Coherent MBR Ti:Sapph laser which supplies most of the light for the experiment. The laser is stabilized to the atomic crossover transition resulting from the saturated spectroscopy signal between the ^{85}Rb $5S_{1/2} \rightarrow 5P_{3/2}$, $F = 3 \rightarrow F' = 3$ and $F = 3 \rightarrow F' = 4$ transitions.

4.1.4 Cavity and Laser Stabilization

The cavity probe beam derives from the MBR laser and is sent through a double-passed acousto-optical modulator to control the frequency. Stabilization of the cavity requires the use of an auxiliary laser with a wavelength far from the atomic resonance. This auxiliary Toptica DL100 diode laser has a center frequency of 820

nm and can be tuned over 20 GHz without mode-hopping. The frequency is tuned to match the resonance condition imposed by the transmission of the 780 nm probe beam. When the two lasers are simultaneously resonant to the cavity, the auxiliary diode laser is locked to a 25 cm confocal Fabry-Perot cavity that has mirrors with high reflectivity at 780 nm and 820 nm and a finesse of 200. This transfer-lock cavity resides on the optical table and is not under vacuum and is stabilized using a Pound-Drever-Hall technique (see reference [56] for a review of this technique) with a beam deriving from the stabilized Ti:sapph laser. The frequency of the auxiliary laser must match the resonance condition for both cavities, which are set by the MBR laser locked to the rubidium atomic resonance. To accomplish this, the beam going to the transfer cavity is frequency shifted by a double-passed acousto-optical modulator before entering the cavity. In addition, the transfer cavity can be scanned over several free spectral ranges to aide in finding a cavity length that is resonant with both lasers.

There are four separate lock circuits (see Fig. 4.2 for a schematic drawing) in all, for successful stabilization of the physics cavity. All of the locks use the Pound-Drever-Hall technique, or slight variations of this method. For the Ti:sapph laser lock and transfer cavity lock, sidebands at 12 MHz are written on the beams using a New Focus electro-optic phase modulator. For the auxiliary laser and cavity lock the sidebands derive from direct modulation of the diode laser current at 26 MHz. The reflected beams off the front mirror of the cavities (or the transmitted saturated spectroscopy signal for the Ti:sapph lock) are detected with fast photodiodes. The photocurrents are demodulated and sent to Stanford Research Systems

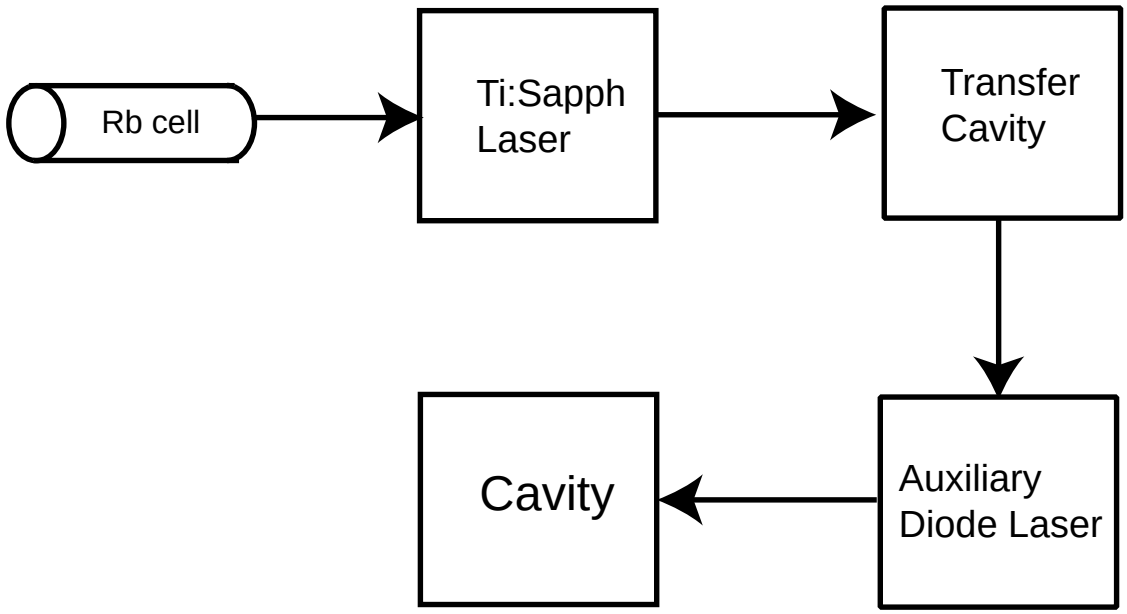

Figure 4.2: Lock schematic.

PID controllers for proportional and integral gain. Finally the output of the PIDs are feed back to control either the cavity length or the laser frequency.

The cavity is stabilized to better than 1/10 of the linewidth with a detection bandwidth of 1 MHz, fulfilling the requirements for stabilization discussed at the beginning of the chapter. Long term drifts in both cavity locks as well as the auxiliary laser lock can be externally monitored and corrected for. The entire lock system is held for several hours without tripping, an essential requirement for cavity QED experiments.

4.2 Atomic Source

4.2.1 Pushed Magneto-Optical Trap

The first generation optical cavity QED experiments in the group utilized a thermal beam of alkali atoms as a source for atoms [11, 57, 58]. Although the beams had a high atomic flux, the mean velocity of the atoms was several hundred m/s. This high velocity results in broadening that washes out or lessens quantum mechanical effects. These mechanisms include Doppler and transit broadening discussed in detail in Ref. [59].

The starting point for most investigations involving cold atoms is the magneto-optical trap (MOT). This trap is widely used in atomic physics experiments (see [60] for a review of magneto-optical trapping). Consider an atom illuminated at the intersection of three pairs counterpropragating beams. If the beams are red-detuned with respect to the atomic resonance the atom can be cooled by optical molasses. The internal structure of the atom can be used to confine these atoms when a magnetic field gradient is introduced to the region. To illustrate this consider an atom with a $J = 0$ ground state and $J = 1$ excited state. In the presence of a magnetic field the magnetic sublevels of the excited state $m = 0, \pm 1$ are split. In one dimension (see Fig. 4.3) it is easy to see that for a red-detuned laser, the atom becomes resonant with the light as the atom moves away from the origin. Applying the appropriate beam polarizations the atom can be preferentially excited by the beam pointing towards the center of the trap. This is done by applying a circular polarization, σ_+ in one direction and σ_- in the counterpropagating direction. In

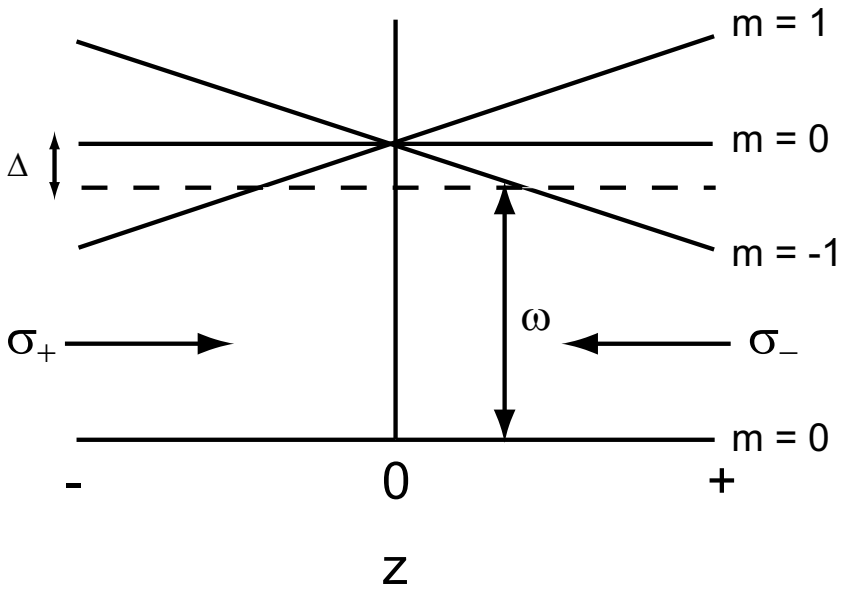

Figure 4.3: Diagram of energy levels for $J = 0 \rightarrow J = 1$ MOT transition. Δ is the MOT beam detuning. The $m = \pm 1$ sublevels of the excited state shift due to the linear magnetic field gradient.

three dimensions the magnetic field gradient is generated using a standard anti-Helmholtz coil configuration.

The experimental apparatus used for the study described in chapter 4 utilizes a three-dimensional MOT of ^{85}Rb collected from the low-velocity tail of a thermal vapor from a dispenser (SAES getters). The MOT is formed in a glass cell with dimensions 1" × 1" × 3" (Hellma). The glass cell is attached to a conflat flange which connects to the cubical chamber that houses the cavity. The MOT is formed approximately 25 cm below the cavity. An additional resonant push beam, which is pulsed on for < 1 ms after the MOT beams are turned off, delivers atoms to the cavity.

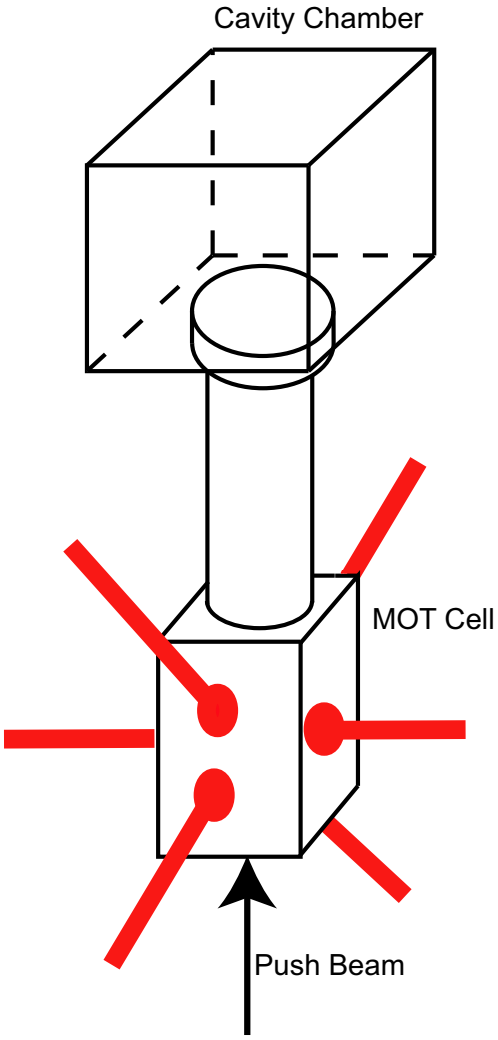

Figure 4.4: Experimental Apparatus: Pushed MOT. Three sets of counterprogating beams intersect in a glass cell where the atoms are released from a rubidium dispenser (SAES getters). The MOT is turned on for a variable time before being released and subsequently pushed from below by a near-resonant push beam towards the cavity chamber.

The pushed atom cloud traverses the cavity mode typically over a timescale of order 1 ms. This is not to be mistaken with the transit time of a single atom across the mode. The mean velocity of the cloud ranges from 5 - 15 m/s, and can be varied by changing the intensity and frequency of the push beam. For a cavity waist of 56 μm the single atom transit time is on the order of several μs.

The initial alignment is achieved by a simple technique. The push beam is aligned to two points: the MOT and the cavity. With the push beam on and passing through the MOT, the effect of the additional beam is to destroy the MOT due to the radiation pressure imbalance. The push beam is aligned to the MOT with one mirror then a second mirror closer to the glass cell is used to align the beam through the center of the cavity. This process is repeated until the beam is walked into perfect alignment between the MOT and cavity.

The cavity serves as a detector for the atoms. Recall from Eq. 2.8 that the transmission of the cavity on the lower branch drops by a factor of $(1+2C)^2$ corresponding to a dip in the transmission of 35 % for a single maximally coupled atom in our cavity. The atoms in the cloud are randomly distributed across the cavity mode. We can speak only of an effective number of atoms due to the averaging that takes place naturally due to this distribution of coupling strengths.

The major drawback to this method of atom delivery is the efficiency. The MOT must be reloaded after each push cycle, which requires at least a 50 ms MOT loading period. The number of effective atoms delivered to the cavity for a cycle of this length is typically less than 5. An extended loading time increases the number of atoms delivered at the expense of lowering the duty cycle. For most experiments

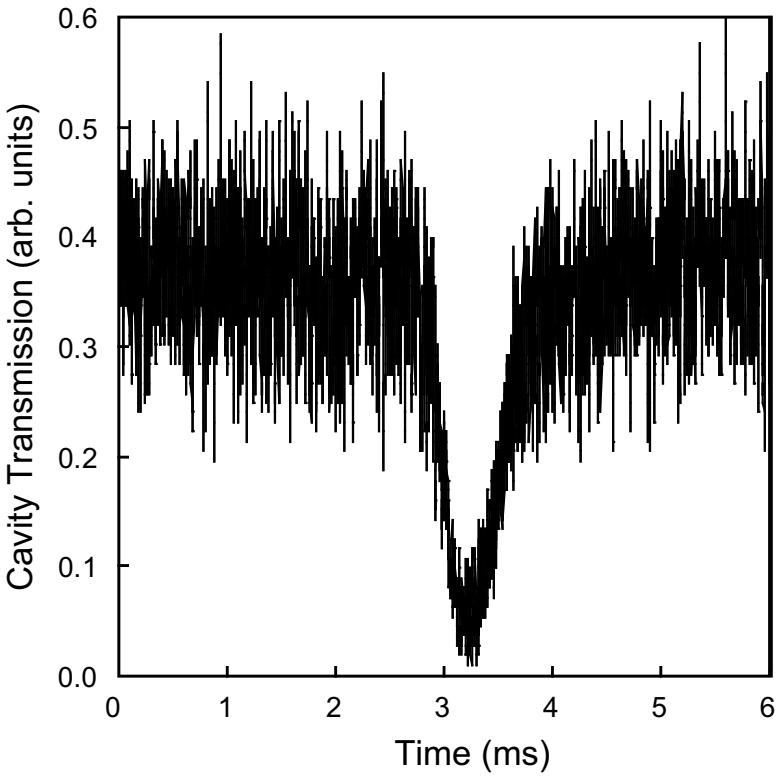

Figure 4.5: Transmission profile of a single-shot measurement of an atom cloud passing through the cavity mode. The detection bandwidth is 1 MHz. The elapsed time is referenced to the push trigger.

we require a MOT loading time of approximately 200 ms, drastically lowering the fractional time the atoms spend in the cavity mode.

4.2.2 LVIS

Next we describe a different apparatus, based on similar principles, which delivers a continuous beam of Rb to the cavity. The Low Velocity Intense Source (LVIS) is a continuous beam of atoms extracted from a modified MOT. The group of Wieman [61] first demonstrated the LVIS using a Cs MOT with a hole drilled through one of the MOT retroreflection mirrors located inside of the vacuum system. They used a gold-coated $\lambda/4$ waveplate mounted inside of the MOT vacuum chamber with a mm-sized hole for atom extraction. The hole casts a shadow on the retroreflected beam, which results in a radiation pressure imbalance in one direction. The Wieman group reported a beam flux of 5 x 10^9 atoms/s with a beam size and divergence given geometrically by the size of the hole and the distance from the mirror to the MOT.

Our implementation of an LVIS system was motivated by the success of the Wieman group and the need to realize a continuous source of atoms for photon counting experiments. The LVIS source constructed consists of an additional chamber for the trap connected above the cubical cavity chamber. A 1.5 mm diameter hole was drilled (done at the NIST Optical Shop) through the center of a 1" diameter gold mirror and $\lambda/4$ waveplate. The optics are mounted 3-4 cm above the cavity. Alignment of the extraction column and cavity was done carefully by eye with the

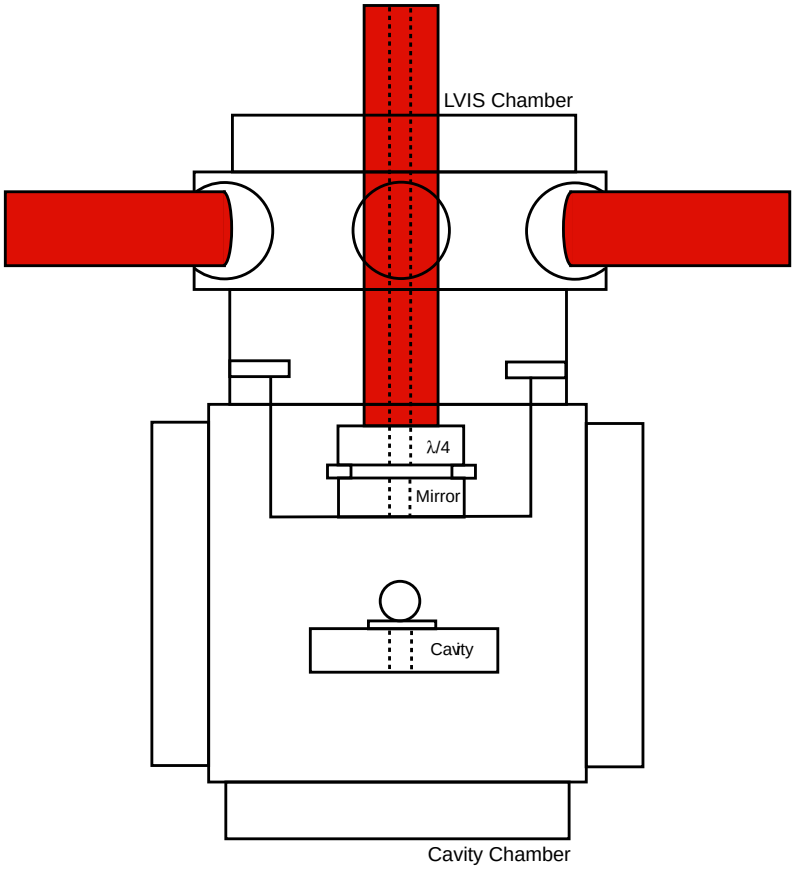

Figure 4.6: Diagram of LVIS apparatus.

aid of a thin ceramic rod fed through the hole and the center of the cavity.

An additional beam counterpropagating the atomic beam passes through the cavity to plug the hole and form a normal MOT. By turning off the plug beam, initial observations are made of atom cloud transits through the cavity. These initial observations showed an increase in the flux from the pushed MOT apparatus. The LVIS beam alignments are adjusted to minimize the transmitted light as the atom cloud passes through the cavity. After maximizing the pulsed LVIS signal, a continuous beam is observed by blocking the plug beam, switching on and off the magnetic field gradient and monitoring the steady state transmission of the cavity.

A maximal 30 percent drop in the transmission has been observed with our LVIS implementation, corresponding to ≈ 1 effective atoms in the cavity in steady state. Work by Sanders and Carmichael [62] show that, for a thermal beam at 300 m/s, 7 atoms randomly distributed in a Gaussian cavity mode corresponds to the equivalent of 1 maximally coupled atom. This number serves us as a guide for assessing the performance of the LVIS and making sure that there will be of order one atom in the cavity mode at all times. The atoms are moving and may not be optimally coupled, but with conditional measurements we are able to extract important information on the quantum properties of the field.

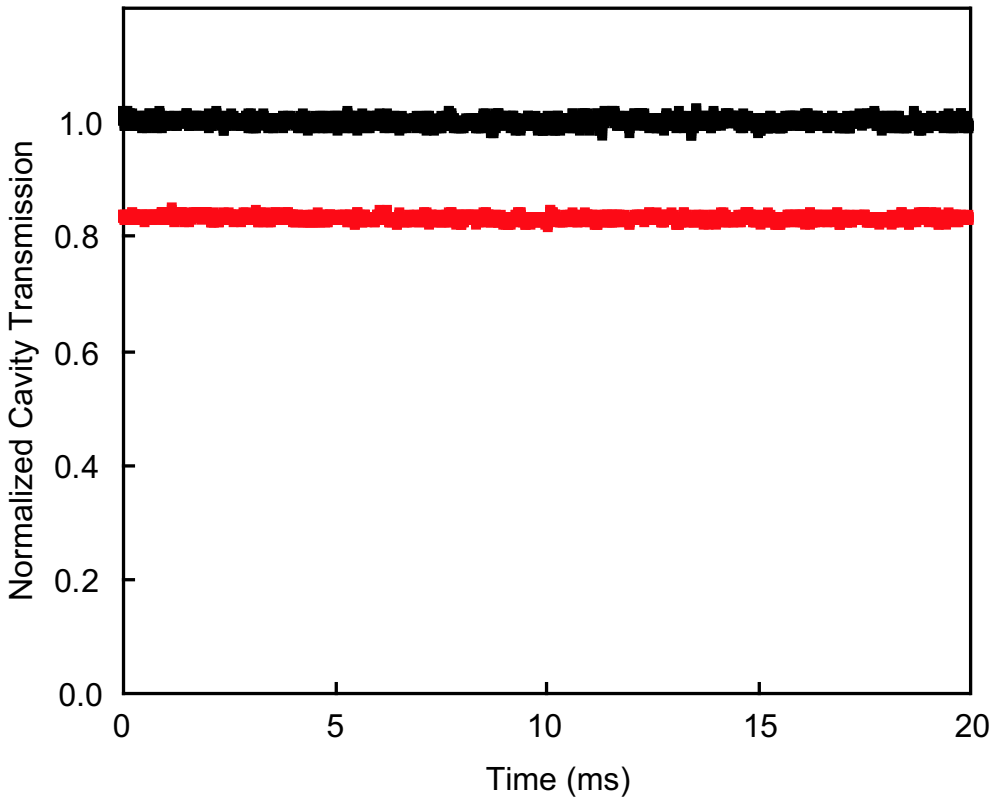

Figure 4.7: LVIS operation: Cavity transmission normalized to the transmission with no atoms present in the cavity. Black trace (LVIS off), red trace (LVIS on).

4.3 Photon Counting Apparatus

4.3.1 Detectors and Hardware

The following chapters discuss cavity QED experiments that rely on the polarization of the input and output cavity beams. Here we will describe the experimental apparatus used to detect single photons emitted from the cavity with different polarizations.

Figure 4.8 shows a schematic of the optics after the cavity and the detectors. The output light beam of the cavity is collimated with a 25 cm lens and passed through a $\lambda/2$ waveplate. The polarization is rotated to the desired angle and the light is passed through a Glan Taylor calcite polarizing beamsplitter. The vertical polarization component is reflected and sent through a long lens tube attached to an aluminium box that is coated on the inside with black paper and has a lid that prevents light from entering. The lens tube houses a telescope with an aperture at the focus to prevent stray light from entering the detector region. At the entrance of the box is an Andover 780 nm spectral bandpass filter that transmits 85 percent of the incident power at this wavelength.

The horizontal polarization beam consists of not only the 780 nm cavity drive, but also the transmission of the 820 nm auxiliary cavity locking laser. The two wavelengths transmit through the beamsplitter and are incident on a diffraction grating (Jobin Yvon) that serves to separate the 780 nm cavity transmission from the 820 nm lock beam. The 1st order diffracted beams are spatially separated by several cm after propagating 25 cm. The 780 nm diffracted beam contains 75 percent

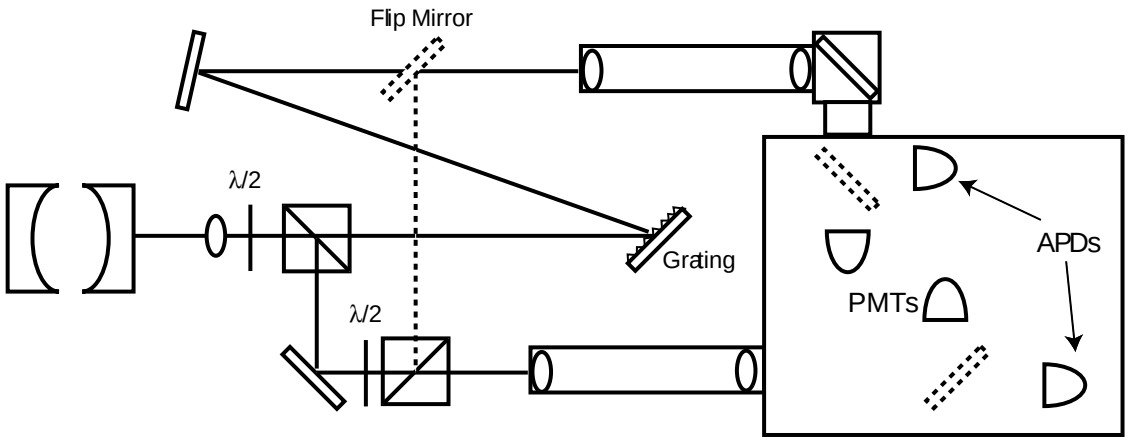

Figure 4.8: Diagram of photon counting apparatus.

of the incident power. It is directed through a second lens tube assembly and into the box.

This box (Fig. 4.8) contains pairs of Hamamatsu photomultiplier tubes (PMTs) and Perkin Elmer avalanche photodiodes (APDs) for photodetection. All have additional spectral filters for 780 nm. The PMTs are primarily used for aligning the cavity, setting up the transfer cavity lock, and for experiments that do not require single photon counting (see chapter 5). The photocurrents from the PMTs are amplified and sent to a digital oscilloscope. Flip mirrors redirect the cavity output to the APDs for photon counting experiments. An additional waveplate and beamsplitter have been included on the vertical polarization arm. This allows some of the vertical beam to be split off and redirected to the second entrance to the box for autocorrelation measurements.

The APDs generate a TTL pulse for each photon detected (35 percent quantum efficiency), which are sent to a Lecroy 3377 time to digital converter (TDC). The

TDC measures the time delay between the arrival of a start pulse and up to 16 subsequent stop pulses with a 0.5 ns time resolution. This data is transferred to a Lecroy 4302 memory module which records up to 16,000 hits. The memory is transferred over a GPIB cable to a computer where a LabWindows/CVI program is used to collect, histogram, and plot the data. Copies of both APD signals are sent to a Stanford Research Systems SR400 photon counter to monitor the stability of the cavity lock and the density of the atomic beam. The arrival of a second start pulse shortly after the arrival of the first restarts the TDC, which has the effect of weighting conditional photon arrivals toward the shorter delay times. The start pulses are stretched with a Lecroy Dual Gate Generator (222) to 1.3 μs to avoid receiving a second start until after the time window we are interested in has elapsed. Most of the conditional dynamics of the system are sufficiently damped after 1 μs. The stop pulses are transmitted through a 350 ft cable before entering the TDC. This allows us to view two-time correlations for negative delay times (stops that arrive before a start).

4.3.2 Correlation Measurements

The measurement of correlation functions discussed in Sec. 2.2.2 requires the binning of photon time arrivals conditioned on a fluctuation in the field. In a weakly driven cavity QED system the detection of a photon is itself a large fluctuation, as the mean intracavity photon number is typically well below one.

A drawback to the setup is a hardware limitation that only allows for an

acquisition window of 2μs. While the conditional dynamics of the system occur on timescales limited by $1/2\kappa$ and $1/\gamma$, a longer window is needed to observe dynamical effects related to individual atom transits through the cavity mode.

For low intensities we have found a simple method of measuring correlations on these longer timescales. Eq. 2.29 states that $g^{(2)}(\tau)$ can be written as an ensemble average of a conditioned state. This method takes this definition to heart by averaging a photocurrent of the detected mode conditioned on a single photon detection. A Lecroy digital storage oscilloscope (Wavepro 7000) triggers on a fluctuation of the photocurrent, while averaging a second photocurrent in real time. A feature of this oscilloscope is a triggering mode, which enable multiple triggers to occur sequentially without refreshing the screen. This drastically reduces dead time between triggers, and can collect up to 1,000 triggers in a sequence.

To compare this new method with the traditional histogram we probe the photon statistics of light emitted from the cavity. A laser operated far above threshold obeys Poissonian statistics, $g^{(2)}(\tau) = 1$ for all τ. However, a classical chaotic source should exhibit bunching, $g^{(2)}(0) > g^{(2)}(\tau)$ [63]. To simulate a chaotic source, a white noise signal with 10 MHz of bandwidth generated from a Stanford Research Systems function generator was written onto the amplitude of the cavity beam through an acousto-optical modulator [64]. The cavity acts as a low pass filter for amplitude fluctuations with a bandwidth given by 2κ. The output of the locked cavity was evenly split on the polarizing beamsplitter by rotating the $\lambda/2$. Figure 4.9 shows bunching in the light as detected by both methods of detection.

Although the two methods show qualitatively similar results there are sig-

nificant differences that must be highlighted. The correlation function $g^{(2)}(\tau)$ is normalized by the average number of photons in the field. For the photocurrent averaging method it is not clear how this normalization should be performed. The oscilloscope not only averages the photocurrents, but also any electronic noise in the signal, adding an offset in the height of the averaged photocurrent that must be accounted when normalizing the signal.

The resolution of the averaging method is limited by the width of the electronic signal generated by a photodetection. The PMT signals detected without amplification through 50 Ω coupling generate pulses with a 5 - 10 ns width while the APDs generate TTL pulses 30 ns long.

When PMTs are used, the averaging method strictly depends on the threshold chosen for the trigger. Setting the threshold too high favors large fluctuations. Despite these apparent disadvantages we have found the averaging method to be a helpful diagnostic tool.

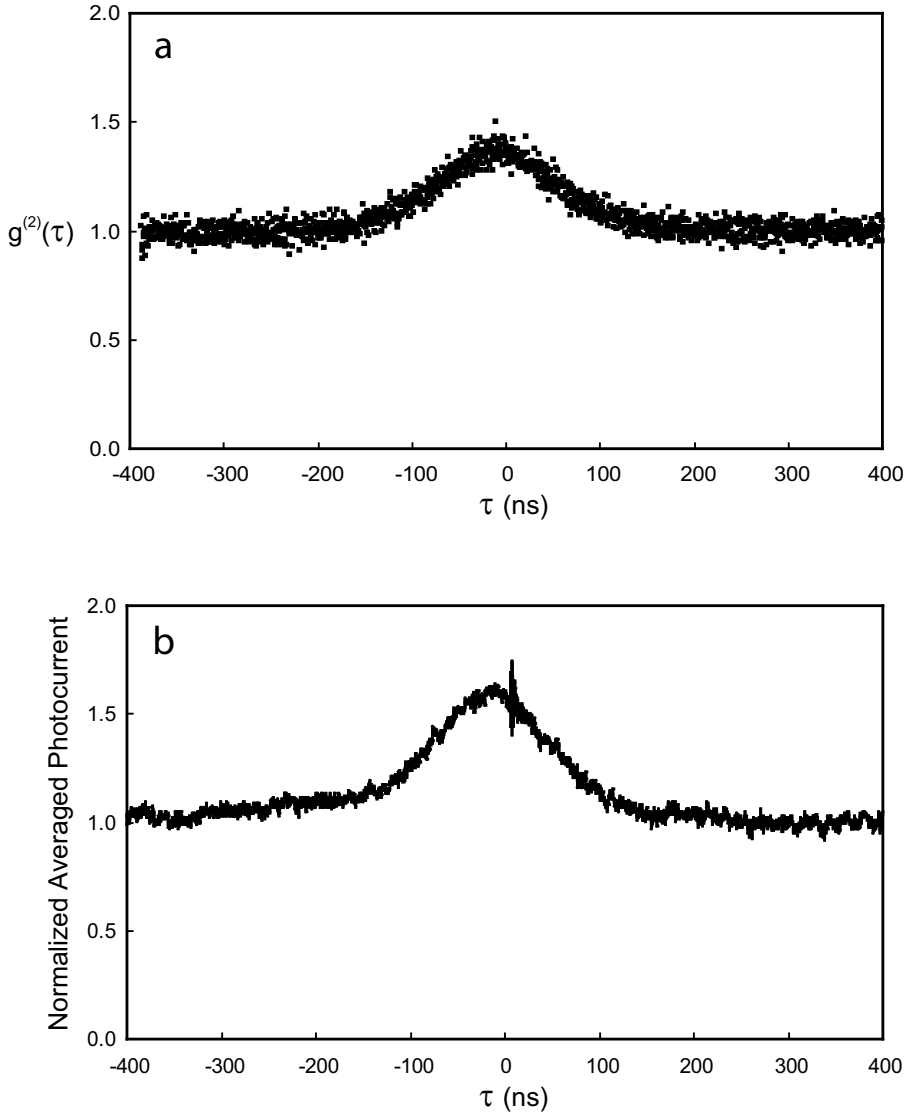

Figure 4.9: A comparision of two methods of measuring correlations simultaneously. a) The traditional method of histogramming the arrival time of a photon conditioned on a photodetection in a second detector. b) A new method of averaging the photocurrent of one detector conditioned on the detection of a fluctuation (photon) on a second. The slight offset of the peak from $\tau = 0$ is due to a trigger offset in the data acquisition. The sharp feature here is due to an electrical reflection in our detector apparatus. The normalization is done with respect to the signal for long τ.

Chapter 5

Spontaneous Emission in the Mode of a Cavity QED System

Spontaneous emission in cavity QED has been regarded as a dissipative process from which information is lost at a rate, γ, to modes other than the preferred cavity mode. Most work in cavity QED spontaneous emission has focused on the enhancement or suppression of the decay rate γ. In the bad cavity limit ($\kappa >> \gamma, g$) the resonant spontaneous emission changes from its free space value as $\gamma \rightarrow \gamma(1 + 2C_1)$ [28]. The enhancement factor ($2C_1$) is related to the ratio of the atomic cross section to the cavity mode cross section multiplied by the average number of reflections inside the cavity. This effect broadens the spectrum, but causes no splitting [65]. There are many experimental demonstrations of enhanced and suppressed spontaneous emission in this regime (see for example the article by Hinds in Ref. [4]). If the reflectivity of the mirrors is high enough and the coupling between the atom and the cavity can become comparable to the two decays ($g \approx \kappa, \gamma$), spontaneous emission into the cavity is reversible.

It is difficult to experimentally study the spontaneous emission in cavity QED. Work in the past has focussed on geometries that allow observation of the atoms from the side [66]. Another approach looks at the fluorescence into the mode of the cavity with the atoms driven by a laser that propagates perpendicular to the cavity axis [10, 67].

Spontaneous emission plays a dual role; it is a decohererence source, but it is also a way to extract information out of the system. An interrogation of the system through spontaneous emission is an unambiguous probe of the state of the atomic part of the atom-cavity system. We follow Birnbaum *et al.* [68] to directly access a small part of the atomic inversion, using the internal structure of the atoms to inform us when a transmitted photon originates in a fluorescence event. Instead of utilizing ^{85}Rb atoms in their stretched states ($m_F = F$ with $\Delta m = 1$) to form a closed two-level system when driven with circularly polarized light, we drive the optical transition with π polarization ($\Delta m = 0$). See Fig. 5.1 a. We can then look at the light emitted out of the cavity separating it into the two linear polarizations, one parallel to the drive and the other orthogonal to the drive. The presence of any light of orthogonal polarization indicates that it has come originally from a spontaneous emission event of an atom that decays with $\Delta m \pm 1$.

Figure 5.1 shows the full atomic structure involved in the experiment (a) and the reduced atomic structure (b) that we utilize to model the system. The Zeeman sublevels are practically degenerate in the experiment as the magnetic field applied is of the order of 1 Gauss, causing the stretched states to be at most 1.4 MHz detuned (less than the HWHM of the atomic transition).

Starting with the atoms in $m = 0$, the process of absorption and emission will effectively create some optical pumping out to the stretched states. This process, however, takes many spontaneous emissions to complete, and we are operating in the low intensity limit where the probability of absorption is very small. We are justified in reducing the full atomic structure to a four-level model. An additional

experimental reason that justifies this simplification is the fresh input flow of atoms that replaces atoms that have been in the cavity for about 10 μs.

The model captures an important feature of cavity QED, the possibility of reabsorption. Although small, it is parameterized by the two coupling constants, g and G, and allows for two different spontaneous emission rates, γ and Γ. G is the atom-cavity coupling constant for the atomic transitions that connect the Zeeman sublevels with $\Delta m = \pm 1$. The relative weight of g and G, and the respective dipole matrix elements are given by the appropriate Clebsh-Gordan coefficients.

5.1 Theory

We need to go beyond the theory of the two-level atom inside a cavity from chapter 2 to describe this multilevel system. Here we present the details of a four-level model of an atom in a driven cavity. The results are directly applicable to our experiments described in the following section.

5.1.1 Two-Mode Cavity QED System

Our cavity QED system consists of a high finesse optical resonator where one or a few atoms interact with two degenerate polarization modes of the cavity. The two modes of the cavity have single atom coupling constants, g and G. The model reduces to the case of a two-level atom in the limit $G \to 0$, and no population in state $|3\rangle$. Although the decay rates and coupling rates can be the same, there may be slight differences arising from the specific Clebsch Gordan coefficients. The system

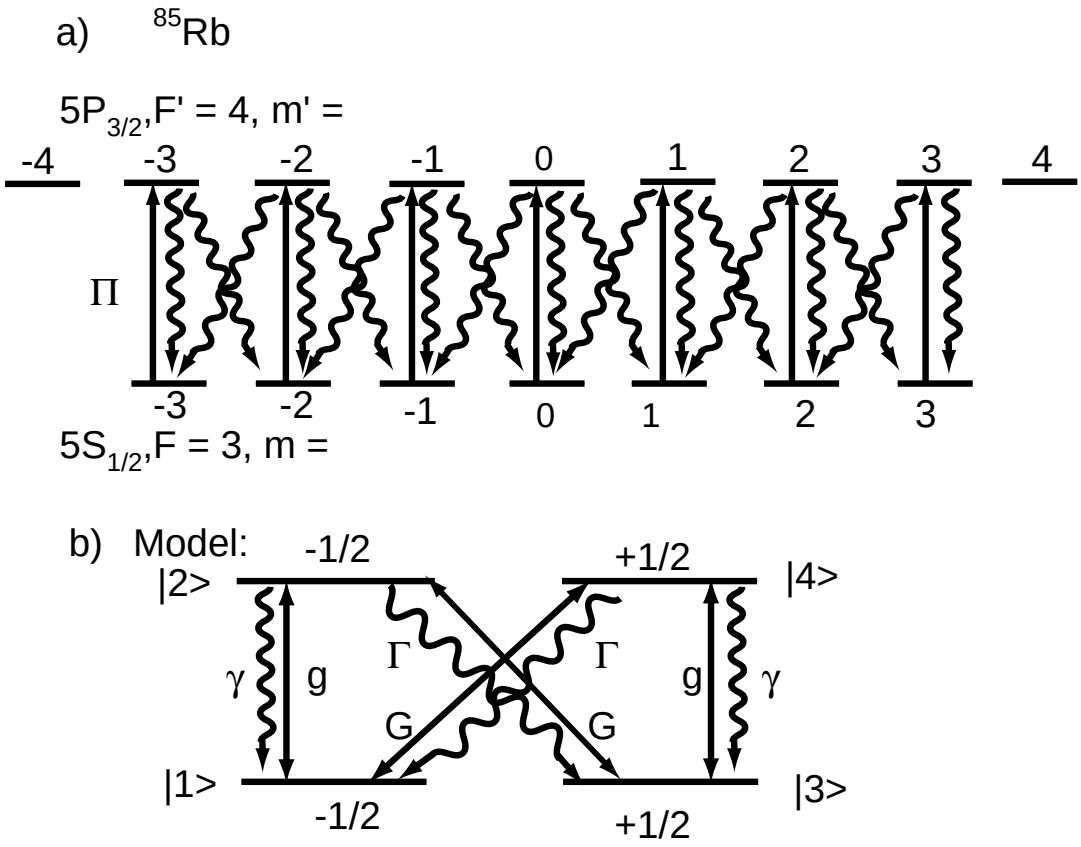

Figure 5.1: a) Energy levels of ^{85}Rb used in the experiment with light in a π transition. b) Simplified diagram used in the model.

is driven on-axis by a classical field that is horizontally polarized, ε/κ, normalized to photon flux units.

The Hamiltonian that governs the time evolution of the system is:

$$\begin{aligned} H &= i\hbar\varepsilon(a-a^\dagger)+i\hbar g(a\sigma_+^1-a^\dagger\sigma_-^1)+i\hbar g(a\sigma_+^2-a^\dagger\sigma_-^2) \\ &\quad +i\hbar G\left[(a+ib)\Sigma_+^R-(a^\dagger-ib^\dagger)\Sigma_-^R\right] \\ &\quad +i\hbar G\left[(a-ib)\Sigma_+^L-(a^\dagger+ib^\dagger)\Sigma_-^L\right] \\ &\quad -i\hbar\kappa(a^\dagger a+b^\dagger b) \\ &\quad -i\hbar\gamma(\sigma_+^1\sigma_-^1+\sigma_+^2\sigma_-^2) \\ &\quad -i\hbar\Gamma(\Sigma_+^R\Sigma_-^R+\Sigma_+^L\Sigma_-^L) \end{aligned} \tag{5.1}$$

where a is the annihilation operator for the driven horizontally polarized cavity mode, b is the annihilation operator for the vertically polarized cavity mode, and the atomic operators are:

$$\sigma_+^1=|2\rangle\langle 1|, \quad \sigma_+^2=|4\rangle\langle 3|, \quad \Sigma_+^R=|4\rangle\langle 1|, \quad \Sigma_+^L=|2\rangle\langle 3| \tag{5.2}$$

The system can be accurately modelled, for weak excitation, as having either zero or one excitations in the coupled modes of the field and the atoms. We follow the quantum trajectory formalism [27] to find the state of the system to first order in the excitation $O(\varepsilon^2)$. In a similar way used in chapter 2, if we assume fixed atomic positions the equilibrium state is the pure state [69]:

$$|\psi_(t)\rangle = c_{001}|0,0,1\rangle+c_{003}|0,0,3\rangle+c_{002}(t)|0,0,2\rangle+$$

$$c_{004}(t)|0,0,4\rangle + c_{101}(t)|1,0,1\rangle + c_{011}(t)|0,1,1\rangle +$$

$$c_{103}(t)|1,0,3\rangle + c_{013}(t)|0,1,3\rangle + O(\varepsilon^4). \tag{5.3}$$

The ket has three numbers, the first two represent the number of excitations in cavity mode with horizontal and vertical polarizations respectively, and the third represents the state of the atom. With these assignments, the first two kets of Eq. 5.3 are the vacuum and they do not have any time evolution. The other coefficients can evolve in time, and the following set of rate equations governs their evolution:

$$\dot{c}_{001} = 0 \tag{5.4}$$

$$\dot{c}_{003} = 0 \tag{5.5}$$

$$\dot{c}_{002} = gc_{101} - \frac{\gamma+\Gamma}{2}c_{002} - iGc_{013} + Gc_{103} \tag{5.6}$$

$$\dot{c}_{004} = iGc_{011} + Gc_{101} + gc_{103} - \frac{\gamma+\Gamma}{2}c_{004} \tag{5.7}$$

$$\dot{c}_{101} = -\varepsilon c_{001} - \kappa c_{101} - gc_{002} - Gc_{004} \tag{5.8}$$

$$\dot{c}_{011} = -\kappa c_{011} + iGc_{004} \tag{5.9}$$

$$\dot{c}_{103} = -Gc_{002} - \varepsilon c_{003} - \kappa c_{103} - gc_{004} \tag{5.10}$$

$$\dot{c}_{013} = -iGc_{002} - \kappa c_{013} \tag{5.11}$$

These equations when solved in the steady state (setting the derivatives to zero) give the following solutions,

$$\begin{aligned}(c_{002})_{ss} = &\left[\frac{\varepsilon(G-g)}{2B_-} - \frac{\varepsilon(G+g)}{2B_+}\right]c_{001} + \\ &\left[\frac{\varepsilon(g-G)}{2B_-} - \frac{\varepsilon(g+G)}{2B_+}\right]c_{003}\end{aligned} \tag{5.12}$$

$$
\begin{aligned}
(c_{004})_{ss} &= \left[\frac{\varepsilon(g-G)}{2B_-} - \frac{\varepsilon(G+g)}{2B_+}\right] c_{001} + \\
&\quad \left[\frac{\varepsilon(G-g)}{2B_-} - \frac{\varepsilon(g+G)}{2B_+}\right] c_{003} && (5.13)\\
(c_{101})_{ss} &= -\left[\frac{\varepsilon A}{2B_+} + \frac{\varepsilon A}{2B_-}\right] c_{001} + \left[\frac{\varepsilon A}{2B_-} - \frac{\varepsilon A}{2B_+}\right] c_{003} && (5.14)\\
(c_{011})_{ss} &= i\frac{G}{\kappa}(c_{004})_{ss} && (5.15)\\
(c_{103})_{ss} &= \left[\frac{\varepsilon A}{2B_-} - \frac{\varepsilon A}{2B_+}\right] c_{001} - \left[\frac{\varepsilon A}{2B_-} + \frac{\varepsilon A}{2B_+}\right] c_{003} && (5.16)\\
(c_{013})_{ss} &= -i\frac{G}{\kappa}(c_{002})_{ss} && (5.17)
\end{aligned}
$$

The most important result for our discussion comes from Eq. 5.15 and Eq. 5.17, which states that the output on the vertical mode of the cavity comes from excitations that originate in the atomic excited states $|2\rangle$ and $|4\rangle$, a spontaneous emission event. Here A and B are defined by:

$$
\begin{aligned}
A &= \frac{G^2}{\kappa} + \frac{\gamma+\Gamma}{2} && (5.18)\\
B &= \kappa A + (G \pm g)^2 && (5.19)
\end{aligned}
$$

This formulation, to lowest order in the excitation, implies the following decorrelation: $\langle a\sigma^+\rangle = \langle a\rangle\langle\sigma^+\rangle + O(\varepsilon^4)$. This is equivalent to the decorrelation of the expectation value of the product of the field and atomic polarization, that recover the Maxwell-Bloch equations [23].

If we assume the atom initially resides in the excited state we can use the steady state results to solve for the average photon number in the driven and undriven modes:

$$
\langle a^\dagger a\rangle = 2\left(\frac{\varepsilon A}{2B_+}\right)^2 + 2\left(\frac{\varepsilon A}{2B_-}\right)^2 \qquad (5.20)
$$

$$\langle b^\dagger b\rangle \;=\; \frac{2G^2}{\kappa^2}(C_-^2 + C_+^2) \tag{5.21}$$

Note that in the limit of G$\rightarrow$ 0 and $\Gamma \rightarrow 0$, the solution for $\langle a^\dagger a\rangle$ reduces to the result for a two-level atom, Eq. 2.20. Figure 5.2 explores the parameter space of this single-atom model to gain physical insight of the system. We plot the dependence of the transmitted intensities of the two modes of the coupling constants, g and G, for a fixed small driving field, ε/κ, in the resonantly driven system.

Experimentally changing the value of g dynamically can be done by moving the atom across the cavity mode and using the spatial structure of the mode to alter the effective coupling of the atom to the mode [3]. This type of control is difficult to achieve and most of the efforts have been to maximize the coupling for quantum information implementations [70]. In our experiments, we use the cooperative nature of the cavity QED system to enhance the coupling of the cavity to a collective atomic polarization. For a collection of two-level atoms the coupling is enhanced by $\sqrt{N}$. To the experimentalist varying N is the equivalent to changing g.

To utilize the single atom model to explain our observations with multiple atoms, we have to add the following assumption: to first order the coupling constants, g and G, are scaled by the square root of the atomic numbers, N and N' (the number of atoms coupled to the undriven mode), as the σ and Σ operators scale as collective operators j and J. This is an oversimplification as the coupling constants depend on the position of the atoms, but it qualitatively shows some of the important features.

The plots in Fig. 5.2 reflect two ways of simulating the resonant response of the

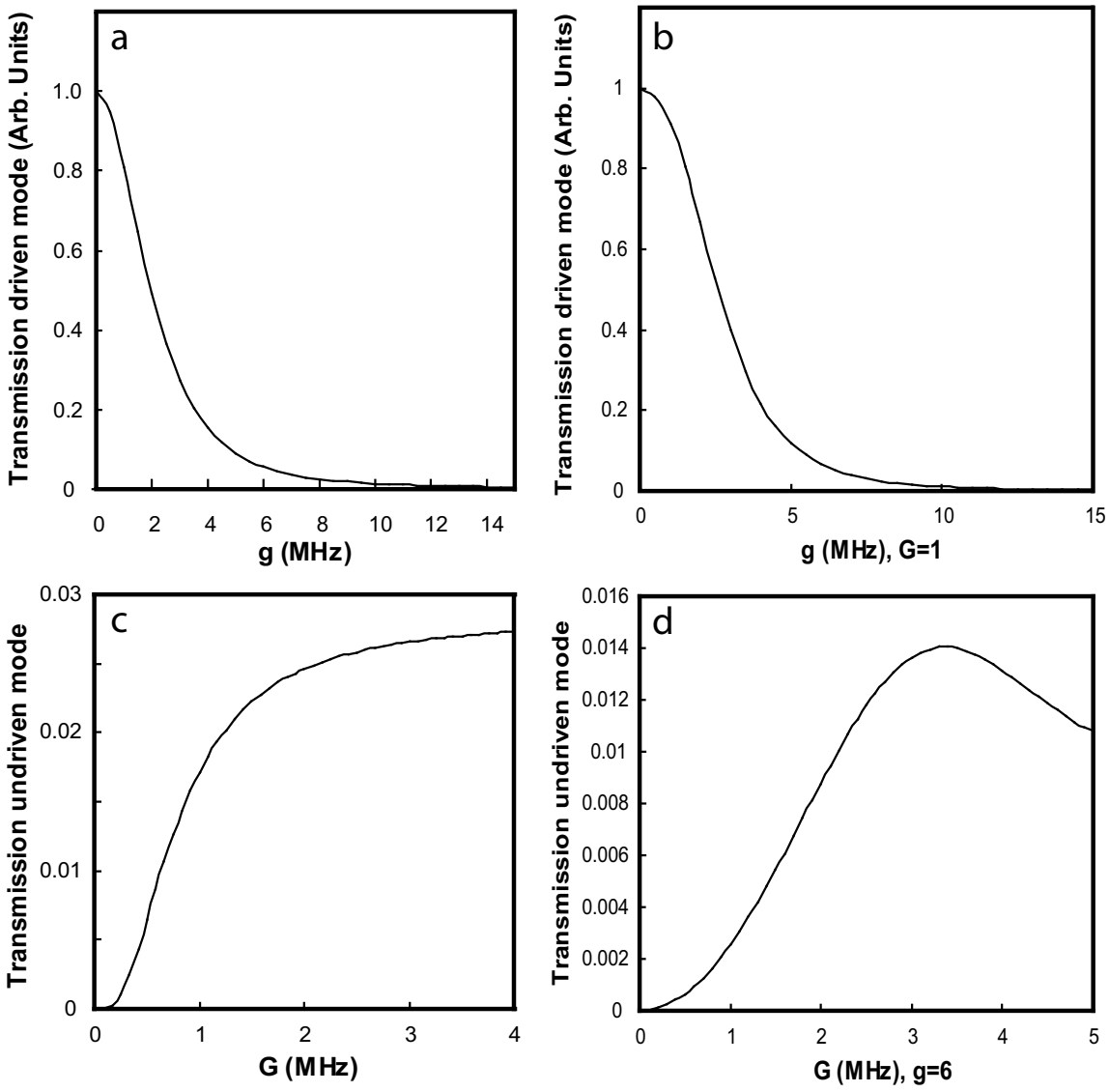

Figure 5.2: Theoretical prediction of the transmission of the driven and undriven modes, with $\kappa/2\pi = 3.2$ MHz and $\gamma/2\pi = 3$ MHz, as a function of g and G. (a) Resonant transmission of the driven mode for g/G fixed to 6. (b) Resonant transmission of the driven mode for $G = 1$. (c) Resonant transmission of the undriven mode for g/G fixed to 6. (d) Resonant transmission of the undriven mode for $g = 6$.

system to strong and weak coupling or equivalently high and low atom number. As we would expect with no atoms, the average photon number of the undriven mode should be zero. The system reduces to two levels, with no way for an atom to decay to $|3\rangle$. Increasing the coupling between these levels makes it possible for population to accumulate in $|3\rangle$ and subsequently, by absorption, into $|4\rangle$. Intuition suggests that an increase of the coupling g should result in a larger G. It is convenient in this case to think of the higher coupling arising from an increase in the intracavity atoms. With more atoms, G should also increase by some factor, $\sqrt{N'}$.

Plots 5.2 (a) and (b) show the transmission of the driven mode for two cuts in the parameter space defined by g, G, γ, and Γ. The first keeps the ratio of g/G constant and equal to 6 while varying g, the second varies g keeping $G = 1$. We use the same convention for the relation between γ and Γ for all the plots shown. Though there is little noticeable difference between the two plots, the predicted transmission for the undriven mode, plots 5.2 (c) and (d) shows qualitatively different behavior. Both plots start at zero transmission for $G = 0$. As G is increased beyond a threshold value in plot (d), the transmission reaches a maximum and begins to decrease monotonically with G. In plot (c) the transmission continues to grow as G is increased. Although the behavior is different, the amount of fluorescence remains within a factor of two of each other.

Off-resonant excitations are important in cavity QED for a complete understanding of the eigenvalue structure of the system. The probe spectrum can give insights into the dynamics of the system, the most obvious example is the vacuum Rabi splitting. The breaking of the degeneracy of the excited states reveals the ef-

fect of the coupling between the two components; cavity and atom. Comprehension of the spectrum is useful for understanding how the system is evolving, which is especially important for a less intuitive system such as ours.

Using the transformations, Eq. 2.7, to introduce off resonance excitation (detunings), we proceed to plot the steady state photon number for both the driven and undriven modes. The response to an off-resonance probe with frequency $\Omega = \kappa\Theta = \gamma\Delta/2$ makes $A \rightarrow A(\Omega),\ B_{\pm} \rightarrow\ B_{\pm}(\Omega),\ C_{\pm} \rightarrow\ C_{\pm}(\Omega)$ keeping the prefactor of $\langle b^{\dagger}b\rangle$, G^2/κ^2 unchanged. The model then predicts probe spectra for the driven mode, see Fig. 5.3, and for the undriven mode, see Fig. 5.4. Figure 5.3 was plotted with a constant $G = 0.07$ MHz. This plot is nearly identical to the same plot with a constant g/G ratio (not shown). Figure 5.4 shows both cases.

The spectrum of the driven mode is qualitatively similar to that of the two-level atom, provided the ratio of g/G is sufficiently large. We chose a ratio of 100 as an estimate of the relative coupling strengths of the two orthogonal modes. The driven mode shows the usual Rabi splitting that agrees closely with the coupling rate g. The decay of energy from this mode is due to enhancement of the spontaneous emission with increased coupling as shown in Eq. 2.20. This loss consequentially results in an increase in the energy of the undriven mode. The undriven mode also shows a doublet for increased coupling, similar to the vacuum Rabi peaks, but with slightly different frequencies. The specific shape of this spectrum is greatly influenced by the value of g/G. If the ratio is close to unity, additional peaks appear; related to the more complicated atomic system. We have restricted our theoretical exploration of the two-mode cavity to ratios between 5 - 100 for g/G as an estimate of the relative

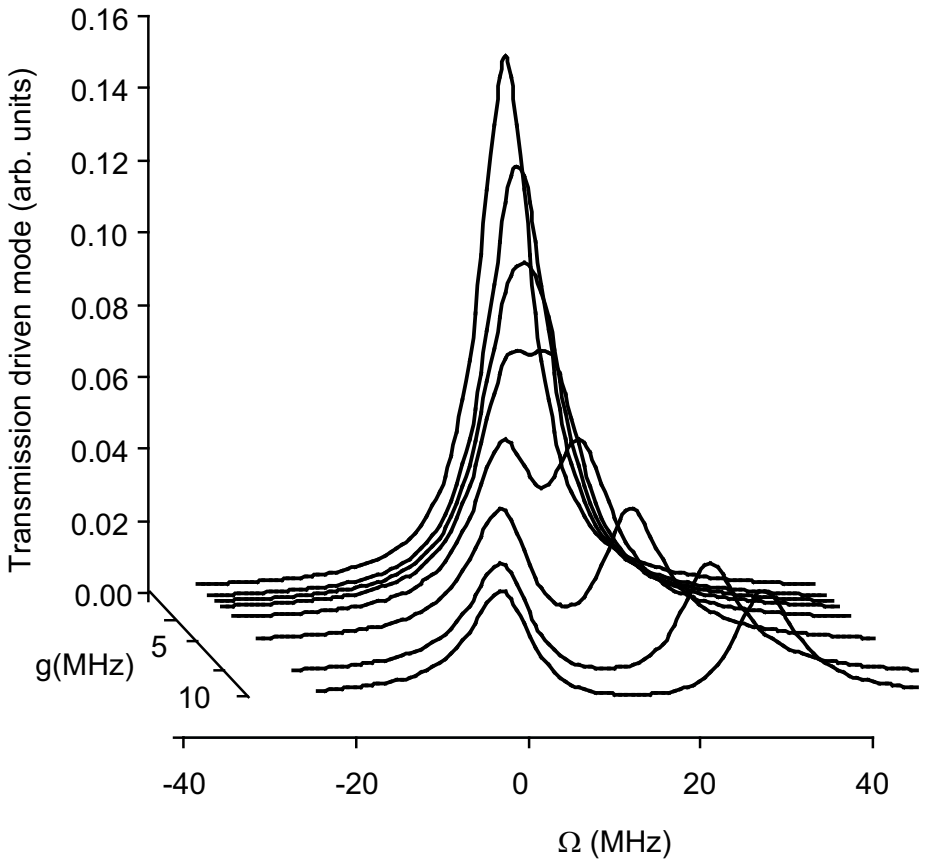

Figure 5.3: Spectrum of the driven mode for $\kappa = 2.6$ MHz, $\gamma/2 = 3$ MHz, and G = 0.07 MHz.

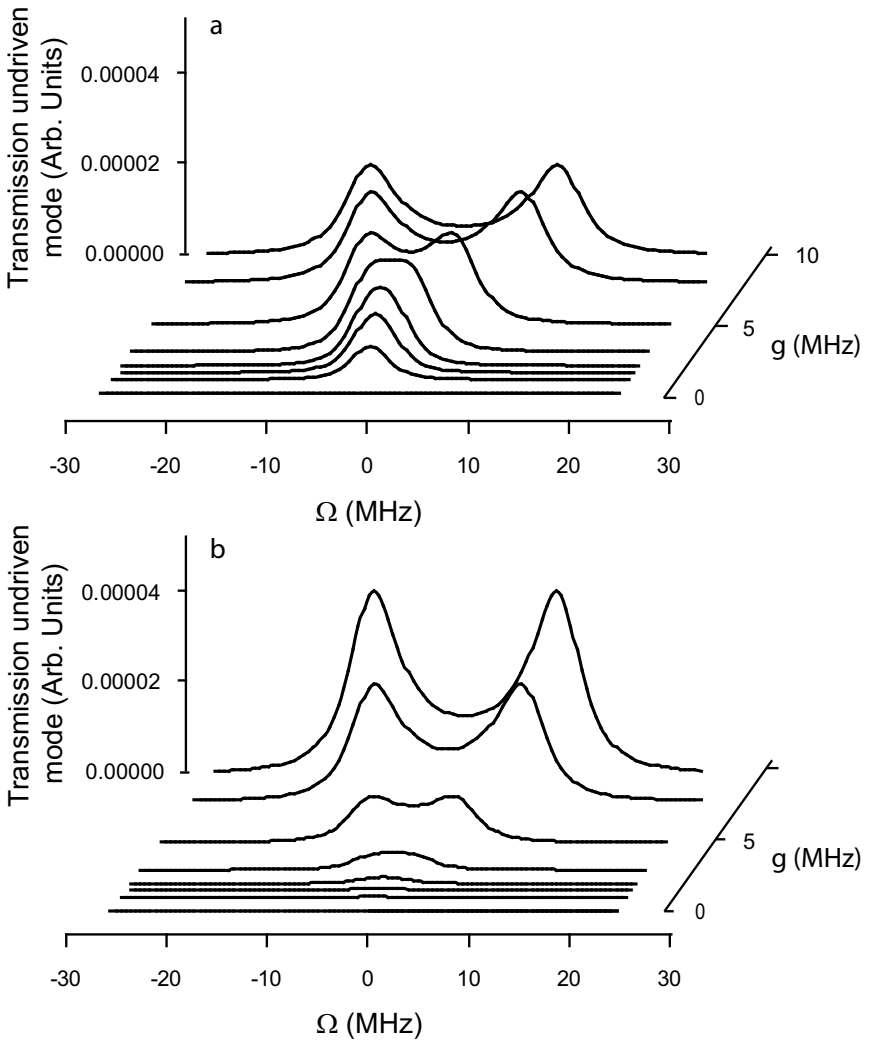

Figure 5.4: Spectrum of the undriven mode for $\kappa = 2.6$ MHz and $\gamma/2 = 3$ MHz. (a) G = 0.07 MHz. (b) $g/G = 100$.

coupling strengths, and κ and γ determined by our experimental values.

5.2 Experimental Results

The atomic source used for this exploration of spontaneous emission in cavity QED is the pushed magneto-optical trap described in section 4.2.1. A general schematic of the apparatus is illustrated in Fig. 5.5. To excite the $\Delta m = 0$ transitions in the cavity, the cavity drive is linearly polarized to better than one part in 10^5 with a high quality Glan Thompson polarizer. As described above, the resulting spontaneous decay can have a polarization component orthogonal to the drive polarization. These components are separated on the cavity output with a Glan Laser polarizing beamsplitter with an extinction ratio of 100,000:1. The two beams are detected with PMTs as described in detail in chapter 4.

The geometry that we use allows only π transitions ($\Delta m = 0$) and no Faraday rotation of the light since an external uniform magnetic field is aligned with the polarization direction of the incoming light. The observed light at the orthogonal polarization must come from spontaneous emission. This light is emitted into the cavity mode so its detection is straightforward. Residual birefringence of the cavity is less than 1×10^4 and we excite the cavity on the axis that minimizes the birefringence (about 8 degrees from the horizontal). The two modes are degenerate to better than 1 MHz.

With the magnetic field in the direction of the polarization, it is possible to optically pump the atoms into the $m = 0$ ground state. This is done with

an additional beam parallel to the cavity axis, in between the atomic source and the cavity. The beam is retroreflected to minimize a radiation pressure mismatch, which would divert the moving atomic sample away from the cavity. The light is tuned to the $5S_{1/2}\ F = 3\ \rightarrow 5P_{3/2}\ F' = 3$ transition. This has a forbidden $m = 0 \rightarrow m' = 0$ transition which allows population to accumulate in the $m = 0$ ground state. Attempts to optically pump the sample cause no discernable effect in the transmission signal of either polarization. The magnetic field was applied with a Helmoltz coil configuration at the cavity region. Later this was replaced with the residual field from LVIS quadrapole field, again with no discernable difference in the signals.

As each launch of atoms (every 150 ms) traverses the cavity, we record the transmission in a digital storage scope for a particular value of the detunings between the probe and the cavity and atomic resonances. For the experiments described below the resonant frequencies of the cavity and atom, $\omega_c = \omega_a$, agree to within 2 MHz. We extract from the raw data plots of the transmission spectrum for a given N, where N is varied naturally as the atomic cloud passes through the cavity. The timing of the loading and push sequence is controlled by a National Instruments DAQ card with eight programmable voltages outputs which control various acousto-optical modulators and other equipment. The digital storage scope is triggered by the DAQ card to synchronize the data acquisition with the arrival of the atomic cloud.

The transit of the atoms through the mode of the cavity is similar to a time of flight measurement of the temperature of the atoms [60]. If the temperature is

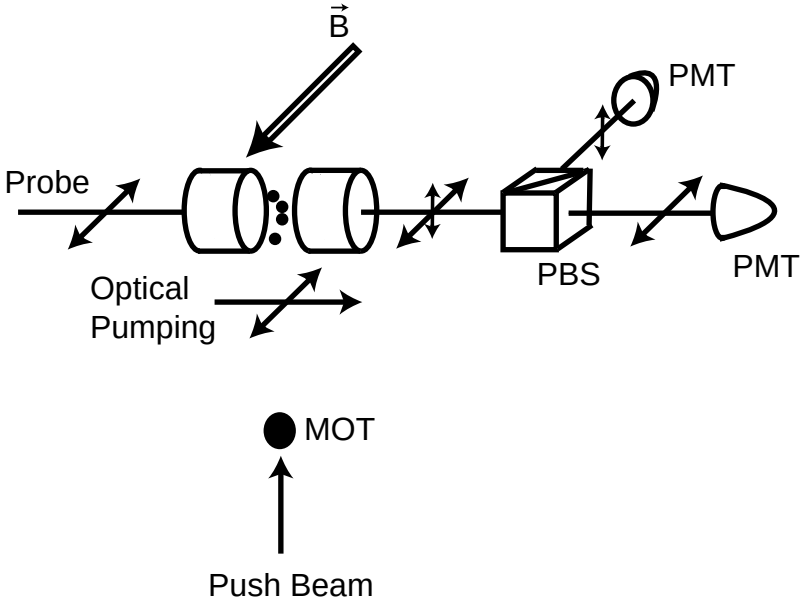

Figure 5.5: Schematic of the experimental apparatus. A polarizer at the output separates the two orthogonal linear polarizations, one parallel to the driving field, the other perpendicular and coming from the decay through $\Delta m = \pm 1$ spontaneous emission.

very cold, there is very little dispersion in the initial velocities and the time it takes for the atoms to traverse the mode is dominated by the distance from the source to the cavity and the initial velocity. The distance between the MOT cloud and the cavity mode is 8 cm. Attempts to see atoms passing by the cavity mode without pushing, letting them fall due to gravity, were unsuccessful as the expansion from the initial temperature (we do not apply optical molasses) is too large. Pushing the atoms with a resonant beam gives them an initial velocity dependent on the intensity of the beam, that can vary from 10 to 20 m/s, but also heats the cloud. This initial velocity is sufficiently high to deliver the atom cloud to the cavity before the expansion of the cloud has time to lower the atomic density to undetectable levels. The range of velocities comes from the different arrival times of the atoms as they arrive at the cavity.

We use our model for the transmission of a two-level atom in a single mode (see chapter 2) to give the cavity transmission as a function of the number of atoms N, $X/Y = (1 + 2C_1N)^{-2}$. Figure 5.7 shows the transmission dip as the atom cloud arrives at the cavity. The solid line represents our model for the temperature of the moving atomic sample. The long tail in the dip represent the coldest atoms in the cloud, which are most likely to feel the effects of the standing wave in the cavity, not accounted for in this our model.

We extract the 1-D temperature of the cloud assuming a Gaussian distribution of velocities at the MOT, with an initial center of mass velocity in the range allowed by the transit measurements (see Fig. 5.6). Fixing the distance and the velocity yeilds a specific temperature. This temperature does not reflect the temperature

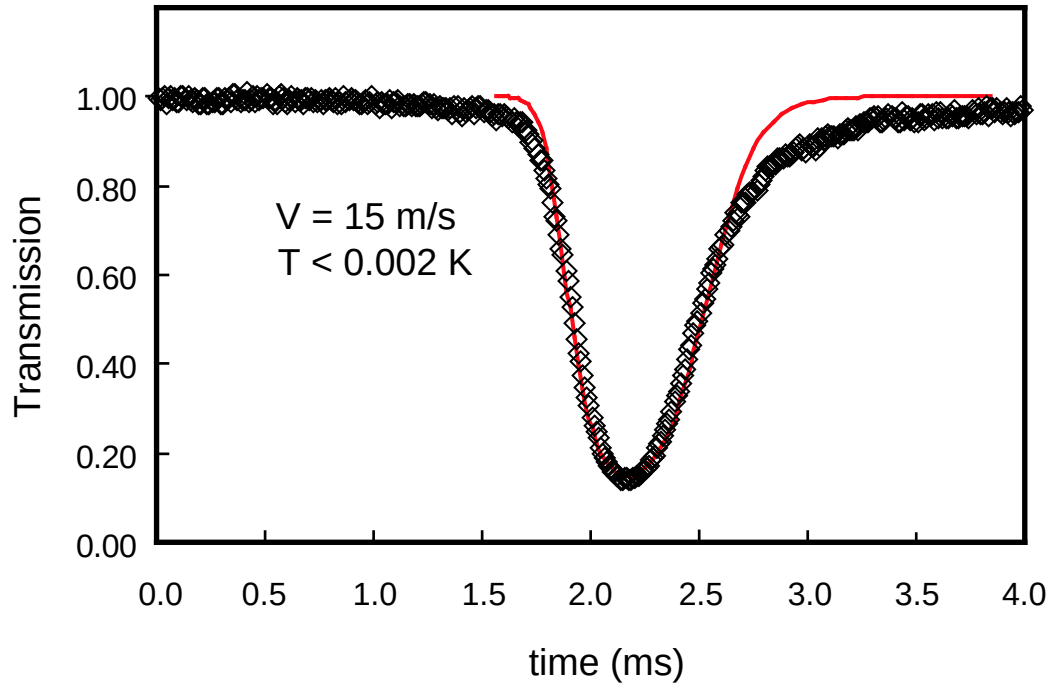

Figure 5.6: The temperature of the atom cloud can be determined by the distribution of atom arrival times at the cavity. The solid line is the fit and the squares are data.

of the MOT, as atoms are heated during the push process. The temperature extracted is an experimental check that nothing is amiss in the alignment and of the performance of the system. The average expansion velocity, $v_{ave} = (8kT/\pi m)^{1/2}$, for this temperature is 0.66 m/s, assuming a Maxwell Boltzmann 1-D distribution. The residual Doppler shift associated with this velocity will be $\vec{k} \cdot \vec{v}_{ave} = 0.85$ MHz, a negligible effect.

The cavity QED transmission is sensitive to the frequency of excitation. We experimentally perform minor adjustments (less than 2 MHz) to ensure that the cavity and the atoms are resonant (better than $\pm$ 2 MHz). This adjustment requires simultaneous changes of the cavity lock frequency derived from the 820 nm laser that

is locked to a transfer cavity and the probe laser, as described in chapter 4. The transmission profile is monitored as the frequencies of the probe and locking laser are adjusted to maximize the depth of the dip in the transmission. This provides a good starting point for finding the atomic resonance of the system.

We optimize the frequency of the driving laser to ensure we are on resonance and proceed to average over 200 launches of atoms. Figure 5.7 shows a typical average over the transmission of both polarizations. The driven mode (horizontal polarization) shown as the thin trace in Fig. 5.7 has a decrease in transmission as the atoms pass through the cavity and start absorbing the light. Note the asymmetry in the dip because of the distribution of initial atom velocities. The thicker trace is the transmission of the vertical polarization (fluorescence) mode, showing an increase in transmission starting from zero as atoms pass through. Then the transmission reaches a maximum, then decreases and increases again as the number of atoms diminishes again. The time axis is converted to the number of atoms by monitoring the dip in the horizontal polarization signal on resonance ($X/Y = (1+2C)^{-2}$), so a single shot measurement probes the response of the system to a variable value of N. The decrease in the signal to noise ratio of the fluorescence signal is due to the lower optical power present in this mode compared to the driven mode. The fluorescence signal has been multiplied by a factor of 250 in Fig. 5.7.

The probe spectrum is obtained by measuring the transmission profile in both polarizations for a variable probe frequency, averaging for 200 launches of atoms for each frequency. The transmitted intensity for a given time (or N equivalently) is plotted versus the probe frequency to reveal the probe spectrum. Figure 5.8 shows

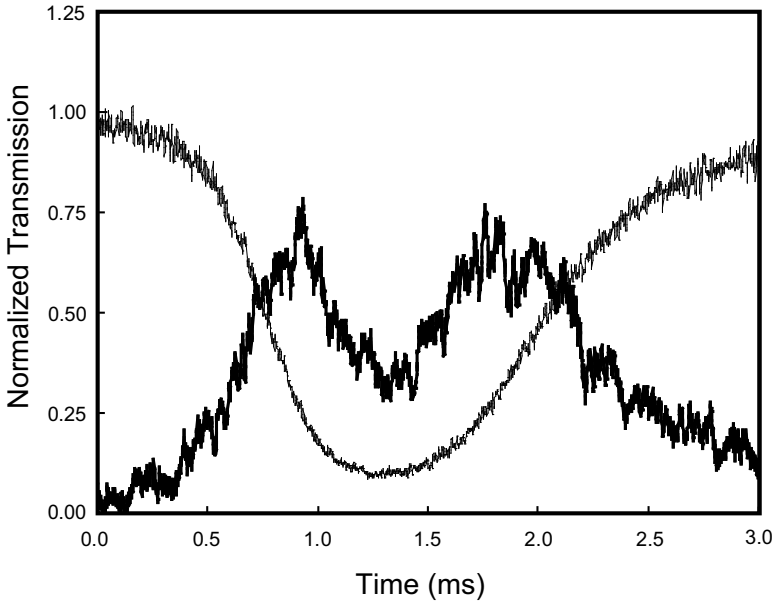

Figure 5.7: Cavity transmission as a function of time for the two orthogonal polarizations: thin line (horizontal) driven mode, thick line (vertical) mode proportional to the spontaneous emission. The transmission of the vertical mode has been multiplied by a factor of 250.

the spectra for the driven and undriven modes for a particular value of C where a vacuum Rabi splitting is observed. The slight asymmetry in the peaks may be due to an off-resonant lock of the cavity by less than a half linewidth (2.6 MHz). Note that the separation of the Rabi doublet for the driven mode is larger than that of the undriven mode, as predicted by the two-mode model with relevant experimental parameters.

Figure 5.9 shows how the peaks evolve as N changes. The increase in the splitting is equivalent to increasing the coupling $g \rightarrow g\sqrt{N}$, as described above due to the collective nature of the atoms in the cavity mode. Recall from chapter 2, Eq. 2.1.3

$$\Omega_{\pm} = \pm\sqrt{-\left(\frac{\gamma}{2}\right)^2 + g^2 N\sqrt{1 + \frac{\gamma}{g^2 N}\left(\frac{\gamma}{2} + \kappa\right)}} \tag{5.22}$$

which gives the peak positions of the vacuum Rabi doublet. In Fig. 5.9 we plot experimentally determined peak positions with the result of Eq. 2.1.3 for N given by the on-resonance value of the transmission dip. We presently do not have a generalized analytic formula for the location of the vacuum Rabi splittings in the four-level, two-mode model. The many equations (more than four) and parameters make it difficult to form a close solution. The theoretical line comes from numerical solutions of the four-level two mode model with experimentally relevant parameters.

At a given time, N is determined by the size of the dip in the horizontal polarization. We use this to parameterize the change in the transmission of the two modes. Figure 5.10 shows the transmission of the driven mode (horizontal polarization) that allows less light as more atoms pass through it, while the orthogonal

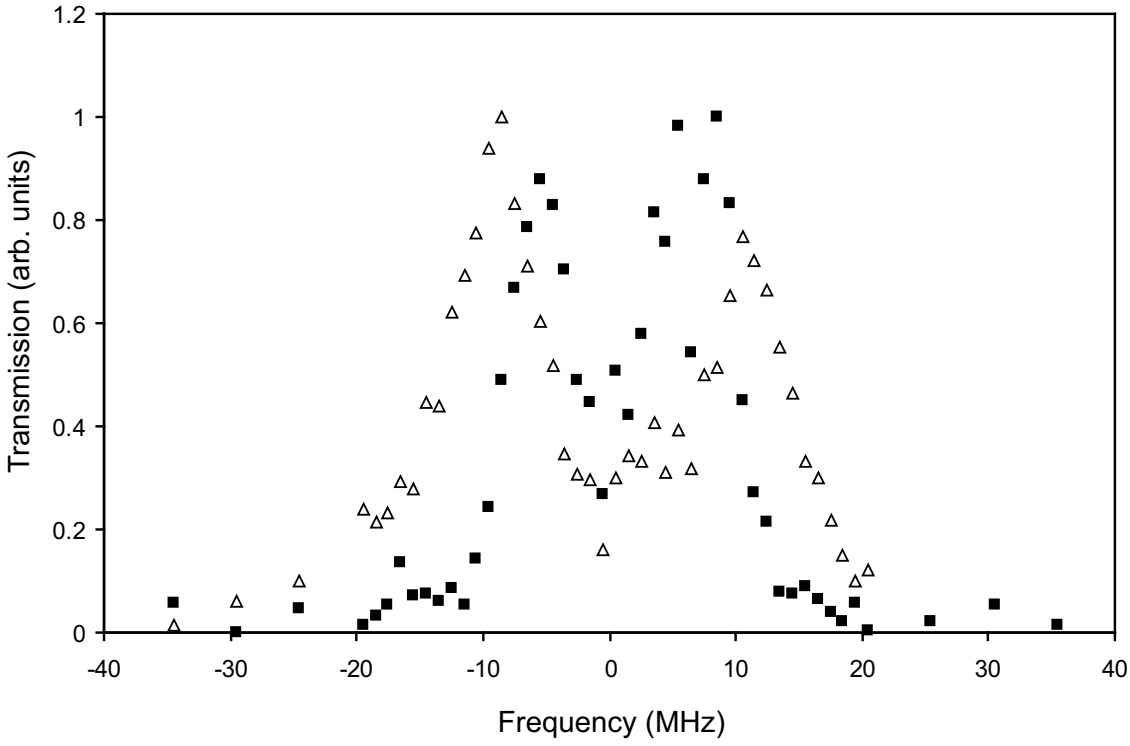

Figure 5.8: Intensity probe spectrum for driven (open triangles) and undriven (closed squares) modes.

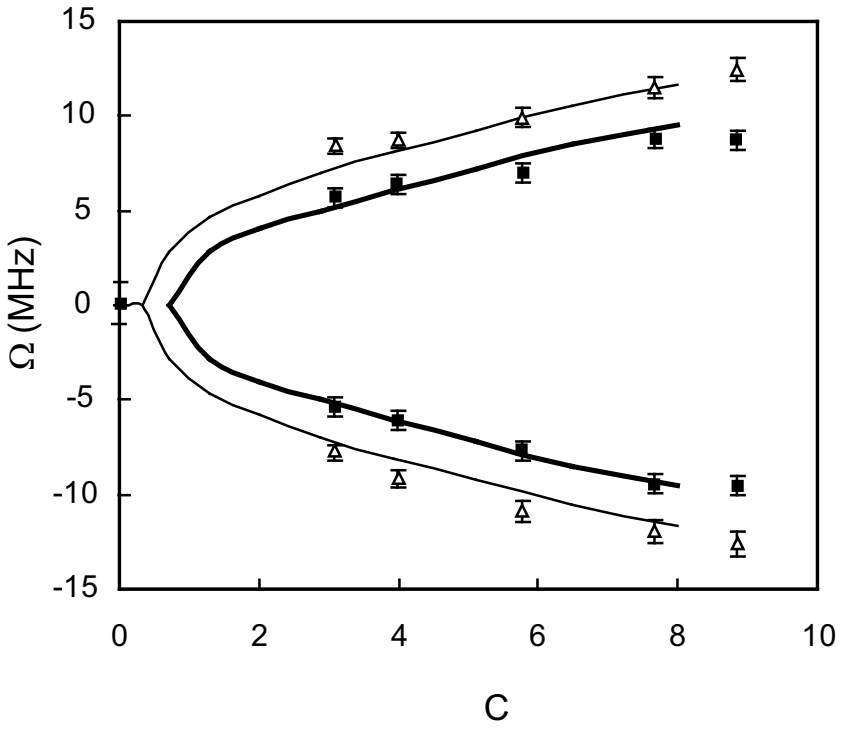

Figure 5.9: Evolution of the position of the splitting in the driven (open triangles) and undriven (closed squares). The driven mode is fitted with $\Omega_{\pm}$, from Eq. 2.1.3 and the undriven mode is fitted with the results of the two-mode theory with relevant experimental parameters.

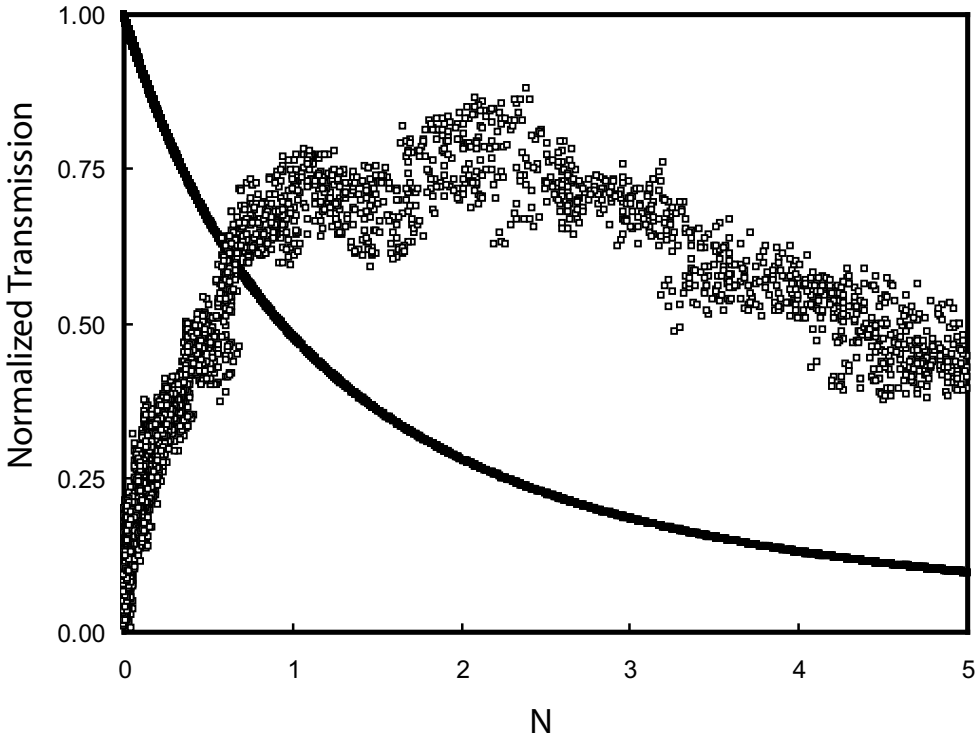

Figure 5.10: Variation of the cavity transmission as a function of the number of atoms in the cavity. Filled boxes driven mode (horizontal polarization). Open boxes orthogonal mode (vertical polarization) proportional to spontaneous emission. The scale for the transmission of the vertical polarization is multiplied by 250.

mode (vertical polarization) shows a maximum in the transmission as the number of atoms increases. Carmichael and Sanders [62] have found that averaging the probability distribution of the atoms over the mode function gives a unique parameter, the effective number of atoms. This parameter can characterize the distribution of atoms in the system. It simplifies the calculations as the atoms are moving across nodes, antinodes and the spatial mode of the cavity.

Figure 5.10 shows another important conclusion of this work, the enhancement

of spontaneous emission into the cavity mode. The amount of spontaneous emission going into the vertical mode is roughly 250 times smaller than what is emitted from the driven mode. Its maximum is in the vicinity of where the driven mode starts to show vacuum Rabi splitting. If the mode of the cavity was simply collecting the spontaneous emission, then the solid angle subtended by the mode would determine the amount of light exiting the vertical polarization mode. The solid angle of the cavity is 3.7×10^{-4} strad, accounting for the fluorescence captured in both directions from the two cavity mirrors. The power missing in the transmitted beam profile (Fig. 5.7) in the horizontal mode is radiated into 4π which accounts for the 75 % drop of the total input power. The total expected fluorescence should be less than $0.75 \times 3.7 \times 10^{-4}/2$ times the input intensity, where the factor of two in the denominator arises from the two linear polarization components of the $\sigma^{\pm}$ light. We find, however, that the measured signal is larger by a factor of 22. This difference shows significant enhanced emission into the cavity mode. In the bad cavity limit it is possible to extract this enhancement as the dynamics of the atom and cavity are clearly delineated. We, however, operate in the intermediate regime of cavity QED, where the bad cavity limit is not valid. The emitted light in the vertical mode comes from spontaneous emission. Our two-mode model predicts the amount of spontaneous emission that will be emitted into the mode (Eq. 5.15 and Eq. 5.17). We see very good agreement in the ratio of detected light in the two polarizations when we use a ratio of g/G=100 in the four level two mode model.

Chapter 6

Photon Counting Measurements

This chapter describes photon counting measurements which utilize the two mode system described in chapter 5. In chapter 4, the technical details of the photon counting apparatus were presented in detail. The apparatus used for photon counting measurements in our two-mode system is similar to the setup described in that chapter, with two major exceptions: the replacement of the PMTs with APDs and the implementation of the LVIS source.

The first change is done simply by placing flip mirrors before the PMTs. These mirrors redirected the cavity output to the single photon detectors. The cavity output beam polarization is temporarily rotated to evenly split the power to the two photodetectors. 5 cm lenses in front of the detectors focus the cavity beam onto the active area of the APDs. Bandpass and high wavelength pass filters placed directly in front of the detectors reduces residual background light as well as eliminates light that is emitted from the APDs during the avalanche process [71]. This light can lead to false peaks in the measured correlation function, however the filters effectively reduce this light to undetectable levels.

The implementation of the LVIS beam is instrumental for the success of photon counting measurements. The pulsed MOT apparatus does not have the capability to provide atoms in the cavity mode for times long enough for sufficient averaging

to take place. The time required to load the MOT, apply the push beam, and the atoms to travel to the cavity, typically requires a 50 ms duty cycle. For this 20 Hz repetition rate the atoms and cavity interact for 20 ms for every 1 s of real time. A 10 percent feature in a correlation function would be resolved with a signal to noise ratio of 1 would require 100 counts per bin, assuming a shot noise limited measurement. Typical count rates are 100,000 counts/s per detector for a measurement of $g^{(2)}(\tau)$ in cavity QED.

Poissonian statistics predict the probability for n photon counts in a time window, Δt, as

$$P_n(R\Delta t) = \frac{e^{-(R\Delta t)}(R\Delta t)^n}{n!} \tag{6.1}$$

where R is the count rate. The probability for two photon counts in a 1 μs window for a total count rate of 200,000 counts/s is 0.0082, where we have taken the output of Eq. 6.1 and divided by 2 to account for the permutations that result in both photons incident on the same detector. This corresponds to a coincidence rate of 8200/s. Here we ignore higher order excitations.

To accumulate 100 counts per bin, assuming a bin size of 1 ns, it would take approximate 12 s to achieve a signal to noise ratio of 1 for a 10 percent effect. The pushed MOT apparatus delivers atoms to the cavity, however the transit time of the atomic cloud across the cavity mode is about 1 ms per launch. With the pushed MOT apparatus operating at 20 Hz it will take 10 minutes of real time to acquire 12 s of interaction time between the atoms and cavity. This illustrates a best case scenario where we assume that the signal is shot noise limited, and there is no dead

time associated with the collection and histogramming of the data. A more realistic situation, which adequately describes our experiment, would require 2 minutes of continuous data taking to accumulate 100 counts per bin. This translates to 100 minutes of real time using the pushed MOT apparatus. To achieve a signal to noise ratio of 5, a more reasonable requirement, we have to multiply our data taking time by a factor of $\sqrt{5}$, requiring about 220 minutes. This demonstrates the necessity to implement a continuous beam of atoms for photon counting measurements in cavity QED.

6.1 Single atom transits

Quantum information protocols require fast detection of single atoms. Two approaches have been implemented in the laboratory: fluorescence detection with large aperture optics [72, 73] and the change of the transmission of a strongly coupled cavity QED system [74].

We start by estimating the signal to noise ratios of these two methods. The fluorescence of a single Rb atom at saturation (radiative lifetime of 26 ns) captured with an $f\# = 1$ imaging system gives a flux, $\Phi = 1/16 \times 1/2\tau = 1.2 \times 10^6$ counts/s. Assuming an overall efficiency of the optics and the detectors of 20 %, and no background and negligible dark counts, the signal to noise ratio, S/N, is $490 \times \sqrt{t}$, where t is the counting time. To get a signal to noise ratio of 3 it is necessary for the detector to integrate for 37 μs. If the S/N ratio is to reach 10, a counting time 420 μs is required.

The approach pioneered by the group of Kimble at Cal Tech utilizes cavity QED to detect transits of atoms through the mode of the cavity. This approach requires strong coupling cavity QED to make sure that the presence of a single atom in the system induces a very large effect. Recall the relation between the normalized input and output intensities, Y and X, for a weakly driven cavity with a single maximally coupled atom is, $Y = X(1 + 2C_1)^2$ [23]. This means that the relative change in the transmission $T = (Y - X)/Y$ is going to be:

$$\delta T = 1 - \frac{1}{(1 + 2C_1)^2} \tag{6.2}$$

For the Cal Tech group, the rates are $(g,\ \kappa,\ \gamma)/2\pi = (11,\ 3.5,\ 2.5)$ MHz resulting in a single atom cooperativity of 6.9. Mabuchi *et al.* [74] found that operating with 1 photon in steady state in the cavity is a reasonable for detection. If the number of photons is too large (i.e. the system resides on the upper branch of the bistability curve), the size of the change in the transmission decreases significantly. On the lower branch the presence of a single atom at an antinode results in nearly total extinction ($\delta T = 1$) of the probe beam.

A detection efficiency of 20 % and a steady state photon number of 1 results in a $S/N = 2970\sqrt{t}$ for the Cal Tech cavity. The time required to detect an atom with a $S/N = 3$ is 1 μs and for $S/N = 10$ is 11 μs, a significant improvement over the imaging method.

Quantum information protocols not only need to detect atoms on fast timescales with high fidelity, but they also require the ability to manipulate the quantum state to perform logic operations. The strong coupling in cavity QED is achieved by

small mirror separations (< 100 μm), severely limiting optical access needed for laser pulses to perform operations or provide trapping potentials. An increase in the mode volume by a factor of 10 results in a decrease of δT of a factor of 40 in the case of the Cal Tech cavity (keeping κ and γ the same). Now for a $S/N = 3$, a 40 μs integration time is required.

Here we present a new method of detecting single atom transits using our two-mode cavity QED system discussed in detail in chapter 5. Detecting the light in the orthogonal mode heralds the arrival of an atom. The method takes advantage of the lack of light in the mode when no atoms are present. The detection of one or two photons can signal the presence of an atom. This eliminates the need to average a photocurrent with many photons to resolve a slight change in the transmission over the shot noise.

An important difference between our cavity and that of Mabuchi *et al.* is the separation between the two mirrors. We have more than 2 mm, compared to the 108 μm of Mabuchi, that permits access for laser beams to interrogate the atom or trap the atom in an optical lattice. A suggested protocol for quantum information processing with neutral atoms in optical lattices in the end requires measurement of the state of the atom via cavity QED, which is sensitive to the hyperfine state of the atom [75].

As an atom traverses the mode of the cavity, it can scatter photons from the driven mode into the cavity mode with orthogonal polarization. The amount of fluorescence emitted into the mode is on the order of 10^{-3} of the light scattered out of the transmitted cavity mode. Typical count rates for the orthogonal mode

in continuous operation using the LVIS beam are 100,000 counts/s, or one every 10 μs on average. Figure 6.1 shows a sample of a time series of photodetections of the transmitted light in the orthogonal mode. The top trace is in the presence of atoms, while the bottom is a background count.

When an atom enters the cavity at about 5 m/s it will remain in the mode for almost 10 μs (mode waist $2\omega_0 = 112\mu$m). There is a very high probability that the atom will fluoresce a few times during its transit as the lifetime of the transition is 26 ns. The detection is aided by the statistics of the photoemissions. The probability of detecting a second photon conditioned on the detection of the first is high on the timescale of an atom transit. In other words, photons emitted from the same atom will be correlated. We measure the autocorrelation of the photoelectric pulses in the presence of atoms and clearly see a broad background peak with a width of a few microseconds. Figure 6.2 shows the resulting autocorrelation function using the photon counting apparatus and scope averaging method described in chapter 4 for long time delays (τ).

The observed enhancement of the probability of two coincidences beyond the uncorrelated coincidences (determined by long time delays) shows the bunching nature of this light. The size of the bunching depends on how high the drive is in the other mode, but does not show a clear saturation for the range of drives explored, which cover up to $> 10^8$ counts/s out of the driven mode.

It is possible in principle to detect atoms with single photons if there were no background light. Typical background counts are 10,000 counts/s for a fluorescence signal of 30,000 counts/s. Measuring atom transits by single photon detection would

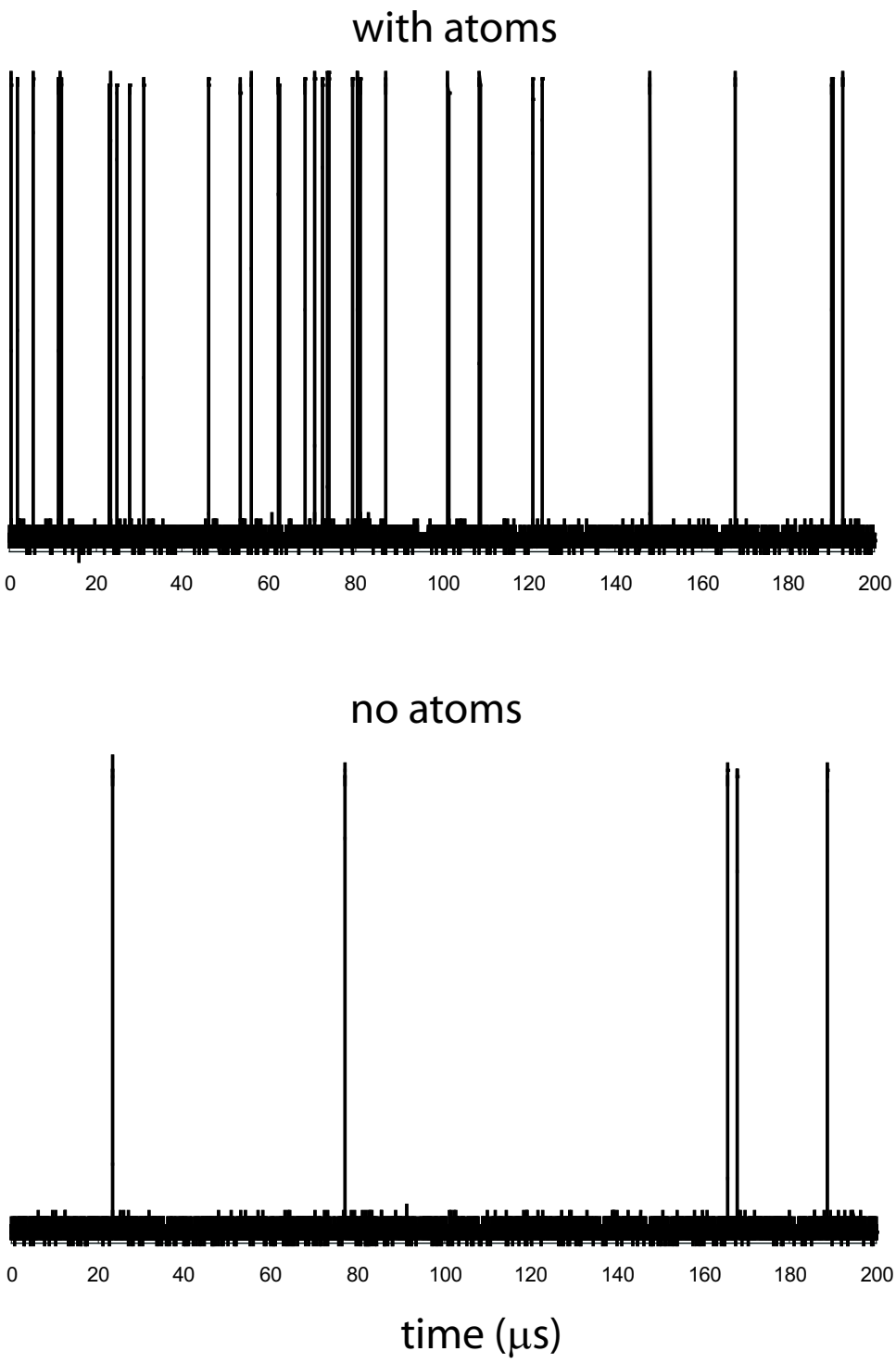

Figure 6.1: Time series of photodetections out of the orthogonal mode of the cavity in the presence (Top) and absence (Bottom) of atoms.

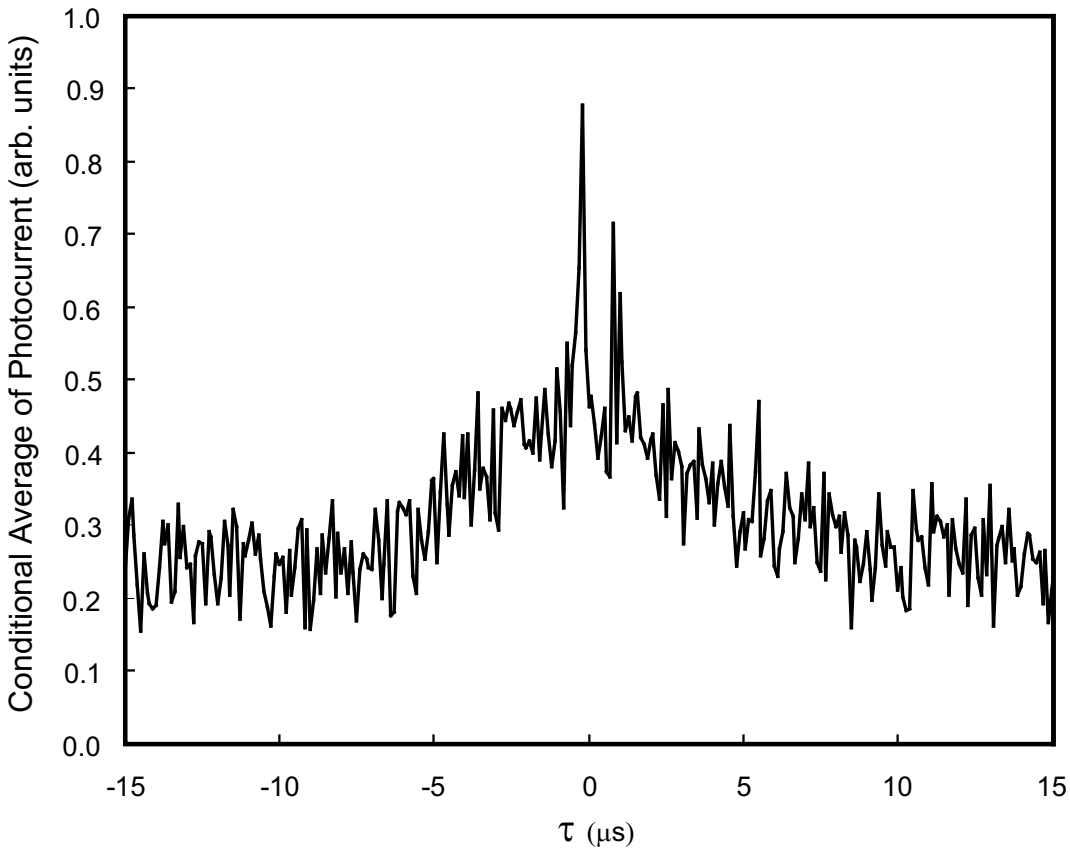

Figure 6.2: Long term autocorrelation of the light emitted out of the orthogonal mode. There is a large bunching background related to the transit of the atom through the cavity mode. The sharp feature at $\tau = 0$ is discussed in section 6.2. The sharp feature shortly after $\tau = 0$ is an electronic artifact.

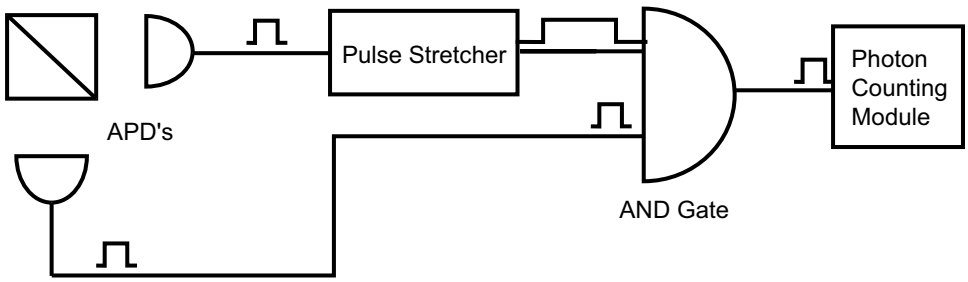

Figure 6.3: Schematic of the apparatus used to study the coincidences from atom transit in the cavity.

result in a false detection 25 % of the time. The bunched signal, however, provides an advantage when multiple photon emissions are used to detect the atoms. Photon coincidences make it possible to detect atom transits with high fidelity in times equal or faster than the methods described above.

Figure 6.3 shows the pulse processing apparatus used to detect the arrival of atoms into the cavity. The first photon detection starts a gate that is opened for a preset time, if a second photon arrives and passes through the gate it will produce a valid count. This way of detecting captures no more than one fourth of all events as we cannot count events that fall consecutively in the same photodetector, nor are coincidences registered when the gated "start" photon arrives after the "stop" photon. If an atom emits two stop photons that arrive after a start photon and within the preset time interval, two coincidences are recorded. This remains a valid trigger for an atom detection (with an even higher fidelity), but must be accounted for if one is counting individual atom transits.

We perform a series of measurements of atom transits at three drive power

levels and with three coincidence window lengths. The photon counting apparatus is identical to that shown in Fig. 4.8 where the APDs are used in place of the PMTs and the flip mirror on the vertical polarization beam redirects half of the fluorescence beam to the detector box.

The pulses generated by the start detector are stretched by a Lecroy Dual Gate Generator to a variable width. The stretched pulse is sent to a EGG linear gate module which allows stop pulses to pass only when the stretched start signal is on. The gated output is sent to a Stanford Research Systems SR400 Photon Counting Module to count the number of coincidences. Figure 6.4 shows the histogram of two photon coincidences as measured by our apparatus. The black bars are the background coincidences, while the white bars are in the presence of atoms for three time gate intervals: 500 ns, 1 μs, and 5 μs. The line shows the theoretic expectations from a purely Poissonian distribution. There is a clear excess in the last bar, coming from the bunching events when an atom fluoresces into the mode more than once as it crosses the cavity. The results shown in Table 6.1 shows fidelities above 90% for all gate lengths and input intensities. The fidelities are limited by the presence of background counts, which can cause false triggers. Our fidelities are calculated by measuring the coincidence counts with the LVIS beam off and dividing by the coincidence counts with the beam on. Counts recorded due to one background and one fluorescence photon are not counted as false, as they do herald the presence of an atom. Also we do not account for multiple stops, which double count a small fraction of the recorded coincidences. For low input drives these multi-photon events are unlikely and account for a low percentage of the total atom counts (see Fig. 6.5).

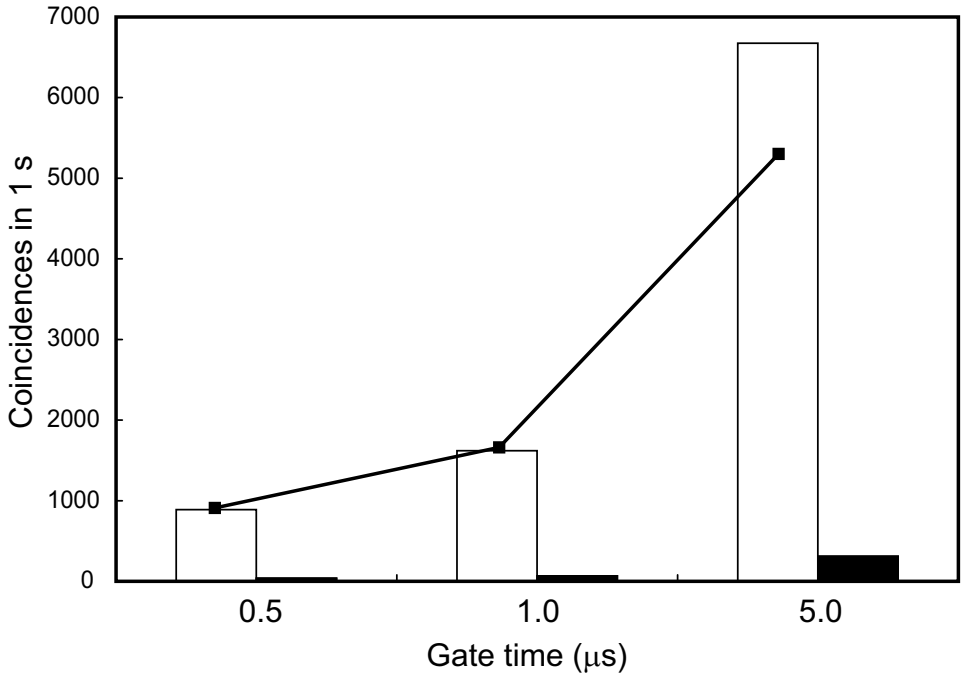

Figure 6.4: Histogram of two photon coincidences in the presence (white) and absence (black) of atoms. The line is the Poissonian prediction.

Table 6.1: Atom transit results.

Input Power (nW)	Δt (μs)	Gated Counts (in 10 s) (beam off)	Gated Counts (in 10 s) (beam on)	Fidelity
1.6	0.5	122	2,313	0.947
	1.0	215	4,318	0.950
	5.0	968	20,885	0.954
4.2	0.5	374	8,897	0.958
	1.0	684	16,203	0.958
	5.0	3114	66,757	0.953
38.4	0.5	2,096	27,484	0.924
	1.0	3,933	47,215	0.917
	5.0	17,518	198,338	0.912

The time series of the APD signals (Fig. 6.1) also gives information on the probability distribution of the process. Figure 6.5 shows the analysis of a time series with atoms (white squares) and background (filled black squares). The analysis, done off line with a computer algorithm, is for time periods of 5 μs. The algorithm analyzes a sequence of APD signals recorded from our Lecroy 7000 scope. The program takes the time interval of interest and counts the number of clicks measured. Then it moves the window one bin (time point) at a time until it traverses the entire sequence, counting the single, double, and triple count events for each iteration. In the end it adds the total number of time windows where two counts, for instance,

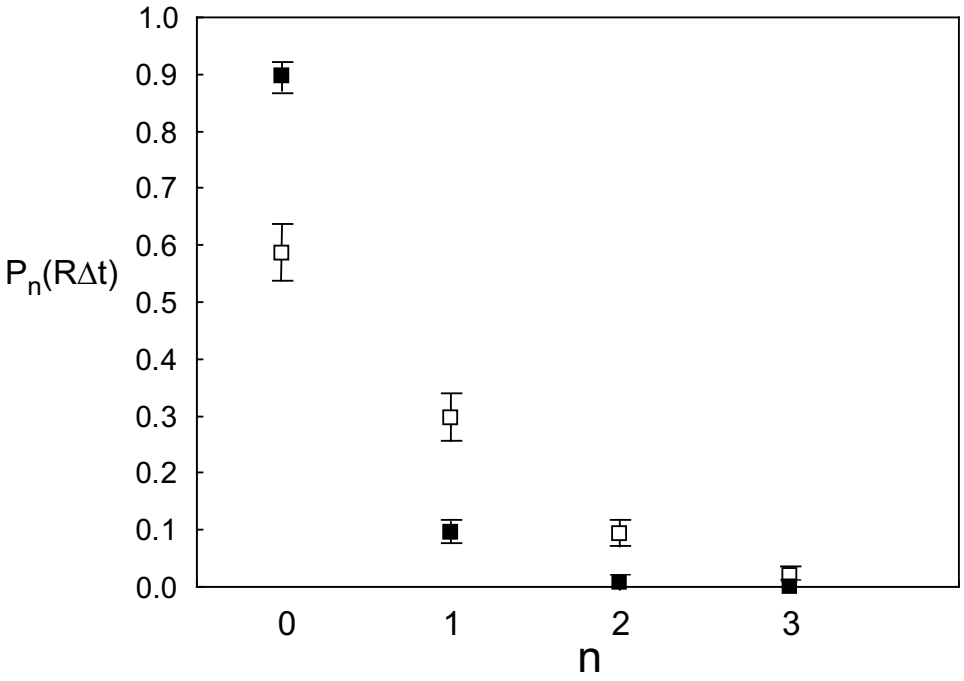

Figure 6.5: Extracted probability that there would be n counts in any interval of 5 μs of a measured time series. White squares represent the probabilities with the atomic beam on, and the black squares with the beam off.

are recorded and divides by the total number of windows (time points) to get a probability. Figure 6.1 shows a clear enhancement of the probabilities of single counts and double coincidences. The triple coincidences are also enhanced, but they are infrequent.

This new method of detecting atom transits is fast, reliable, and does not require strong coupling in cavity QED.

6.2 Cross-correlation Measurements

A measurement of entanglement in cavity QED is a difficult endeavor due to the very small amount of entanglement in the system. A first glance of the system wave function reveals the large vacuum component that dominates the steady state. In other words, most of the time there are no excitations in the system at all. It is the presence of rare excitations that can lead to an entanglement between the atoms and the mode of the cavity. The measurement of this entanglement requires a powerful tool that can neglect the vacuum component and extract information about the one and two excitation probability amplitudes. In quantum optics, we have such a tool at our disposal; the correlation function. As stressed in chapter 3 of this thesis, traditional correlation functions (Hanbury-Brown and Twiss for example) are unable to measure the entanglement, because they typically only probe one component of the entangled pair. Cross-correlations, as the name implies, correlates fluctuations from two separate systems, in our case the atom and cavity mode, making it possible to extract a measurement or witness of entanglement

Recall from chapter 3 that a cross-correlation, $j^2(\tau)$, is an entanglement witness for cavity QED

$$j^{(2)}(\tau) = \frac{\langle \sigma_+(0)a^\dagger(\tau)a(\tau)\sigma_-(0)\rangle}{\langle a^\dagger a\rangle_{ss}\langle \sigma_+\sigma_-\rangle_{ss}} \tag{6.3}$$

An entanglement witness is not proportional to the entanglement. However, it does track the entanglement and can give an indication as to how the entanglement is affected by the environment. A common measure of entanglement is given by the concurrence, $\mathcal{C} = \sqrt{4(A_{1g}A_{0e} - A_{1e})^2}$ for the cavity QED system. This depends on

the probability amplitudes of the steady state wave function. In order to access the probability of coincident cavity and fluorescent emissions, a cross-correlation, such as $j^{(2)}(\tau)$, is needed to simultaneously record these correlated events with respect to the probability of having only one cavity or only one atomic excitation.

To gain an understanding of cross-correlations, we turn to the quantum trajectory formalism pioneered by H. J. Carmichael (see his book [76] for detailed lectures on the topic in the context of quantum optics). This approach to studying an open quantum system derives formally from the master equation, and treats the time evolution of the system as a sum over possible "trajectories" that can be interrupted by a series of collapses. These collapses correspond directly to experimental measurements, such as the detection of a transmitted photon from a cavity. This method allows us to consider an initially pure state that evolves due to a non-Hermitian Hamilitonian. The norm of the wave function is conserved after each time step in the evolution by renormalizing the wave function. The collapses are probabilistically determined. Summing over many trajectories recreates an ensemble average of the quantum dynamics of the system. Correlation functions naturally arise from these simulations by simply correlating collapses, exactly as is done in the laboratory.

Carmichael *et. al.* [77] have independently derived a two-mode model inspired in part by our experimental endeavors. They have performed quantum trajectories that simulate our system, with the appropriate experimental parameters. The model is simplified in that it only contains two atomic levels, but the quantum trajectory formalism allows for multiple excitations which make an analytical solution impossible. Later we present the results of these quantum simulations to compare with

our data.

As presented in the previous section, when an atom traverses the cavity mode it emits photons in an otherwise "dark" mode. The detection of one or two photons reliably heralds the arrival of an atom. On the other hand, for a small number of atoms ($N_{eff} < 1$) in the cavity, the driven mode is relatively insensitive to the presence of an atom in the intermediate coupling regime. With no atoms in the cavity the transmitted beam is a coherent state and the photon flux is large. For these reasons it seems natural to first examine the autocorrelation of the undriven mode. Light can only be emitted (neglecting the background) when atoms are present. In a sense this is a purified measurement in that there is no contamination of the statistics due to time intervals when no atoms are present.

Figure 6.6 presents our results of an autocorrelation, $g^{(2)}_{FF}(\tau)$, performed on the fluorescence emitted in the vertical mode of our cavity QED system. We define this autocorrelation in the language of the two-mode model presented in chapter 5 as:

$$g^{(2)}_{FF}(\tau) = \frac{\langle \Psi | b^\dagger(0) b^\dagger(\tau) b(\tau) b(0) | \Psi \rangle}{\langle b^\dagger b \rangle^2} \tag{6.4}$$

where the the subscript, F, denotes the detection of fluorescence. The measurement shows a clear bunching. The peak decays on a time scale that is consistent with 2κ. Figure 6.2 is a measurement of the same signal using the scope averaging method described in chapter 4. The bunching peak is clearly noticeable at $\tau = 0$. The feature sits on top of a large Gaussian shaped pedestal that is attributed to correlated photons emitted by single atoms that transit the cavity mode. We compared our results with Fig. 6.7, a quantum trajectory simulation of the autocorrelation with

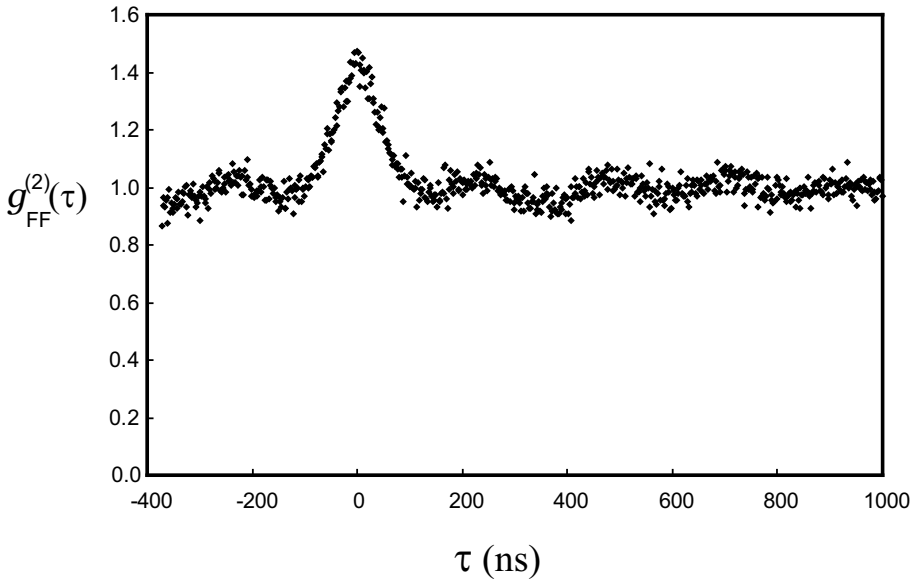

Figure 6.6: Bunching shown in an autocorrelation of the fluorescence mode.

a large driving field (15 photons in the driven mode). Our results are qualitatively and quantitatively consistent with the quantum trajectory simulation of Carmichael [77]. The bunching signal is clearly the main feature in the correlation function. It becomes visible less than a minute after the start of data acquisition. The long term oscillations in Fig. 6.6 depend on the magnetic field present at the cavity and sit on top of the atomic transit induced bunched peak.

Next we define a new cross-correlation, again based on the two-mode model of chapter 5:

$$g^{(2)}_{TF}(\tau) = \frac{\langle \Psi | b^\dagger(0) a^\dagger(\tau) a(\tau) b(0) | \Psi \rangle}{\langle b^\dagger b \rangle \langle a^\dagger a \rangle} \tag{6.5}$$

where the subscript, T, represents the transmitted driven mode. This correlation is similar to the $j^{(2)}(\tau)$ function presented in chapter 3, but here the mode that receives the spontaneous emission is used to measure the correlation.

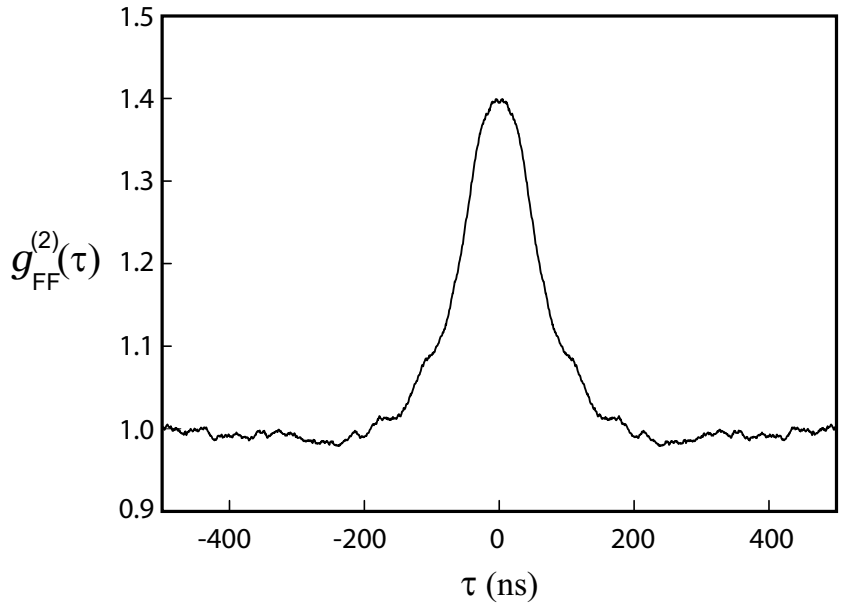

Figure 6.7: Quantum trajectory simulation of the autocorrelation, $g^{(2)}_{FF}(\tau)$ from H. Carmichael and H. Eleuch. For this simulation there are 15 photons in the undriven mode.

The basic requirements for the measurement are: a high density LVIS beam, stable cavity and laser locks, and fine control of the polarization of the input and output cavity beams. The LVIS beam must produce enough atoms to produce a count rate in the undriven mode on the order of 20,000-70,000 counts/s. There is a background due to stray beams and dark counts of about 5,000 counts/s in the APD aligned to this mode. In addition, the birefringence of the cavity is responsible for 5,000-20,000 counts/s depending on the strength of the input drive. Minimizing the background due to the birefringence is a delicate procedure. The cavity transmission is monitored while making small rotations of the polarizer before the cavity input. The waveplate on the cavity output must then be rotated to extinguish as much of the light in the driven mode as possible. We iterate many times until the input polarization is extinguished by a factor greater than 10^4.

Figure 6.8 represents our first measurement of $g^{(2)}_{TF}(\tau)$. There is clearly an anti-correlation in the signals defined by the dip at $\tau = 0$, with count rates for the driven and undriven modes of 4.7×10^7 photons/s and 2.3×10^4 photons/s respectively. Decreasing the drive (see Fig. 6.9) by a factor of 10 results in a peak appearing out of the depression at $\tau = 0$ in the cross-correlation. The size of these effects are on the order of $1 - 2$ % and require about 30 minutes of data taking to resolve the features with a good signal to noise ratio.

Again the quantum trajectory simulations show behavior that qualitatively similar to the data. Figure 6.10 is another plot from Carmichael that captures the interesting features of the measured cross correlation. Carmichael has warned us that he has not performed a careful check of all the experimental parameters, so

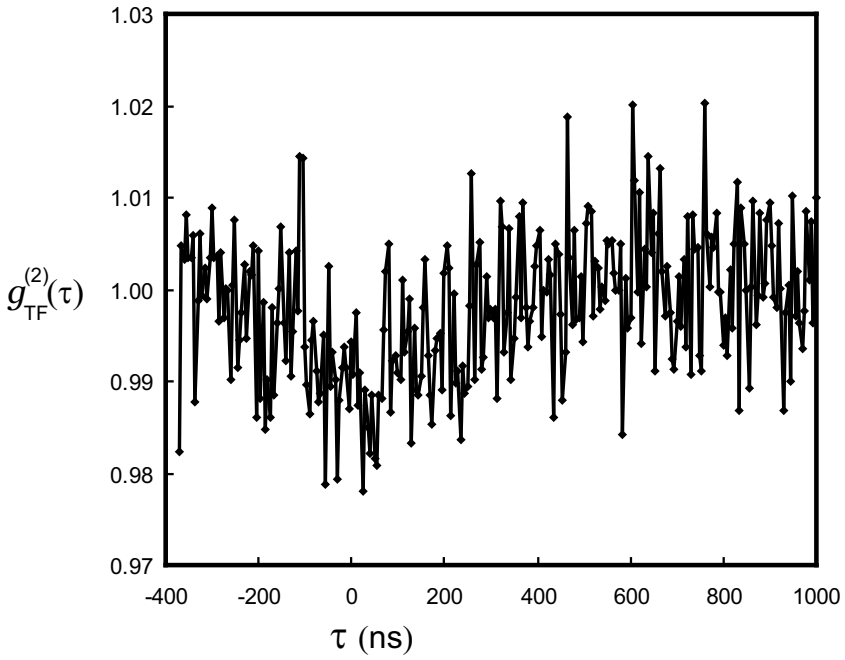

Figure 6.8: Cross correlation between the driven (T) and undriven (F) modes with ≈ 1.2 photons in the driven mode.

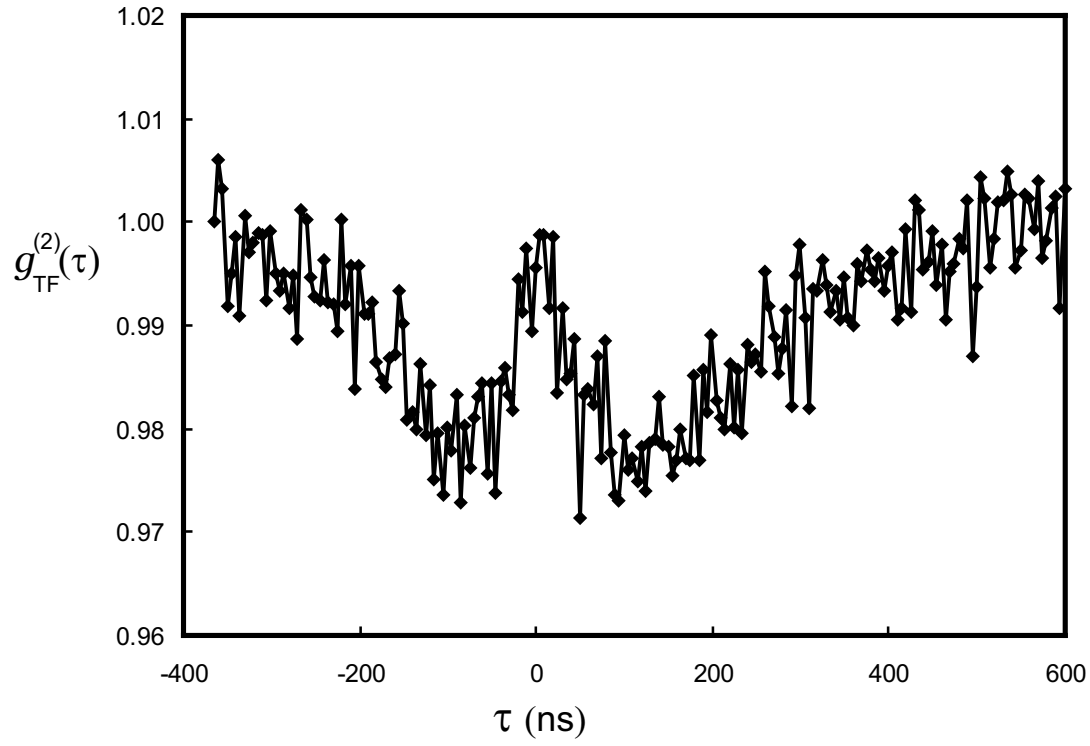

Figure 6.9: Cross correlation between the driven (T) and undriven (F) modes with ≈ 0.15 photons in the driven mode.

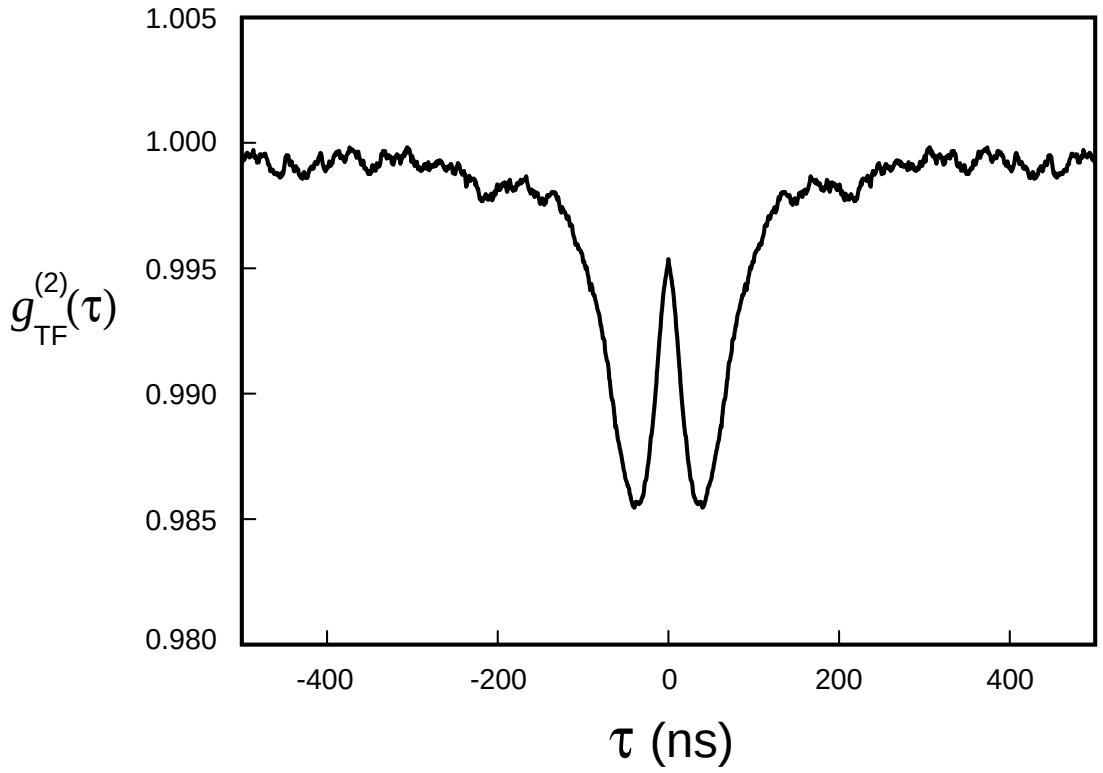

Figure 6.10: Quantum trajectory simulation of $g^{(2)}_{TF}(\tau)$ from H. Carmichael and H. Eleuch. For this simulation there are 3 photons in the driven mode and 0.1 photons in the undriven mode.

there remains a mismatch of the timescale for these dynamics. Higher order excitations (3 photons in the driven mode and 0.1 in the undriven mode) are needed in the simulations to exhibit this type of behavior. While measuring the cross-correlations we monitor the number of photons detected from the driven and undriven modes. These rates are important as they allow us to extract information relevant for quantifying the entanglement.

Recall from chapter 3 that the calculations of the concurrence for a driven cavity QED are done in the weak driving limit with a two-level atom. The fluorescence

detection in chapter 3 is assumed to be measured in free space with no cavity. Rather than attempt a correction for this, we proceed here and use our measurements to extract a value of $j^{(2)}(0)$ from $g^{(2)}_{TF}(0)$ for these two cross-correlation measurements. Strictly speaking any information obtained about entanglement would be related to the entanglement between the two modes of our cavity. Recall, however, that the light in the undriven mode comes from an excitation in the atom, Eq. 5.15 and Eq. 5.17.

Experimentally the ratio of steady state photons in the cavity is less than the saturation photon number, n_0; however formally speaking, we are away from the low intensity limit. We have developed the theory in the low intensity limit but expect the relationship between the probabilities of single counts and coincidences to hold. We have some justification for this as Gea Banacloche *et. al.* [55] have found that the correlation functions remain valid entanglement witnesses with strong driving fields in cavity QED, where the steady state photon number is larger than n_0.

Guided by the results of chapter 3, we can try to extract a concurrence estimate from the plots of Fig. 6.8 and Fig. 6.9. This gives a lower bound or witness of entanglement. Here we note the relationship between the concurrence and $j^{(2)}(0)$:

$$\begin{aligned} \mathcal{C} &= \sqrt{4(A_{1g}A_{0e} - A_{1e})^2} && (6.6)\\ &= \sqrt{4(A_{1g}A_{0e})^2(1 + j^{(2)}(0) - 2\sqrt{|j^{(2)}(0)|})} && (6.7)\\ &\approx \sqrt{4(A_{1g}A_{0e})^2(1 + g^{(2)}_{TF}(0) - 2\sqrt{|g^{(2)}_{TF}(0)|})} && (6.8) \end{aligned}$$

where $j^{(2)}(0) = |A_{1e}|^2/(|A_{0e}|^2|A_{1g}|^2)$. The value of $j^{(2)}(0)$, as indicated by the last equation, comes from the fractional difference from unity of the normalized cross-

correlations that we measure, $g^{(2)}_{TF}(0)$. The rate, R, of single photon detections can give us the probability of the single excitations by solving for the intracavity photon number, n, for the two modes, where $R = 4\pi n\kappa$. Recall from chapter 2 that $X = \langle a^\dagger a\rangle / n_0$ where n_0 is 5.3 for our system. The square root gives us the value of the single excitation probability amplitude. Our calculation here does not account for the quantum efficiencies of the detectors or other losses which raises the detected counting rates and increases the concurrence. This is especially critical for a careful measurement of entanglement as the efficiencies enter twice in the formula.

The results for the two measurements are plotted in Fig. 6.11. They gives an estimate of the concurrence on the order of 10^{-5} with an uncertainty on the individual measurements of $\pm 4 \times 10^{-5}$, with the error dominated by the residual shot noise in the coincidence measurements. Here we calculate the uncertainty based on the dominant contributions to be:

$$\delta\mathcal{C} = A_{1G}A_{0e}\delta(j^{(2)}(0)) \tag{6.9}$$

Although our entanglement witness in cavity QED is not yet a good bound, we should compare our measurement to the measurement of entanglement between a single trapped ion and a single photon from the group of C. Monroe [78]. They measure correlations between the state of the ion and the polarization of the photon and obtain a success probability of 1.6×10^{-4} of entanglement, which is of the same order as our concurrence. Further work is necessary to compare the two measurement strategies and to improve our results.

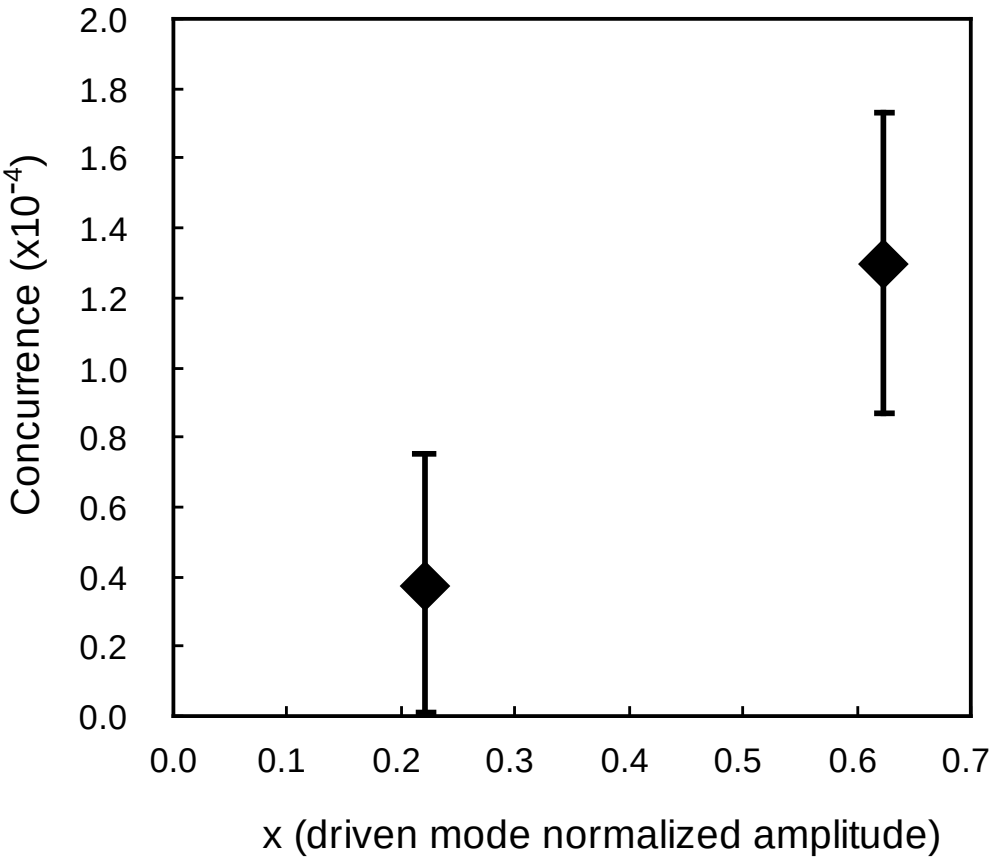

Figure 6.11: Measured concurrence for our system derived from two cross-correlation measurements.

Chapter 7

Conclusions

The cavity QED system provides a unique test bed for exploring the nature of entanglement in open quantum systems. The mechanisms responsible for loss and decoherence in the atom-cavity system, are avenues for interrogating the system. This has long been known and exploited, but here we take advantage of *both* the cavity decay and spontaneous emission to probe the dynamics of system in the time and frequency domains.

The two-mode model we have presented is rich with physics not yet uncovered by our experimental explorations. We have seen interesting probe spectrum that hint at an underlying structure that is related to the presence of the second mode and the relative coupling strengths of the two. Our first attempts to probe the spontaneous emission from the atoms have revealed a far more interesting system than expected.

The implementation of the LVIS beam for cavity QED experiments has been a huge boost for our group. We are past the age of using thermal atomic beams for these experiments. This next generation, cold atom beam apparatus will provide many years of fruitful investigations without the adverse effects of fast, hot atoms traversing the cavity mode.

The success of the LVIS apparatus is directly responsible for our new results

in the photon counting regime. The continuous atom beam has made it possible to measure cross-correlations of the two modes in our system as a step towards developing a witness measurement of entanglement. A broad range of experiments are now possible for measuring cross-correlations and their use as a probe to track the time evolution of entanglement. The results of this experiment should prove useful for developing a deeper understanding of entanglement in cavity QED.

BIBLIOGRAPHY

[1] M. Brune, "Cavity Quantum Electrodynamics," in *Les Houches 2003 Session LXXIX, Quantum Entanglement and Information Processing*, p. 161 (Elsevier, Amsterdam, 2004).

[2] G. Khitrova, H. M. Gibbs, M. Kira, S. W. Koch, and A. Scherer, "Vacuum Rabi Splitting in Semiconductors," Nature Phys. **2**, 81 (2006).

[3] G. R. Guthohrlein, M. Keller, K. Hayasaka, W. Lange, and H. Walther, "A Single Ion as a Nanoscopic Probe of an Optical Field," Nature **414**, 49 (2001).

[4] P. R. Berman, ed., *Cavity Quantum Electrodynamics*, Advances in Atomic, Molecular, and Optical Physics (Academic Press, Boston, 1994). Supplement 2.

[5] E. T. Jaynes and F. W. Cummings, "Comparison of Quantum and Semiclassical Radiation Theories with Applications to the Beam Maser," Proc. IEEE **51**, 89 (1963).

[6] H. Paul, Ann. Phys. (Leipzig) **11**, 411 (1963).

[7] J. J. Sánchez Mondragón, N. B. Narozhny, and J. H. Eberly, "Theory of Spontaneous-Emission Line Shape in an Ideal Cavity," Phys. Rev. Lett. **51**, 550 (1983).

[8] J. Gripp, S. L. Mielke, and L. A. Orozco, "Evolution of the Vacuum Rabi Peaks in a Detuned Atom-Cavity System," Phys. Rev. A **56**, 3262 (1997).

[9] J. Gripp, S. L. Mielke, L. A. Orozco, and H. J. Carmichael, "Anharmonicity of the Vacuum Rabi Peaks in a Many-Atom System," Phys. Rev. A **54**, R3746 (1996).

[10] M. Hennrich, A. Kuhn, and G. Rempe, "Transiton from Antibunching to Bunching in Cavity QED," Phys. Rev. Lett. **94**, 053,604 (2005).

[11] G. T. Foster, S. L. Mielke, and L. A. Orozco, "Intensity Correlations in Cavity QED." Phys. Rev. A **61**, 053,821 (2000).

[12] G. Rempe, R. J. Thompson, R. J. Brecha, Q. Turchette, and H. J. Kimble, "Atoms in an Optical Cavity," in *Atomic Physics 13*, H. Walther, T. W. Hänsch, and B. Neizert, eds., vol. 275 of *AIP Conference Proceedings*, p. 305 (AIP, New York, 1993).

[13] S. L. Mielke, G. T. Foster, and L. A. Orozco, "Non-Classical Intensity Correlations in Cavity QED," Phys. Rev. Lett. **80**, 3948 (1998).

[14] H. J. Carmichael, H. M. Castro-Beltran, G. T. Foster, and L. A. Orozco, "Giant Violations of Classical Inequalities through Conditional Homodyne Detection of the Quadrature Amplitudes of Light," Phys. Rev. Lett. **85**, 1855 (2000).

[15] R. H. Brown and R. Q. Twiss, "Correlation Between Photons in Two Coherent Beams of Light," Nature **177**, 27 (1956).

[16] A. Einstein, B. Podolsky, and N. Rosen, "Can a Quantum-Mechanical Description of Reality be Considered Complete?" Phys. Rev. **47**, 777 (1935).

[17] E. Schrodinger, "The Present Situation in Quantum Mechanics," Naturwissenschaften **48**, 807 (1935).

[18] J. Bell, "On the Problem of Hidden Variables in Quantum Mechanics," Rev. Mod. Phys. **38**, 447 (1966).

[19] A. Aspect, P. Grangier, and G. Roger, "Experimental Realization of Einstein-Podolsky-Rosen-Bohm Gedanken Experiment; a New Violation of Bell's Inequalities," Phys. Rev. Lett. **49**, 91 (1982).

[20] C. H. Bennett, G. Brassard, C. Crepeau, R. Jozsa, A. Peres, and W. Wootters, "Teleporting an Unknown Quantum State via Dual Classical and EPR Channels," Phys. Rev. Lett. **70**, 1895 (1993).

[21] N. Gisin, G. Ribordy, W. Tittel, and H. Zbinden, "Quantum Cryptography," Rev. Mod. Phys. **74**, 145 (2002).

[22] D. DiVincenzo, "Quantum Computation," Science **270**, 5234 (1995).

[23] L. A. Lugiato, "Theory of Optical Bistability," in *Progress in Optics*, E. Wolf, ed., vol. XXI, pp. 69–216 (North-Holland, Amsterdam, 1984).

[24] R. J. Brecha, P. R. Rice, and M. Xiao, "N Two-Level Atoms in a Driven Optical Cavity: Quantum Dynamics of Forward Photon Scattering for Weak Incident Fields." Phys. Rev. A **59**, 2392 (1999).

[25] J. Gripp and L. A. Orozco, "Evolution of the Vacuum Rabi Peaks in a Many-Atom System," Quantum Semiclass. Opt. **8**, 823 (1996).

[26] J. Gripp, "Evolution of the vacuum Rabi sidebands," Ph.D. thesis, State University of New York at Stony Brook (1997).

[27] H. J. Carmichael, *An Open Systems Approach to Quantum Optics, Lecture Notes in Physics*, vol. 18 (Springer-Verlag, Berlin, 1993).

[28] H. J. Carmichael, R. J. Brecha, and P. R. Rice, "Quantum Interference and Collapse of the Wavefunction in Cavity QED," Opt. Commun. **82**, 73 (1991).

[29] R. J. Glauber, "Photon Correlations," Phys. Rev. Lett. **10**, 84 (1963).

[30] R. J. Glauber, "The Quantum Theory of Optical Coherence," Phys. Rev. **130**, 2529 (1963).

[31] H. J. Kimble, M. Dagenais, and L. Mandel, "Photon Anti-Bunching in Resonance Fluorescence," Phys. Rev. Lett. **39**, 691 (1977).

[32] A. Peres, "Collective Tests for Quantum Nonlocality," Phys. Rev. A **54**, 2685 (1996).

[33] C. H. Bennett, D. P. DiVincenzo, J. A. Smolin, and W. K. Wootters, "Mixed-state entanglement and quantum error correction," Phys. Rev. A **54**, 3824 (1996).

[34] W. K. Wootters, "Entanglement of Formation of an Arbitrary State of Two Qubits," Phys. Rev. Lett. **80**, 2245 (1998).

[35] M. B. Plenio, "Logarithmic Negativity: A Full Entanglement Monotone That is not Convex." Phys. Rev. Lett. **95**, 090,503 (2005).

[36] H. Nha and H. J. Carmichael, "Entanglement within the Quantum Trajectory Description of Open Quantum Systems," Phys. Rev. Lett. **93**, 120,408 (2004).

[37] K. Chen, S. Albeverio, and S. Fei, "Concurrence of Arbitrary Dimesional Bipartite Quantum States," Phys. Rev. Lett. **59**, 040,504 (2005).

[38] A. Uhlmann, "Fidelity and Concurrence of Conjugated States," Phys. Rev. A **62**, 032,307 (2000).

[39] P. Rungta, V. Buzek, C. Caves, M. Hillery, and G. J. Milburn, "Universal State Inversion and Concurrrence in Arbitrary Dimensions," Phys. Rev. A **64**, 042,315 (2001).

[40] S. Albeverio and S. Fei, "A Note On Invariants And Entanglements," J. Opt. B **3**, 233 (2001).

[41] P. R. Rice, J. Gea-Banacloche, M. L. Terraciano, D. L. Freimund, and L. A. Orozco, "Steady State Entanglement in Cavity QED," Opt. Exp. **14**, 4514 (2006).

[42] M. L. Terraciano, R. Olson, D. L. Freimund, L. A. Orozco, and P. R. Rice, "Fluorescence spectrum into the mode of a cavity QED system," arXiv.org **quant-ph/0601064**.

[43] H. J. Carmichael, R. J. Brecha, M. G. Raizen, H. J. Kimble, and P. J. Rice, "Subnatural Linewidth Averaging for Coupled Atomic and Cavity-Mode Oscillators," Phys. Rev. A p. 5516 (1989).

[44] R. J. Glauber, "Coherent and Incoherent States of the Radiation Field," Phys. Rev. **131**, 2766 (1963).

[45] L. Mandel and E. Wolf, *Optical Coherence and Quantum Optics* (Cambridge University Press, New York, 1995).

[46] P. Grangier, G. Roger, A. Aspect, A. Heidmann, and S. Reynaud, "Observation of Photon Antibunching in Phase-Matched Multiatom Resonance Fluorescence," Phys. Rev. Lett. **57**, 687 (1986).

[47] A. Kuzmich, W. P. Bowen, A. D. Booze, A. Boca, C. W. Chou, and L.-M. D. adn H J Kimble, "Generation of nonclassical photon pairs for scalable quantum communication with atomic ensembles," Nature **423**, 731 (2003).

[48] D. V. Regelman, U. Mizrahi, D. Gershoni, E. Ehrenfund, W. V. Schoenfeld, and P. M. Petroff, "Semiconductor Quantum Dot: A Quantum Light Source of Multicolor Photons with Tunable Statistics," Phys. Rev. Lett. **87**, 257,401 (2001).

[49] A. J. Berglund, A. C. Doherty, and H. Mabuchi, "Photon Statistics and Dynamics of Fluorescence Resonance Energy Transfer," Phys. Rev. Lett. **89**, 068,101 (2002).

[50] M. G. Moore and P. Meystre, "Optical control and entanglement of atomic Schrödinger fields," Phys. Rev. A **59**, 1754 (1999).

[51] J. Leach, C. E. Strimbu, and P. Rice, "Nonclassical cross-correlations of transmitted and fluorescent fields in cavity QED systems," J. Opt. B: Quantum Semiclass. Opt **6**, S722 (2004).

[52] M. Stobińska and K. Wódkiewicz, "Witnessing entanglement with second-order interference," Phys. Rev. A **71**, 032,304 (2003).

[53] H. J. Carmichael, G. T. Foster, J. E. Reiner, L. A. Orozco, and P. R. Rice, "Intensity-Field Correlations of Non-Classical Light," in *Progress in Optics*, E. Wolf, ed., vol. 46, p. 355 (Elsevier, Amsterdam, 2004).

[54] G. T. Foster, L. A. Orozco, H. M. Castro-Beltran, and H. J. Carmichael, "Quantum State Reduction and Conditional Time Evolution of Wave-Particle Correlations in Cavity QED," Phys. Rev. Lett. **85**, 3149 (2000).

[55] J. Gea-Banacloche, P. R. Rice, and L. A. Orozco, "Entangled and Disentangled Evolution for a Single Atom in a Driven Cavity," Phys. Rev. Lett. **94**, 053,603 (2005).

[56] E. D. Black, "An Introduction to Pound-Drever-Hall Laser Frequency Stabilization," Am. J. Phys. **69**, 79 (2001).

[57] J. Gripp, S. L. Mielke, and L. A. Orozco, "Cascaded Optical Cavities with Two-Level Atoms: Steady State," Phys. Rev. A **51**, 4974 (1995).

[58] J. E. Reiner, W. P. Smith, L. A. Orozco, H. M. Wiseman, and J. Gambetta, "Quantum Feedback in a wakly driven Cavity QED system," Phys. Rev. A **70**, 0238,119 (2004).

[59] J. E. Reiner, F. M. Dimler, and L. A. Orozco, "Broadening mechanisms and their effects in non-classical correlations on cavity QED with atomic beams," J. Opt. B: Quantum Semiclass. Opt. **6**, 135 (2004).

[60] H. J. Metcalf and P. Straten, *Laser Cooling and Trapping* (Springer, New York, 1999).

[61] Z. T. Lu, K. L. Corwin, M. J. Renn, M. H. Anderson, E. A. Cornell, and C. E. Wieman, "Low-Velocity Intense Source of Atoms from a Magneto-Optical Trap," Phys. Rev. Lett. **77**, 3331 (1996).

[62] H. J. Carmichael and B. C. Sanders, "Multiatom Effects in Cavity QED with Atomic Beams," Phys. Rev. A **60**, 2497 (1999).

[63] R. Loudon, *The Quantum Theory of Light*, 2nd ed. (Oxford University Press, New York, 1983).

[64] G. T. Foster, S. L. Mielke, and L. A. Orozco, "Intensity Correlations of a Noise-Driven Diode Laser," J. Opt. Soc. Am. B **15**, 2646 (1998).

[65] D. J. Heinzen, J. J. Childs, J. E. Thomas, and M. S. Feld, "Enhanced and inhibited visible spontaneous emission by atoms in a confocal resonator," Phys. Rev. Lett. **58**, 1320 (1987).

[66] J. J. Childs, K. An, M. S. Otteson, R. R. Desari, and M. S. Feld, "Normal Mode Line Shapes for Atoms in Standing-Wave Optical Resonators," Phys. Rev. Lett. **77**, 2901 (1996).

[67] Y. Zhu, A. Lezama, T. W. Mossberg, and M. Lewenstein, "Vacuum-Field Dressed-State Pumping," Phys. Rev. Lett. **61**, 1946 (1988).

[68] K. M. Birnbaum, A. Boca, R. Miller, A. D. Boozer, T. E. Northup, and H. J. Kimble, "Photon Blockade in an Optical Cavity with One Trapped Atom," Nature **436**, 87 (2005).

[69] J. P. Clemens, Private Communication (2006).

[70] J. McKeever, J. R. Buck, A. D. Boozer, A. Kuzmich, H.-C. Ngerl, D. M. Stamper-Kurn, and H. J. Kimble, "State-Insensitive Cooling and Trapping of Single Atoms in an Optical Cavity," Phys. Rev. Lett. **90**, 133,602 (2003).

[71] A. L. Lacaita, F. Zappa, S. Bigliardi, and M. Manfredi, "On the Bremsstrahlung Origin of Hot-Carrier-Induced Photons in Silicon Devices," IEEE Trans. Electron Devices **ED 40**, 577 (1993).

[72] S. Kuhr, W. Alt, D. Schrader, M. Mueller, V. Gomer, and D. Meschede, "Deterministic Delivery of a Single Atom," Science **293**, 278 (2001).

[73] N. Schlosser, G. Reymond, I. Protsenko, and P. Grangier, "Sub-poissonian loading of single atoms in a microscopic dipole trap," Nature **411**, 1024 (2001).

[74] H. Mabuchi, Q. A. Turchette, M. S. Chapman, and H. J. Kimble, "Real-Time Detection of Individual Atoms Falling Through a High-Finesse Optical Cavity," ol **21**, 1393 (1996).

[75] W. D. Phillips, Private Communication (2005).

[76] H. J. Carmichael, "Quantum Trajectory Theory for Cascaded Open Systems," Phys. Rev. Lett. **70**, 2273 (1993).

[77] H. Eleuch and H. J. Carmichael, "2-mode correlation function of a cavity QED system," preprint (2006).

[78] B. B. Blinov, D. L. Moehring, L.-M. Duan, and C. Monroe, "Observation of entanglement between a single trapped atom and a single photon," Nature **428**, 153 (2004).